



**MODELLING AND CONTROLLER DESIGN FOR A BLADE OPERATION  
OF A MOTOR GRADER**

**EKİN CANSU ÖZKAN ÖZTÜRK**

**SEPTEMBER 2022**

**ÇANKAYA UNIVERSITY**

**GRADUATE SCHOOL OF NATURAL AND APPLIED SCIENCES**

**DEPARTMENT OF MECHATRONICS ENGINEERING**

**MASTER THESIS IN**

**MECHATRONICS ENGINEERING**

**MODELLING AND CONTROLLER DESIGN FOR A BLADE OPERATION  
OF A MOTOR GRADER**

**EKİN CANSU ÖZKAN ÖZTÜRK**

**SEPTEMBER 2022**

## **ABSTRACT**

### **MODELLING AND CONTROLLER DESIGN FOR A BLADE OPERATION OF A MOTOR GRADER**

OZKAN OZTURK, Ekin Cansu

**Master of Science in Mechatronics Engineering**

Supervisor: Assistant Professor Dr. Halit ERGEZER

September 2022, 110 pages

The subject of this study is the creation of a system that will provide automatic height control of the motor grader blade mechanism. It is aimed to increase both working precision and working efficiency with automatic height control. The height of the blade from the ground was determined by reference to the right and left cutting edges. Two hydraulic cylinders, right and left, provide the up and down movement of the blade. The relationship between the position of the hydraulic cylinders and the cutting edges of the blade was determined using polynomial surface fitting method. The behavior of the hydraulic system was examined with the test records taken on the real machine and the transfer functions were obtained by using the system identification method. The effect of the flow generated by the hydraulic pump (at a certain RPM value) through the electro-hydraulic valve and the elapsed time were investigated. Forward and feedback control methods were used in Matlab/Simulink model created for cylinder movements. Simulation outputs and real test records were examined. Using the functions obtained by the polynomial surface fitting method, the positions of the right and left edges in three axes were calculated against a height input. The terrain was designed in the simulation environment and the behavior of the model was observed at different altitudes. Cylinder speed coefficients were obtained for different RPM values to be examined in the future studies, and the dynamic model of the vehicle

was examined for possible disturbances from the road and the effect on the blade edges of the blade was observed.

**Keywords:** Motor Grader, Semi-Autonomous Systems, Position Control, Feedforward Control, Feedback Control, System Identification.



## ÖZ

# MOTOR GREYDER BIÇAK HAREKETLERİNİN MODELLENMESİ VE KONTROLÜ

ÖZKAN ÖZTÜRK, Ekin Cansu  
Mekatronik Mühendisliği Yüksek Lisans

Danışman: Doç. Dr. Halit ERGEZER

Eylül 2022, 110 sayfa

Bu çalışmanın konusu bir motor greyder aracının bıçak mekanizmasının otomatik yükseklik kontrolünü sağlayacak sistemin oluşturulmasıdır. Otomatik yükseklik kontrolü ile hem çalışma hassasiyeti hem de çalışma verimliliğinin artırılması amaçlanmaktadır. Bıçağın yerden yüksekliği kesici kenarının sağ ve sol ucu referans alınarak belirlenmiştir. Bıçağın yukarı aşağı hareketini sağ ve sol olmak üzere iki hidrolik silindir sağlamaktadır. Hidrolik silindirlerin pozisyonu ile bıçağın kesici uçları arasındaki ilişki polinomial yüzey dönüşümü metodu kullanılarak belirlenmiştir. Hidrolik sistemin davranışı gerçek makine üzerinde alınan test kayıtları ile incelenmiş ve sistem tanılama yöntemi kullanılarak transfer fonksiyonlar elde edilmiştir. Hidrolik pompa tarafından oluşturulan akışın (belirli bir RPM değerinde) elektro-hidrolik valflerden geçme süresi ve miktarının hidrolik silindirlerin hızına etkisi incelenmiştir. Silindir hareketleri için oluşturulan Simulink modelinde ileri ve geri beslemeli kontrol yöntemleri kullanılmıştır. Simülasyon çıktıları ve gerçek test kayıtları incelenmiştir. polinomial yüzey dönüşümü metodu ile elde edilen fonksiyonlar kullanılarak girilen bir yükseklik değerine karşılık sağ ve sol uçların üç eksenindeki konumları hesaplanmıştır. Simülasyon ortamında arazi tasarlanmış ve farklı yükseklik değerinde modelin davranışı gözlemlenmiştir. Devam eden çalışmalarda incelenmek üzere farklı RPM değerleri için silindir hız katsayıları elde edilmiş ve yoldan gelmesi muhtemel

düzensizlikler için aracın dinamik modeli incelenmiştir ve bıçağın uç noktalarına etkisi gözlemlenmiştir.

**Anahtar Kelimeler:** Motor Greyder, Yarı Otonom Sistemler, Pozisyon Kontrolü, İleri Beslemeli Kontrol, Geri Beslemeli Kontrol, Sistem Tanılama.





To My Mother

## ACKNOWLEDGEMENT

I would like to express my sincere gratitude to my family especially to my mother and Kenan for their support and sacrifice to me. I have successfully completed this difficult period with your support.

Special thanks to my supervisor Asst. Prof. Dr. Halit Ergezer for the excellent guidance and providing me with an excellent atmosphere to conduct this research. I would like to thank Prof. Dr. Klaus Werner Schmidt and Prof. Dr. Yavuz Samim Ünlüsoy for their help, support and guidance. My special gratitude also goes to the rest of the thesis committee Prof. Dr. Kemal Leblebiciođlu and Asst. Prof. Dr. Ulař Beldek for the encouragement and insightful comments.

I would like to thank to Motor Grader Engineering Department Manager Dr. İlhan Varol, Design Executive Emre Altınkaya, Control and Software Team Leader Ufuk Akpınarlı, and my colleagues for their understanding and assistance. Finally, I would like to thank Founder of the Hidromek Inc. Hasan Basri Bozkurt, Chairman of Hidromek Inc. Mustafa Bozkurt and General Manager of Hidromek Inc. Ahmet Bozkurt for providing such a working and research environment for Hidromek Inc. engineers.

This study is supported by Hidromek Inc.



## TABLE OF CONTENTS

<b>STATEMENT OF NONPLAGIARISM .....</b>	<b>iii</b>
<b>ABSTRACT .....</b>	<b>iv</b>
<b>ÖZ.....</b>	<b>vi</b>
<b>ACKNOWLEDGEMENT .....</b>	<b>ix</b>
<b>TABLE OF CONTENTS.....</b>	<b>x</b>
<b>LIST OF TABLES .....</b>	<b>xii</b>
<b>LIST OF FIGURES .....</b>	<b>xiii</b>
<b>LIST OF SYMBOLS AND ABBREVIATIONS .....</b>	<b>xviii</b>
<b>CHAPTER I.....</b>	<b>1</b>
<b>INTRODUCTION.....</b>	<b>1</b>
1.1. BACKGROUND.....	1
1.2. APPLICATIONS.....	6
1.3. LITERATURE SURVEY .....	7
1.3.1. Automatic Function Control .....	7
1.3.2. Mechanism Analysis .....	10
1.3.3. Hydraulic Works .....	12
1.4. OBJECTIVE OF THE THESIS .....	13
1.5. THESIS OUTLINE .....	13
<b>CHAPTER II .....</b>	<b>15</b>
<b>MECHANISM ANALYSIS.....</b>	<b>15</b>
2.1. PROBLEM DESCRIPTION AND SOLUTION .....	27
2.2. POLYNOMIAL SURFACE FITTING .....	31
<b>CHAPTER III .....</b>	<b>37</b>
<b>HYDRAULIC SYSTEM AND SYSTEM IDENTIFICATION .....</b>	<b>37</b>
3.1. Slow (20% Joystick Value) .....	42
3.1.1. Down Direction.....	43

3.1.2. Upper Direction.....	44
3.2. Intermediate (50% Joystick Value) .....	44
3.2.1. Down Direction.....	45
3.2.2. Upper Direction.....	46
3.3. Fast (80 % Joystick Value).....	46
3.3.1. Down Direction.....	47
3.3.2. Upper Direction.....	48
<b>CHAPTER IV.....</b>	<b>56</b>
<b>CONTROLLER DESIGN.....</b>	<b>56</b>
<b>CHAPTER V.....</b>	<b>71</b>
<b>TEST RESULTS, SIMULATIONS AND MATHEMATICAL MODEL FOR FUTURE WORKS.....</b>	<b>71</b>
5.1. TEST RESULTS FOR HYDRAULIC SYSTEM AND HEIGHT SIMULATIONS.....	71
5.2. TERRAIN DESIGN.....	75
5.3. MATHEMATICAL MODEL FOR FUTURE WORKS.....	76
5.3.1. Different RPM-JV Relationship.....	76
5.3.2. Disturbances.....	79
<b>CHAPTER VI.....</b>	<b>87</b>
<b>CONCLUSION.....</b>	<b>87</b>
<b>REFERENCES.....</b>	<b>88</b>

## LIST OF TABLES

<b>Table 2.1:</b> Coefficients for all Axes Equations .....	28
<b>Table 2.2:</b> Polynomial Coefficients.....	36
<b>Table 4.1:</b> Calculated Cylinder Speeds .....	65
<b>Table 4.2:</b> Calculated Cylinder Speeds for other JVs .....	65



## LIST OF FIGURES

<b>Figure 1.1:</b> Motor Grader .....	1
<b>Figure 1.2:</b> First Motor Grader .....	2
<b>Figure 1.3:</b> Attachments .....	2
<b>Figure 1.4:</b> Representation of Joystick (left) and Levers (right).....	3
<b>Figure 1.5:</b> Typical Road Cross Section .....	3
<b>Figure 1.6:</b> Different Orientations.....	4
<b>Figure 1.7:</b> Blade Mechanism and Its Components .....	4
<b>Figure 1.8:</b> Blade Mechanism and Its Components .....	5
<b>Figure 1.9:</b> Chart of Proposed Grader Blade Stabilization System.....	8
<b>Figure 1.10:</b> The machine frame and the designed alignment relationship .....	8
<b>Figure 1.11:</b> Representation of Combined Automated Blade Control.....	9
<b>Figure 1.12:</b> Representation of Automatic Switching for Bulldozer Blade.....	10
<b>Figure 1.13:</b> Blade and Rotation Axis Representation.....	12
<b>Figure 1.14:</b> Hydraulic Scheme Representation for Wheel Loader .....	12
<b>Figure 2.1:</b> Upper Mechanism .....	15
<b>Figure 2.2:</b> Lower Mechanism .....	16
<b>Figure 2.3:</b> Blade is Parallel to the Ground.....	17
<b>Figure 2.4:</b> Blade is in Cross Slope.....	17
<b>Figure 2.5:</b> Neutral Position .....	18
<b>Figure 2.6:</b> Tool Selection.....	19
<b>Figure 2.7:</b> Coordinate Axes .....	19
<b>Figure 2.8:</b> Analysis, Step 1 .....	20
<b>Figure 2.9:</b> Analysis, Step 2 .....	21
<b>Figure 2.10:</b> Analysis, Step 3 .....	22
<b>Figure 2.11:</b> Analysis, Step 4 .....	23
<b>Figure 2.12:</b> Analysis, Step 4 .....	23
<b>Figure 2.13:</b> Analysis, Step 5 .....	24

<b>Figure 2.14:</b> Data Set Representation .....	24
<b>Figure 2.15:</b> Data Set Graph for B1 Point in x-axis.....	25
<b>Figure 2.16:</b> Data Set Graph for B1 Point in the y-axis.....	25
<b>Figure 2.17:</b> Data Set Graph for B1 Point in the z-axis .....	26
<b>Figure 2.18:</b> Data Set Graph for B1 Point in x-axis.....	26
<b>Figure 2.19:</b> Data Set Graph for B1 Point in y-axis.....	26
<b>Figure 2.20:</b> Data Set Graph for B1 Point in z-axis .....	27
<b>Figure 2.21:</b> Optimization Result Error Graph for B1 Point in x-axis.....	28
<b>Figure 2.22:</b> Optimization Result Error Graph for B1 Point in y-axis.....	29
<b>Figure 2.23:</b> Optimization Result Error Graph for B1 Point in the z-axis.....	29
<b>Figure 2.24:</b> Optimization Result Error Graph for B4 Point in the x-axis.....	30
<b>Figure 2.25:</b> Optimization Result Error Graph for B4 Point in y-axis.....	30
<b>Figure 2.26:</b> Optimization Result Error Graph for B4 Point in the z-axis.....	31
<b>Figure 2.27:</b> Error Graphs for Polynomial Fitting in x-axis data for B1 Point, RH .	32
<b>Figure 2.28:</b> Error Graphs for Polynomial Fitting in x-axis data for B4 Point, LH..	33
<b>Figure 2.29:</b> Error Graphs for Polynomial Fitting in y-axis data for B1 Point, RH .	34
<b>Figure 2.30:</b> Error Graphs for Polynomial Fitting in y axis data for B4 Point, LH..	34
<b>Figure 2.31:</b> Error Graphs for Polynomial Fitting in z-axis data for B1 Point, RH..	35
<b>Figure 2.32:</b> Error Graphs for Polynomial Fitting in z-axis data for B4 Point, LH..	35
<b>Figure 3.1:</b> Schematic of Electro-Hydraulic System .....	37
<b>Figure 3.2:</b> Representation of Valve Model.....	38
<b>Figure 3.3:</b> Representation of Hydraulic Cylinder.....	39
<b>Figure 3.4:</b> Electro-Hydraulic Valve Working Principle .....	39
<b>Figure 3.5:</b> Test Setup .....	40
<b>Figure 3.6:</b> Siko Draw-Wire Encoder .....	40
<b>Figure 3.7:</b> Draw-Wire Encoder Representation Mounted in Cylinder .....	41
<b>Figure 3.8:</b> Sensor Mounted on Cylinder.....	41
<b>Figure 3.9:</b> Down Direction for Left Lifting Cylinder, Joystick Value 20 % .....	43
<b>Figure 3.10:</b> Down Direction for Right Lifting Cylinder, Joystick Value 20 %.....	43
<b>Figure 3.11:</b> Up Direction for Left Lifting Cylinder, Joystick Value 20 % .....	44
<b>Figure 3.12:</b> Up Direction for Right Lifting Cylinder, Joystick Value 20 % .....	44
<b>Figure 3.13:</b> Down Direction for Left Lifting Cylinder, Joystick Value 50 % .....	45
<b>Figure 3.14:</b> Down Direction for Right Lifting Cylinder, Joystick Value 50 %.....	45
<b>Figure 3.15:</b> Up Direction for Left Lifting Cylinder, Joystick Value 50 % .....	46

<b>Figure 3.16:</b> Up Direction for Right Lifting Cylinder, Joystick Value 50 % .....	46
<b>Figure 3.17:</b> Down Direction for Left Lifting Cylinder, Joystick Value 80 % .....	47
<b>Figure 3.18:</b> Down Direction for Right Lifting Cylinder, Joystick Value 80 % .....	47
<b>Figure 3.19:</b> Up Direction for Left Lifting Cylinder, Joystick Value 80 % .....	48
<b>Figure 3.20:</b> Up Direction for Right Lifting Cylinder, Joystick Value 80 % .....	48
<b>Figure 3.21:</b> Up Direction, 20% Joystick Value/PWM/Current Start Time Comparison RH and LH .....	49
<b>Figure 3.22:</b> Down Direction, 20% Joystick Value/PWM/Current Start Time Comparison RH and LH .....	49
<b>Figure 3.23:</b> Up Direction, 50% Joystick Value/PWM/Current Start Time Comparison RH and LH .....	50
<b>Figure 3.24:</b> Down Direction, 50% Joystick Value/PWM/Current Start Time Comparison RH and LH .....	50
<b>Figure 3.25:</b> Up Direction, 80% Joystick Value/PWM/Current Start Time Comparison RH and LH .....	50
<b>Figure 3.26:</b> Down Direction, 80% Joystick Value/PWM/Current Start Time Comparison RH and LH .....	51
<b>Figure 3.27:</b> Up and Down Directions, 20% Joystick Value, LH.....	51
<b>Figure 3.28:</b> Up and Down Directions, 20% Joystick Value, RH .....	52
<b>Figure 3.29:</b> Up and Down Directions, 50% Joystick Value, LH.....	52
<b>Figure 3.30:</b> Up and Down Directions, 50% Joystick Value, RH .....	52
<b>Figure 3.31:</b> Up and Down Directions, 80% Joystick Value, LH.....	53
<b>Figure 3.32:</b> Up and Down Directions, 80% Joystick Value, RH .....	53
<b>Figure 3.33:</b> Up and Down Direction vs Current Graph, 50% Joystick Value, RH .	54
<b>Figure 3.34:</b> Closer look to Figure 3.32 .....	54
<b>Figure 3.35:</b> Up and Down Direction vs Current Graph, 50% Joystick Value, LH .	54
<b>Figure 3.36:</b> Close look to Figure 3.34 .....	55
<b>Figure 4.1:</b> Pole-Zero Map for Down Direction .....	56
<b>Figure 4.2:</b> Pole-Zero Map for Up Direction .....	57
<b>Figure 4.3:</b> Matlab Simulink Model for 50 % Joystick Value's Transfer Functions	57
<b>Figure 4.4:</b> Matlab Simulink Model for 50 % Joystick Value's Transfer Functions	58
<b>Figure 4.5:</b> Matlab Simulink Model for 50 % Joystick Value's Transfer Functions	58
<b>Figure 4.6:</b> Down Direction, 50 % Joystick Value RH with PI Controller .....	59
<b>Figure 4.7:</b> Up Direction, 50 % Joystick Value LH with PI Controller.....	60

<b>Figure 4.8:</b> Up Direction, 50 % Joystick Value RH with PI Controller .....	60
<b>Figure 4.9:</b> Down Direction, 20 % Joystick Value with PI Controller RH and LH .	61
<b>Figure 4.10:</b> Up Direction, 20 % Joystick Value with PI Controller RH and LH ....	62
<b>Figure 4.11:</b> Down Direction, 80 % Joystick Value with PI Controller RH and LH	63
<b>Figure 4.12:</b> Up Direction, 80 % Joystick Value with PI Controller RH and LH ....	64
<b>Figure 4.13:</b> Cylinder Speed Calculation using Test Data.....	65
<b>Figure 4.14:</b> Cylinder Speed Calculation using Test Data.....	66
<b>Figure 4.15:</b> 20 % JV Graphic to Show JV Effects to Equalize the Desired and Actual Stroke Openings .....	67
<b>Figure 4.16:</b> 50 % JV Graphic to Show JV Effects to Equalize the Desired and Actual Stroke Openings .....	67
<b>Figure 4.17:</b> 80 % JV Graphic to Show JV Effects to Equalize the Desired and Actual Stroke Openings .....	67
<b>Figure 4.18:</b> Overall Control Concept for Hydraulic System .....	68
<b>Figure 4.19:</b> Valve Characteristics as an Integrator (Hydraulic System TF).....	68
<b>Figure 4.20:</b> Feedforward Control .....	68
<b>Figure 4.21:</b> Feedback Control.....	69
<b>Figure 4.22:</b> Switch.....	69
<b>Figure 4.23:</b> Simulink model of Hydraulic System Control .....	69
<b>Figure 4.24:</b> Simulink output for Right Lifting Cylinder.....	70
<b>Figure 4.25:</b> Simulink output for Left Lifting Cylinder.....	70
<b>Figure 5.1:</b> KP Value 1, Test Result for Left Lifting Cylinder up/down directions	71
<b>Figure 5.2:</b> KP Value 2,5, Test Result for Left Lifting Cylinder down direction....	72
<b>Figure 5.3:</b> KP Value 2.5, Test Result for Right Lifting Cylinder down direction .	72
<b>Figure 5.4:</b> Calculation model for Desired Stroke when input is Desired Height ...	73
<b>Figure 5.5:</b> Overall Height Model.....	74
<b>Figure 5.6:</b> Blade right edge desired and actual output with approximately 0,5 cm difference.....	74
<b>Figure 5.7:</b> Right lifting cylinder desired and actual stroke openings .....	74
<b>Figure 5.8:</b> Blade left edge desired and actual output with approximately 0,3 cm difference.....	75
<b>Figure 5.9:</b> Left lifting cylinder desired and actual stroke openings .....	75
<b>Figure 5.10:</b> Side view from y-axis.....	76
<b>Figure 5.11:</b> Top view from z-axis .....	76

<b>Figure 5.12:</b> Cylinder Speed Calculation using Test Data for 1000 RPM.....	76
<b>Figure 5.13:</b> Cylinder Speed Calculation using Test Data for 1200 RPM.....	77
<b>Figure 5.14:</b> Cylinder Speed Calculation using Test Data for 1400 RPM.....	77
<b>Figure 5.15:</b> Cylinder Speed Calculation using Test Data for 1600 RPM.....	78
<b>Figure 5.16:</b> Cylinder Speed Calculation using Test Data for 1800 RPM.....	78
<b>Figure 5.17:</b> Cylinder Speed Calculation using Test Data for 2000 RPM.....	79
<b>Figure 5.18:</b> Cylinder Speed Calculation using Test Data for 2200 RPM.....	79
<b>Figure 5.19:</b> Side view from y-axis.....	80
<b>Figure 5.20:</b> Front view from x-axis .....	80
<b>Figure 5.21:</b> Back view from x-axis.....	81
<b>Figure 5.22:</b> Spring-Damper Forces on Machine Schematics .....	81
<b>Figure 5.23:</b> Configuration of the coordinate frames.....	84
<b>Figure 5.24:</b> Simulink Model for Pitch, Roll and Jump Motion of Machine COG ..	86



## **LIST OF SYMBOLS AND ABBREVIATIONS**

### **SYMBOLS**

Cm : Centimeter

Mm : Milimeter

### **ABBREVIATIONS**

JV : Joystick Value

CW : Clockwise

CCW : Counter-Clockwise

## CHAPTER I

### INTRODUCTION

#### 1.1.BACKGROUND

Construction machines are multi-purpose, high-performance machines used in water canals, road constructions, airport and bridge construction, marble industry, and agriculture. These machines can be classified according to their functions, purpose of usage, and sizes. Motor graders are one of the preferred construction machines in works such as leveling, road construction, grading applications, snow plowing, etc. Motor graders have articulated frames, six wheels, and diesel engines that can also be fitted with various attachments depending on usage. The motor grader can be seen in Figure 1.1.



**Figure 1.1:** Motor Grader

The first self-propelled motor grader in history is found in the 20th century. The first motor grader obtained by modifying a tractor with a blade attachment was made by the Russell Grader Manufacturing Company in 1919 [15].



**Figure 1.2:** First Motor Grader

Motor graders are machines that can reach various speeds. While it performs tasks such as fine/rough grading, speeds will be 2-3 km/h and 6-10 km/h, and it moves at higher speeds in works such as snow plowing. The motor grader needs various attachments to perform the mentioned works. The blade positioned in the middle of the machine is a permanent attachment. According to the need, attachments such as a ripper, scarifier, push plate, snow plow attachment, and front dozer blade can be mounted on the front and rear of the machine.



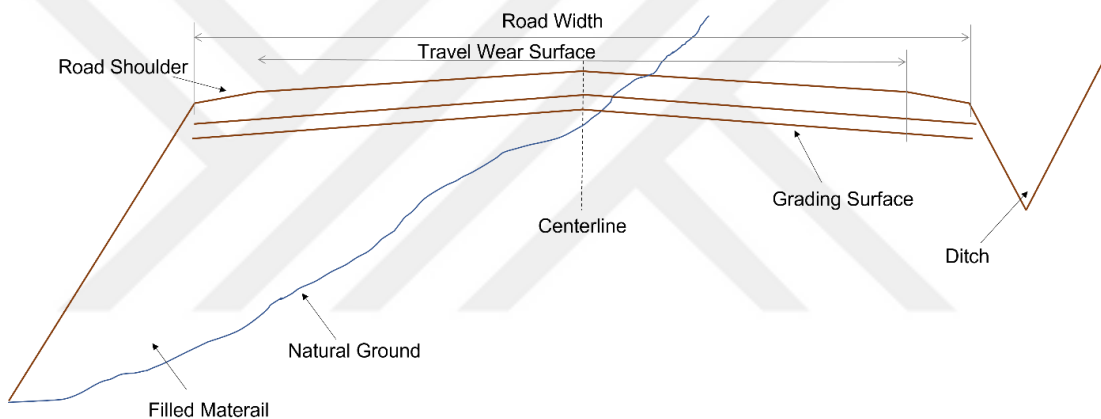
**Figure 1.3:** Attachments

The permanent attachment of the motor grader, the blade, can operate in various positions. In the traditional method, the position control of the blade is carried

out by the operator from inside of the cabin using joysticks (electronically) or levers (mechanically).



**Figure 1.4:** Representation of Joystick (left) and Levers (right)



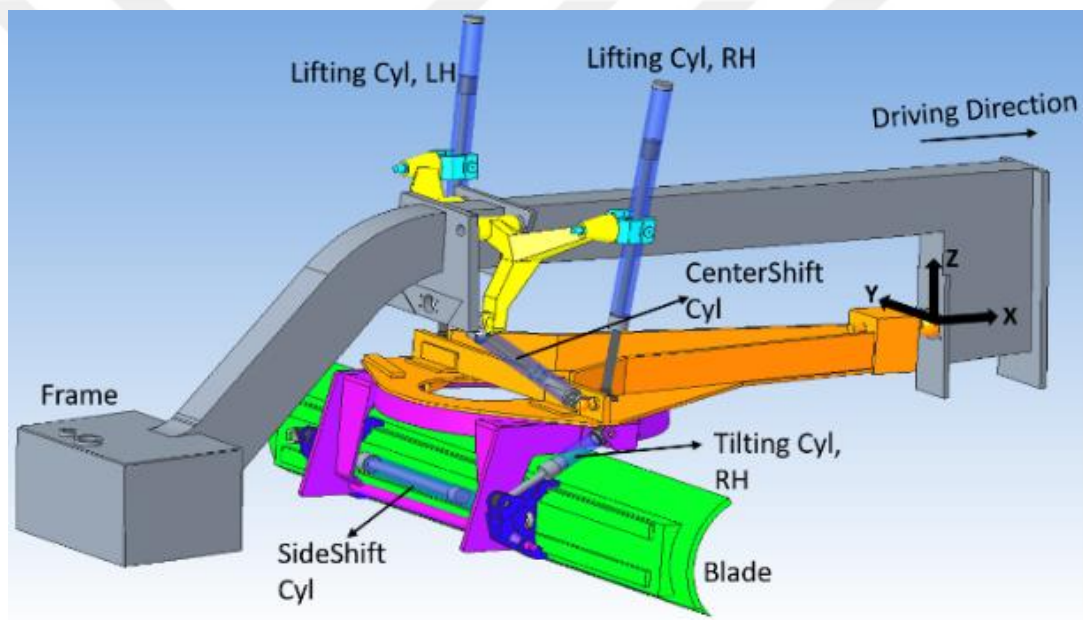
**Figure 1.5:** Typical Road Cross Section

Figure 1.5 shows a typical road cross-section. Road construction is one of the construction works that require precision. In road construction, motor graders are often used to make a slope to the road cross slope or/and longitudinal slope, to level the surface and open rain channels. The cross slope is the type of slope determined according to a certain standard. The longitudinal slope is the slope in the direction of the vehicle preferred in mountainous terrains. The ditch is the name given to the polygonal-shaped channels where rainwater is collected. The grading/leveling surface is the part where the final slope and height of the road are given. Then, asphalt pouring can be done on the surface [1, 12].



**Figure 1.6:** Different Orientations

Various hydraulic components provide blade positions. A typical motor grader blade mechanism has two lifting cylinders, two tilting cylinders, a center-shift cylinder, a side-shift cylinder, and a hydraulic motor.



**Figure 1.7:** Blade Mechanism and Its Components

Figure 1.8 should be studied for a better understanding of the movements. In that figure, the XYZ coordinate system is positioned on the front frame of the machine. In the presentation, z is the vertical axis, y is the lateral axis, and x is the driving direction of the machine. The lifting cylinders provides the blade moves along the z-axis up and down direction and rotates around the x-axis. The retraction and/or extraction of the tilting cylinders changes the position of the blade's cutting edge relative to the ground, which means it rotates the blade around the y-axis CW/CCW. The side shift cylinder moves the blade on the left and right sides of the machine, which means the blade moves along the y-axis +/- direction. The purple component in



Figure 1.7 can be named a circle and the hydraulic motor mounted inside it. The movement of the hydraulic motor rotates the blade around the z-axis CW/CCW. The slope cutting angle position is shown in the first orientation in Figure 1.6, and it can happen by the movement of the center-shift cylinder.



**Figure 1.8:** Blade Mechanism and Its Components

Works such as leveling and road construction require high precision. Traditionally, the operators decide on the height at which the blade should enter the ground. The vehicle may need to work in the same area many times to achieve the desired sensitivity in the field. Thus, the vehicle consumes more fuel, the time required to complete the job is extended, and the operator has to work for long hours in a dusty, vibrating, and noisy environment, which results in time, money, and health loss problems.

Motor graders perform their functions while the machine is traveling. Both steering and attachment control can be challenging for operators. For such reasons, the interest in automatic systems in construction machinery has increased. Equipping vehicles with various sensors can provide a faster and more safe working environment. Thanks to the algorithms developed with the information received from the sensors, the machines can become smart.

## 1.2. APPLICATIONS

US-based construction and agricultural machinery manufacturer John Deere uses various intelligent systems in its motor graders. AutoshiftPlus is an automatic gear shift application, and the operator can control the machine using only gas and brake pedal without changing the gear or pushing the inching pedal. MachineDamageAvoidance application prevents the machine and tires from damaging when the blade operates at various angles. AutoPass application automatically controls the blade's up and down movement, rotation, and cutting edge angle. With AutoArticulation, the articulation between the rear and front chassis of the machine is performed automatically [17].

Caterpillar, another motor grader manufacturer, prefers 2D, 3D and StableBlade systems in its graders. In the 3D system, the machine is equipped with a GNSS antenna, mainfall sensor for the machine's pitch angle, blade slope sensor, position sensing system for side shift and RTK radio. Thus, the blade's position can be controlled in real-time during work. In the 2D system, the slope of the blade and the leveling height is automatically determined by the system. The StableBlade system detects vibrations in the stable blade application and warns the operator to slow down. This plays an important role in reducing grading errors [18].

Leica Geosystem is a company that designs intelligent systems for construction machines. They offer 2D and 3D systems for motor graders. In the 2D system, the machine is equipped with a slope sensor, a tilt sensor, a trisonic (2 axes- ultrasonic) sensor, or a laser system for the blade's position. The operator can observe the information about the rotation and tilt of the blade. Thanks to trisonic sensor and laser system, the height of the blade relative to the ground can be adjusted automatically. In 3D systems, slope sensor for the blade, tilt sensor for the blade cutting edge, GNSS antennas and receivers are used [19].

Companies such as Topcon [13], Trimble, and Moba offer similar systems as Leica as shelf products. These products can be applied to any brand of machine, but calibration is important since the specifications of each machine can be different.

Motor graders, excavators, Wheel loaders, etc., are also automated. Wheel loaders are construction machines used for crushing, filling, laying and loading materials in areas such as excavation, road construction, construction works, and marble industry, and these works are carried out with the bucket mounted in front of the machine. Wheel loaders are equipped with GPS and laser systems and tilt sensors.

Automated and even wheel loaders take the load from one place and unload to the truck in the working area. The position and height of the truck are determined by the GPS and laser system on a machine. Excavators are another construction machine used for digging the soil and lifting and carrying the load. Automatic systems are widely preferred in excavators. GPS systems and angle sensors determine the position of the bucket and machine. Thus, the machines can decide on the depth of the soil to be excavated.

Automatic function control studies on Wheel loaders, bulldozers, and excavators are abundant both as a shelf product and in the literature. The most important factor in directing many companies to these machines as shelf products is that these machines are highly preferred in construction. Functionality and ease of use are also important reasons for this preference. On the other hand, the studies on motor graders are not enough compared to other machines. When the studies are examined, the complexity of the mechanism may be one of the reasons. In addition, these machines are used at high speeds while performing their functions. This may be an important factor in less work being done. It is very important to automate these machines for mentioned reasons.

### **1.3. LITERATURE SURVEY**

The literature survey is described under three headings. First, automatic system studies on motor graders and similar machines are included. Then, studies on the motor grader mechanism were carried out were added. Finally, studies on the control of hydraulic actuators are mentioned.

#### **1.3.1. Automatic Function Control**

Sobczyk et al. [2] stated in their study that the height errors of the blade (moldboard) were due to the position of the front wheels. The grader's front wheels can be leaning or/and steering. Also, the wheels can wear out over time. The surface quality of the terrain is an important factor for grading errors. The authors aimed to prevent possible grading errors with the stabilization system they presented in their study. The proposed model's receivers are mounted on the machine's front frame and front wheels. In addition, the ground reference and stationary signal sources are placed in the working area. Thus, the changes in the position of the front frame during the movement of the machine are recorded. Accordingly, the position of the platform



(drawbar) is determined. By looking at the difference between the fixed reference and the blade's height value, the hydraulic cylinders' stroke values can be calculated, and the blade can be repositioned.

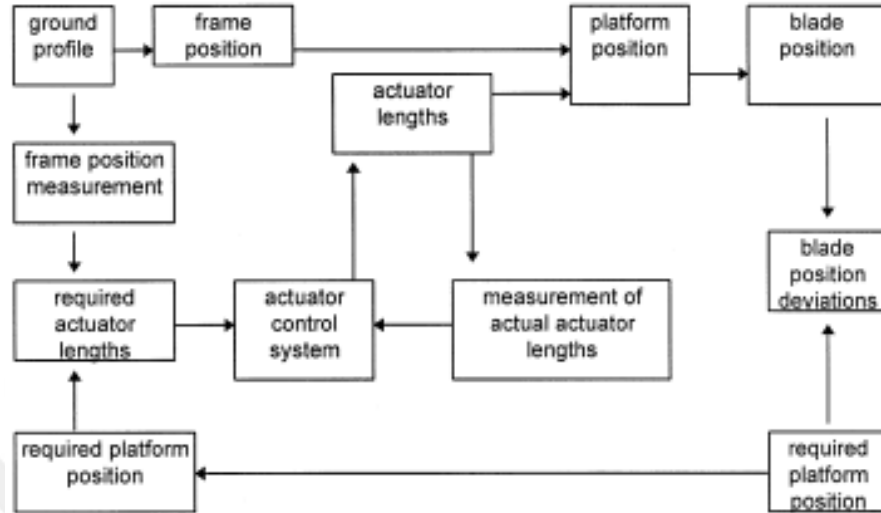


**Figure 1.9:** Chart of Proposed Grader Blade Stabilization System

Retscher [24, 25] mentioned the necessity of expressing the orientation and position of the machine and attachment in real-time according to the terrain in 3D systems. For this, a coordinate system embedded in the machine's center of gravity is placed. The position and orientation of the machine and its attachment were estimated using Kalman and Wiener filter algorithms. RTK, GPS, and inclinometer data were used.

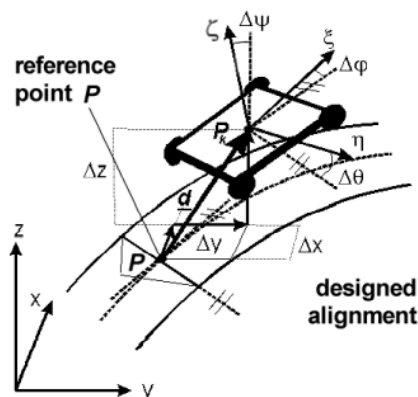


**Figure 1.10:** The machine frame and the designed alignment relationship

Sakai [3], in his study for motor graders used in snow plowing works, mentioned a control system in which tilting cylinders for the position of the blade cutting edge and lifting cylinders for the height of the blade from the ground can be controlled together. In the system, pressure sensors for blade pushing force, snow sensors for snow height of the road, and angle sensors to determine the angle of the blade's cutting edge are used. The study observed that the smaller the angle formed by the blade's cutting edge with the ground, the less the road created by the snow on the blade surface and the higher the working efficiency. Thus, it aims to increase productivity with the automatic control of the height and the blade angle.

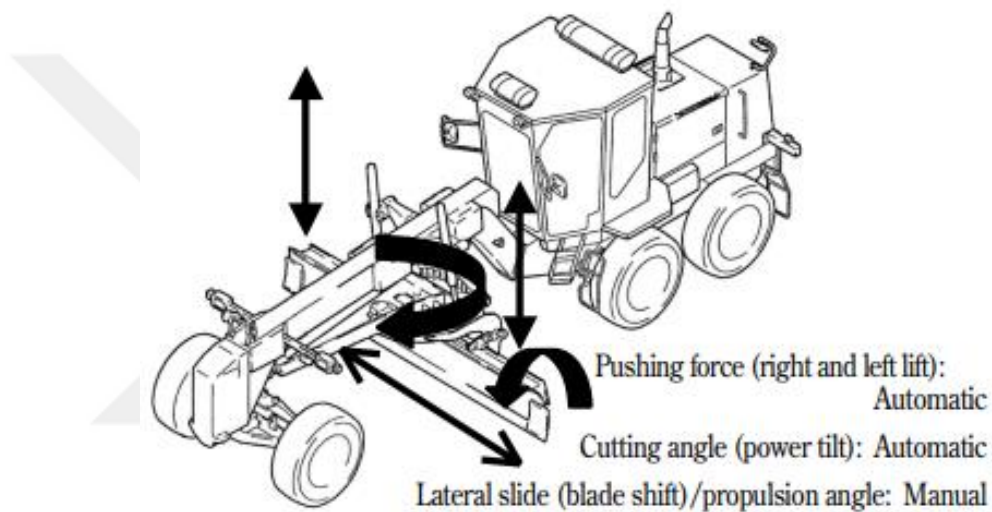


**Figure 1.11:** Representation of Combined Automated Blade Control

Hayashi et al. [6] conducted an automatic control system study for the bulldozer blade. In the study, not only level but also soil digging and soil scrapping works were done for the automatic control system. In the system, the GNSS antenna is placed on the top of the cabin. Stroke sensors are placed in the cylinders that control the bulldozer blade so that the GNSS antenna can measure the position of the bulldozer blade in the correct coordinate system. In this way, the blade's position can be known in real-time. The study prevented surface deterioration by creating an automatic transition system for digging and leveling applications. As the determined surface height approaches, the load applied to the blade will be decreased, so the machine could automatically switch from digging mode to leveling mode.

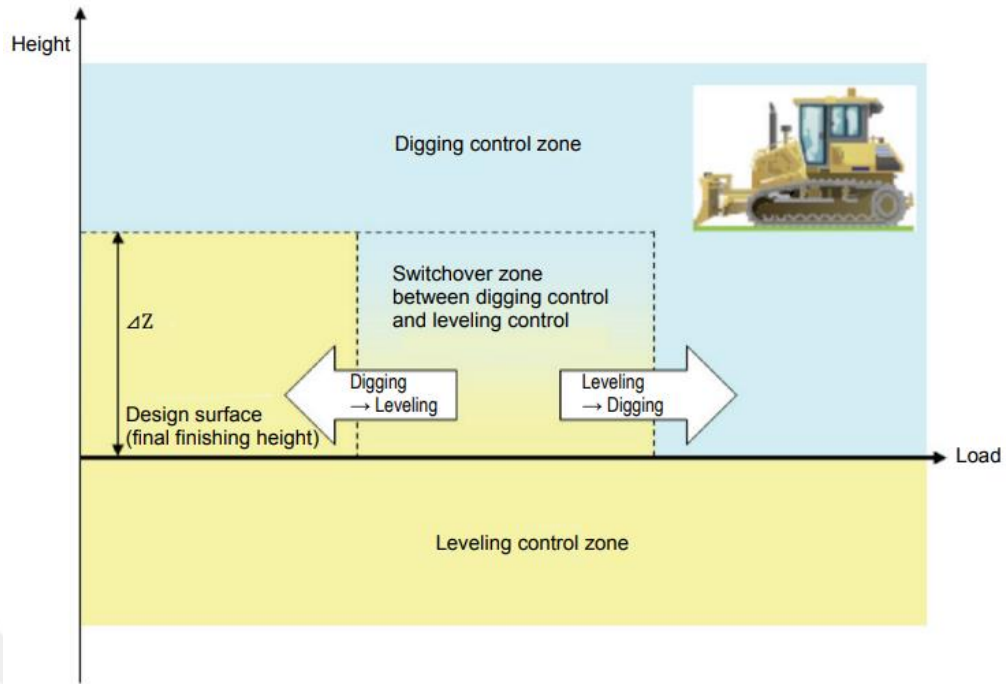


**Figure 1.12:** Representation of Automatic Switching for Bulldozer Blade

Sun et al. [9] performed pose and position estimation studies on three axes for dozer blade. The study used an IMU sensor and RTK GPS on the machine. The IMU sensor is inside the cabin, and the GPS antennas are located at both edges of the dozer blade. The modified Kalman filter was used in the pose estimation application for the blade. Forward kinematics was used for the position of the blade cutting edges.

### 1.3.2. Mechanism Analysis

Shevchenko and Beztsennaya [26] mentioned that the design criteria of the motor grader are created depending on the hydraulic performance of the machine. Also, during the selection and design of the blade cylinders, changing the length of only one of the lifting cylinders affects the angles of the other cylinder. They stated that the calculations were made without paying attention to the force distributions on the cylinders. For this reason, their studies examined the loading patterns formed on the lifting cylinders. For this, they placed a coordinate plane on the spherical joint, the connection point of the drawbar, and the front frame. Then, they calculated the changes in the loads on the axle levers, taking into account the angles of the drawbar in 3 axes as a result of the movement of the lifting cylinders. Axis rotations were defined using rotation matrices.

Pan ve Callejo [7], examined the motor grader blade mechanism the most detailed in their study. They have explained in detail all the components of the blade mechanism. They extracted the mechanism's topology and divided it into two structures: spatial parallel and spatial serial mechanism. Their study addressed the spatial parallel mechanism part, which includes the components that provide the blade's upper and down way movement. They took the mechanism in 3 different orientations according to the robot terminology and expressed the mechanism equations using the neutral coordinate system [5]. Then, an optimization problem was defined for parallel lifting, lifting and scraping applications for 3 different mechanisms and the results were compared.

Pan ve Hou [8], as a continuation of the work in [7], focused on the 3RRPS-S mechanism, one of the three mentioned mechanisms, in detail. Again, they obtained the mechanism equations by using the neutral coordinate method. Then, sensitivity analysis was performed for the mechanism. This is to see how the design parameters affect the objective function defined for optimization. Then, the optimization results for parallel lifting and lifting functions were compared.

Korytov, Scherbakov and Titenko [11] pointed out that the angle occurred by the motor grader blade to the X0 axis should be calculated based on its rotation in around the Y0 axis. The rotation around the X0 axis is called the cross slope, and the rotation around the Y0 axis is called the blade angle (See Figure 1.9). It was put forward that the blade angle affects the cross slope angle of the blade and causes errors on the road surface. As a result of the study, it was mentioned that the slope of the road depends on the cross slope and blade angle, the blade angle should be adjusted according to  $\gamma_{P0}$  to adjust the angle of the road correctly, and the blade angle should be changed up to certain value to minimize the cross slope error.

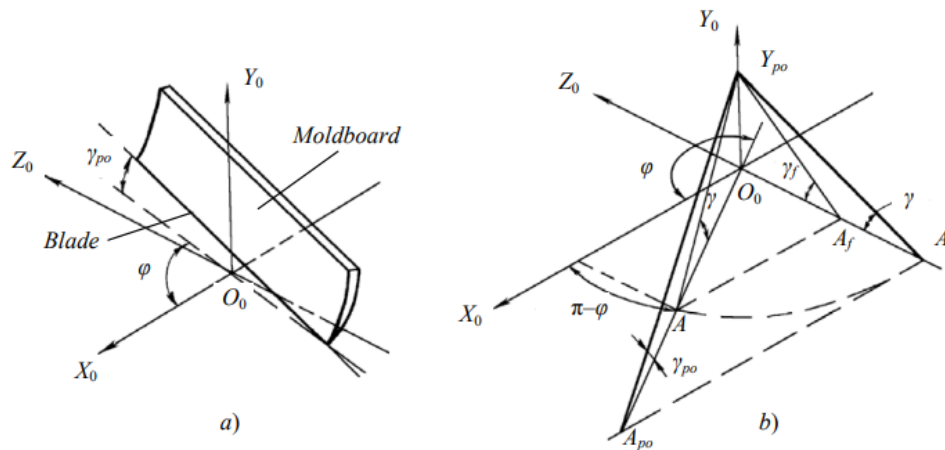


Figure 1.13: Blade and Rotation Axis Representation

### 1.3.3. Hydraulic Works

Fales, Kelkar, Spencer, Chipperfield and Wagner [4], analyzed the Wheel loader mechanism and the calculations of the hydraulic system in their studies. The hydraulic system of Wheel loader consists of an electro-hydraulic valve, hydraulic cylinders and load sensing pump like a motor grader. In the study, the pump, orifice and cylinder equations required for the dynamic calculations of the hydraulic system were written. Then, the equations of motion of the mechanism were obtained. For the controller design, linearization was made using obtained dynamic equations.

Fales and Kelkar [27] applied the  $H_{\infty}$  design technique for the Wheel loader control system in the continuation of the study in [4]. The purpose of the control system to be designed is to adjust the height of the Wheel loader bucket from the ground. For this reason, hydraulic equations, mechanism equations were obtained again.

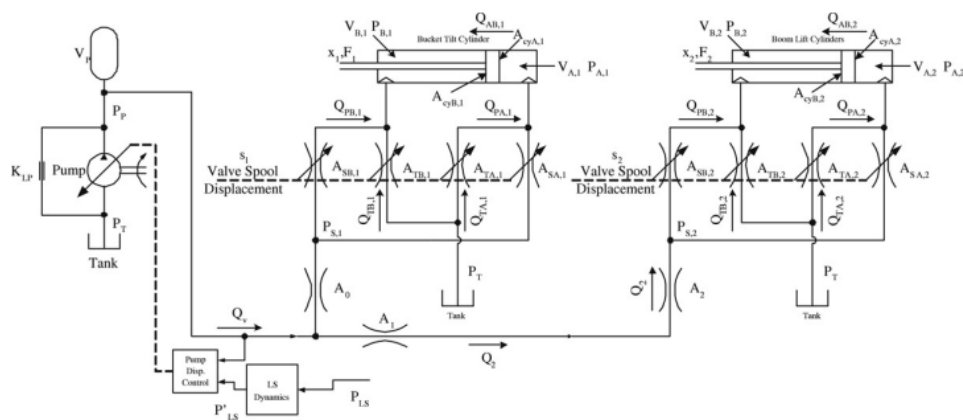


Figure 1.14: Hydraulic Scheme Representation for Wheel Loader

#### **1.4. OBJECTIVE OF THE THESIS**

The main purpose of this thesis is to provide automatic position/height control of a mechanism with high degrees of freedom. The inverse kinematics method can be used to solve the mechanism. Still, in this study, the 3D CAD model of the real mechanism was used, some assumptions were made, and an optimization technique was used to express the cylinder stroke/blade edge relationship. The equations are validated using the measurements taken from the wire-draw sensors on the real mechanism, and the accuracy of the analysis was verified. Then, step input was given to the system to observe the response of the hydraulic system to the desired height and the movements of the hydraulic cylinders were recorded. Since the cylinders providing height control can be controlled independently from each other, the system can be expressed as MIMO/Multi Input-Multi Output System. Using the input/output relationship, the transfer functions of the system were obtained using the system identification method.

Hydraulic system equations were not needed during the height control. The load sensing hydraulic pump in the machine has the power to generate enough flow to feed the hydraulic system. The hydraulic system can adjust the flow reaching the cylinders thanks to electrohydraulic valves. This study has studied a model to ensure that the flow to the cylinders is interrupted as soon as the desired height is reached.

Then, the dynamic movements occurring in the center of gravity of the machine were modeled in Matlab®/Simulink® [21] environment. Again, using the terrain created in the Matlab®/Simulink®, various disturbances were given to the machine's tires. It was observed how the movements in the center of gravity affected the position of the blade's edge.

The methods applied during this study can be studied for other mechanisms and machines. We hope this study will contribute to future studies since the motor grader mechanism is quite complex, and the studies for this machine in the literature are minimal compared to other machines.

#### **1.5. THESIS OUTLINE**

Chapter I includes a brief introduction of the motor grader, the smart applications used/preferred in construction machines, the literature survey and thesis content.

In Chapter II, the mechanism of the machine is explained in more detail, the movements of the mechanism in various axes are mentioned, the data collecting method is explained, the analysis of the mechanism is solved using optimization methods, and the graphic outputs are compared.

Chapter III is the section where transfer functions are obtained using the system identification method of the input/output relationship during leveling using the sensor outputs mounted on the real mechanism.

In Chapter IV, the controller design concepts were mentioned.

In Chapter V, the test results for the hydraulic system were compared, the terrain was created and the effects of road disturbances were examined.



## CHAPTER II

### MECHANISM ANALYSIS

The motor grader blade mechanism can be examined in two systems. The first is the upper part of the mechanism, called parallel manipulator in terminology [7, 8]. The upper mechanism consists of right and left lifting cylinders, a center shift cylinder, and a drawbar (See Figure 1.7 for detail). According to parallel robot terminology, the mechanism is named 2RRPS-SPS-S. The right and left arms consist of 3 limbs; the center shift arm consists of 2 limbs, so the total limb number of the upper mechanism is 11. See Figure 2.1.

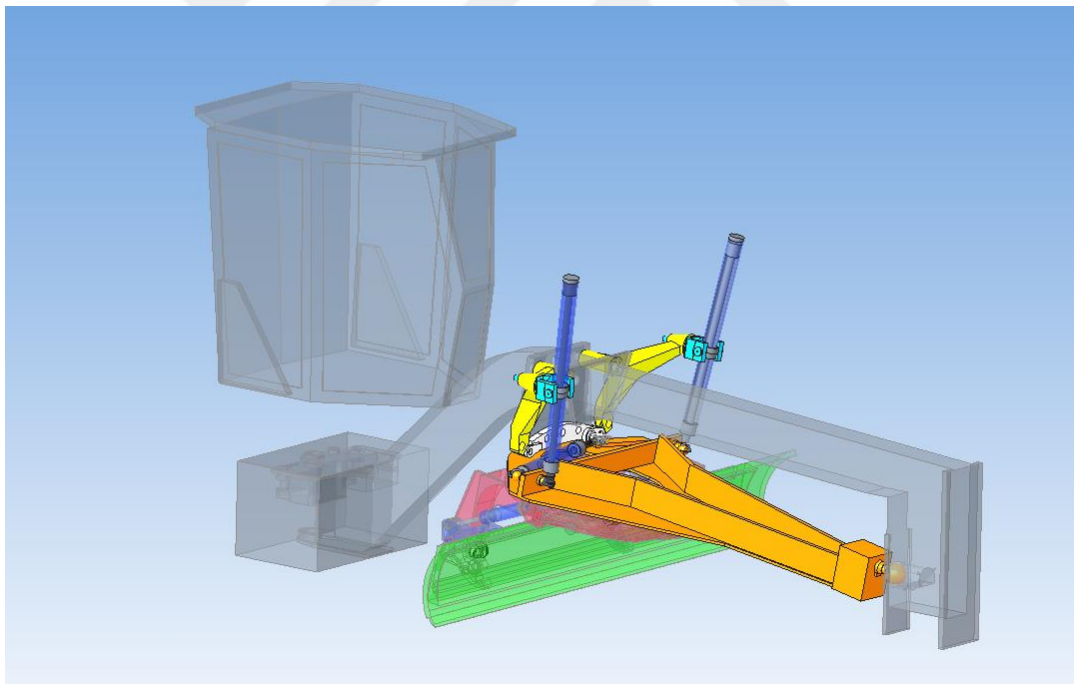


**Figure 2.1:** Upper Mechanism



The Second system consists of the lower part of the mechanism. This part contains the side shift cylinder, tilting cylinders, circle and blade (See Figure 1.7 for detail). The analysis of the lower parts was not included in the height control, but the blade's position as a result of the movement of the lifting cylinders was examined. See Figure 2.2.

It was mentioned in Chapter I that the movement of the lifting cylinders is needed to control the mechanism-ground distance. Considering the similarity of the upper mechanism to the Stewart platform, the positions of the right/left lifting cylinder and center shift cylinder can be calculated with the inverse kinematic method according to the position of the drawbar, which is the movable component, in three axes [23]. However, the availability of 3D CAD data of the mechanism allowed the cylinder/blade edge relationship to be recorded using the mechanism analysis methods of the CAD program instead of writing complex kinematic equations.

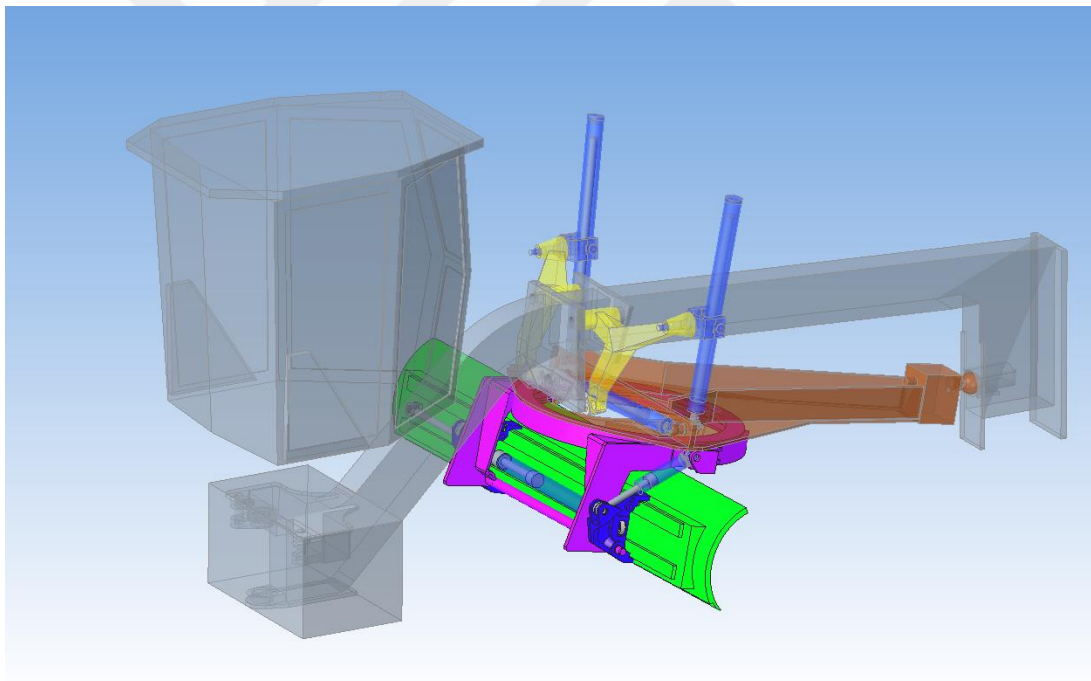


**Figure 2.2:** Lower Mechanism

As a result of the movement of the lifting cylinders, two different movements of the blade occur (See Figures 1.7 and 1.8). When the right and left cylinders have the same stroke value, the blade's cutting edge is parallel to the ground. In this case, the mechanism can be called a parallel mechanism (See Figure 2.3). However, as seen in general applications, various road profiles and slopes should be given according to

the needs of the road. In such cases, the lifting cylinders are positioned in the field with the blade inclined by taking different stroke openings. This position can also be called an un-parallel mechanism (See Figure 2.4).

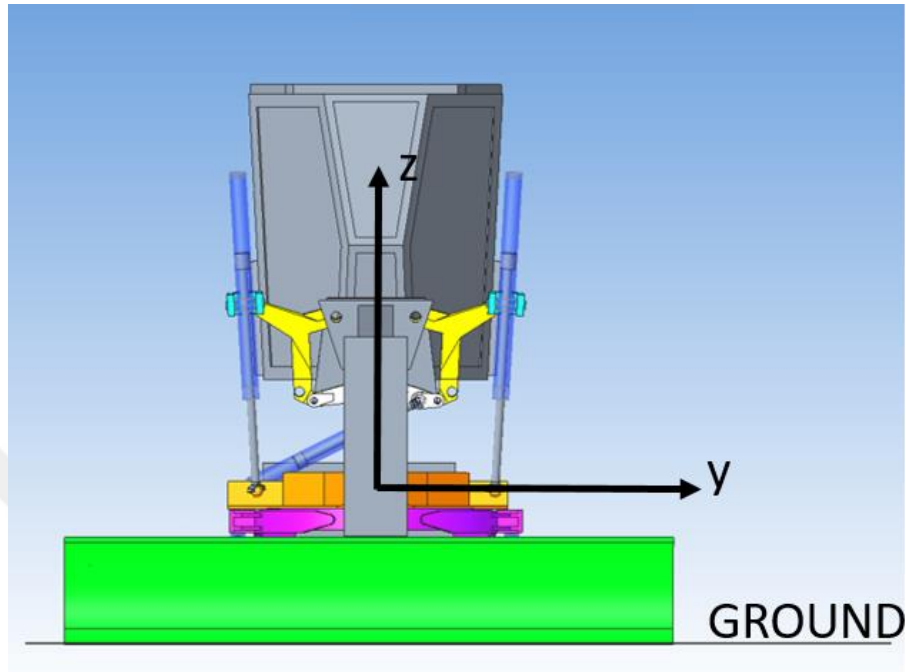


**Figure 2.3:** Blade is Parallel to the Ground

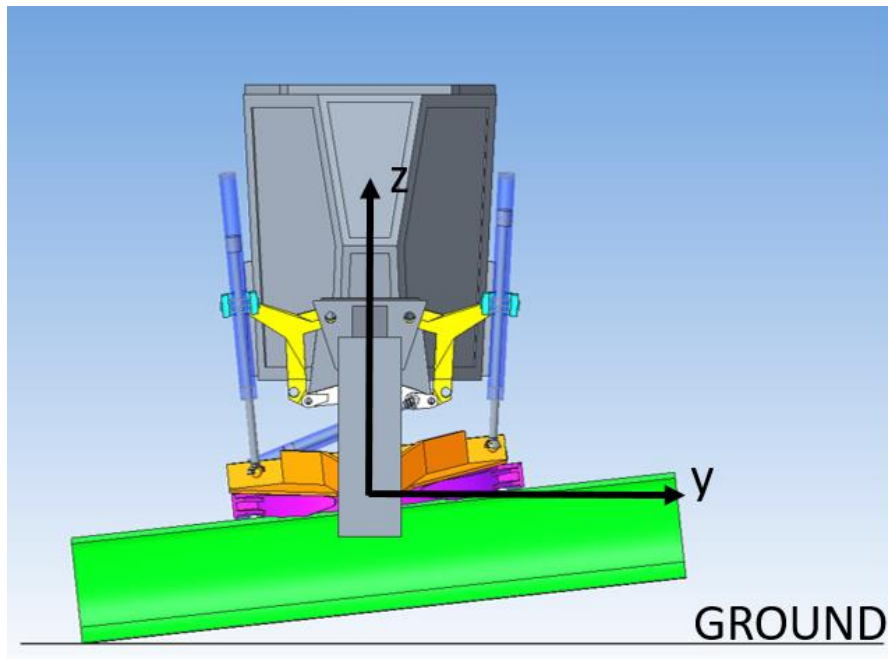


**Figure 2.4:** Blade is in Cross Slope

Some assumptions have been made about the mechanism to express the relationship between the lifting cylinders/blade position. Thus, the elevation change in the vertical axis can be observed without mentioning other axis orientations.

These assumptions are listed below,

- Rear and front frame should be in straight position. (No articulation angle)
- Front wheels are in straight position. (No leaning and steering)
- Side shift cylinder should be centered.
- Tilting Cylinders should fully open. (Blade cutting edge perpendicular to the ground)
- Circle rotation should be zero. (Blade front area is perpendicular to the x-axis.)
- Lifting cylinders should be fully closed and parallel to each other. (For initial position)

The mechanism obtained from the assumptions mentioned above is called the neutral position. Then, considering the direction of movement of the machine, the right and left side of the blade cutting edge are named as B1 and B4, respectively. See Figure 2.5.

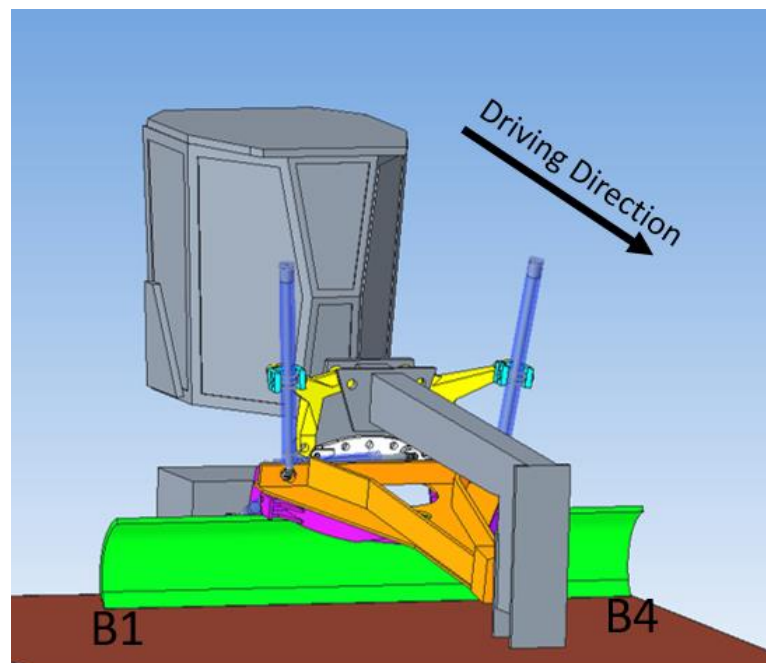


**Figure 2.5:** Neutral Position

Then, using the Mechanism feature of the 3D CAD model created in PTC CREO® 7.0.1.0 [22], under the Applications tab of the program, motion trajectories of B1 and B4 points were obtained for various situations of lifting cylinders.

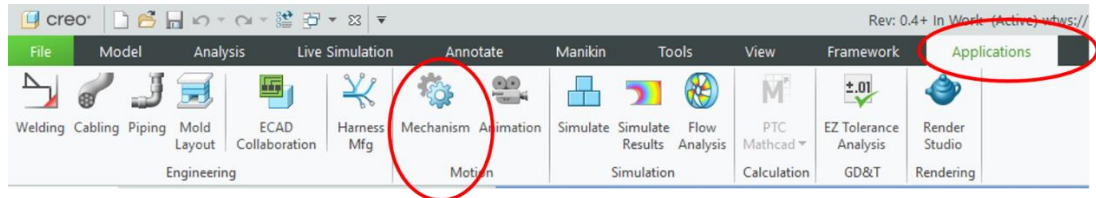


**Figure 2.6:** Tool Selection

For this, XYZ coordinate systems are placed at B1 and B4 points. The XYZ coordinate system, which is also located on the front frame of the machine, was accepted as the reference coordinate system. This reference system is chosen on the front frame because the selected point is fixed and its height from the ground is constant during the analysis.

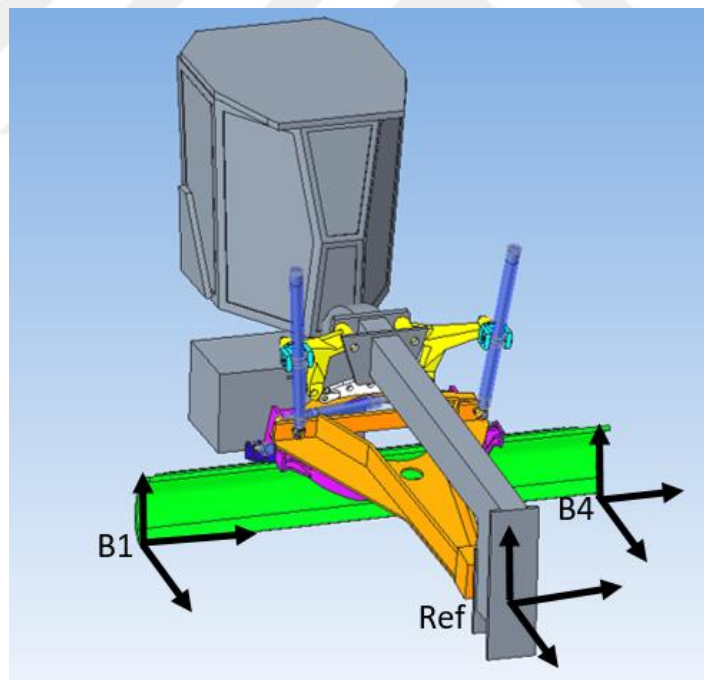


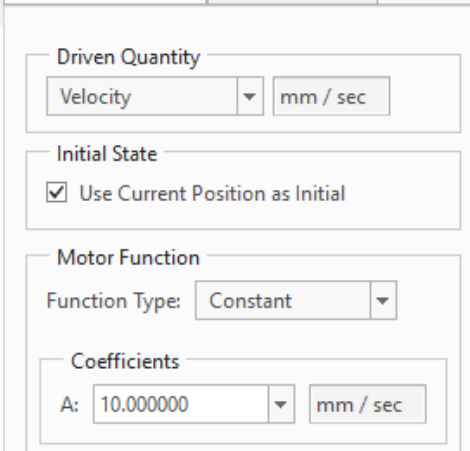
**Figure 2.7:** Coordinate Axes

The situation where the lifting cylinders' strokes are fully open does not apply to the neutral position of the mechanism; it is preferred in the right or left slope cutting angle position. In the case of levelling, it is sufficient for the blade to sweep the working surface a little. For this reason, during the analysis, the maximum stroke value

was preferred not as much as the cylinder's stroke value but as the stroke value where the blade touched the ground. For this mechanism, the maximum stroke value can be taken as  $strokeValue/2$ . In parallel and un-parallel situations, the position where the blade touches the ground in Figures 2.3 and 2.4.

Analysis steps are described as follows,

1. The cylinder to be opened from 0 mm to maximum mm is decided. The motor that will provide the movement is placed in that cylinder. Figure 2.8 shows the screen where the features are selected for the mentioned motor function during analysis. The velocity was chosen in mm/sec for data collection at 10 mm resolution.
2. Then the starting position must be determined. When the mechanism is neutral, the cylinder that provides the movement is in the 0 mm position, while the other cylinder gets a certain stroke value. For example, let the left one be the cylinder that provides the movement. Let the stroke value of the right cylinder be accepted as 200 mm. Thus, the starting position of the analysis is left cylinder stroke 0 mm and right cylinder stroke value 200 mm. See Figure 2.9.



The image shows a software configuration window for a motor function. It is divided into four sections: 'Driven Quantity', 'Initial State', 'Motor Function', and 'Coefficients'. In the 'Driven Quantity' section, 'Velocity' is selected from a dropdown menu, and the units are 'mm / sec'. In the 'Initial State' section, the checkbox 'Use Current Position as Initial' is checked. In the 'Motor Function' section, 'Constant' is selected from the 'Function Type' dropdown. In the 'Coefficients' section, the value 'A: 10.000000' is entered, with units 'mm / sec'.

**Figure 2.8:** Analysis, Step 1

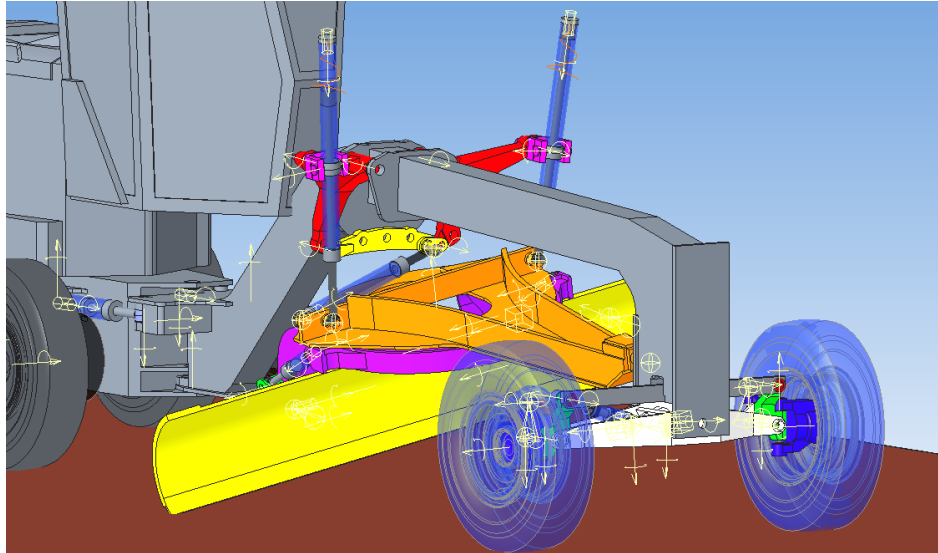


**Figure 2.9:** Analysis, Step 2

3. Then, from the *Analysis Definition* window opened with the *Mechanism Analysis* option, the analysis type will be the position, the end time will be the maximum stroke value, and the initial configuration will be as mentioned in Step 2. In Figure 2.10, the end time is selected as 30 seconds because the maximum stroke value is 300 mm. Then, the analysis will run. See Figure 2.10.

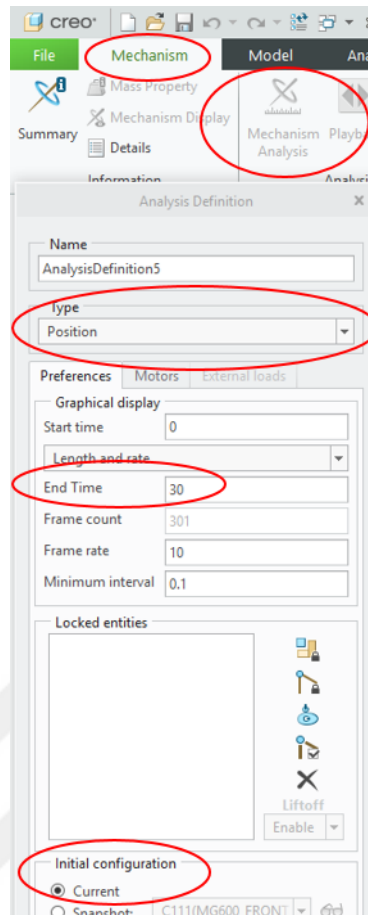


**Figure 2.10:** Analysis, Step 3

4. To obtain the trajectory obtained by the right and left edges of the blade as a result of the movement, the *Trace Curve* option is selected under the *Analysis* tab. In the window that opens, the point whose trajectory is desired to be drawn is selected on the CAD model. The *Curve Type* is marked as 3D and the last saved analysis is chosen to draw the trajectory. These steps must be done separately for both B1 and B4 points. See Figure 2.11. The curve drawn by the B1 point as a result of the analysis is shown in red in Figure 2.12. The initial position indicates B1's position at the beginning of the analysis, and the Final position indicates the position of B1 at the end of the analysis. See Figure 2.12.



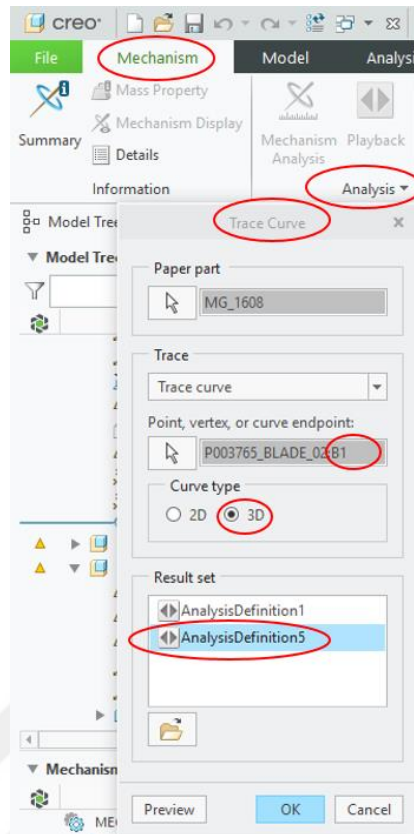


**Figure 2.11:** Analysis, Step 4

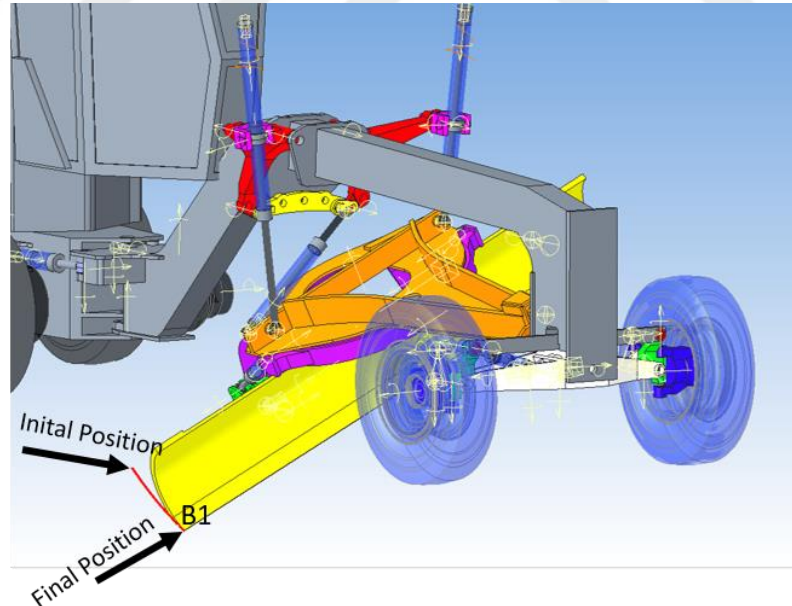


**Figure 2.12** Analysis, Step 4

5. Finally, the position of each point forming the trace curve in the coordinate plane is obtained according to the coordinate system on the front frame selected as reference. See Figure 2.13.



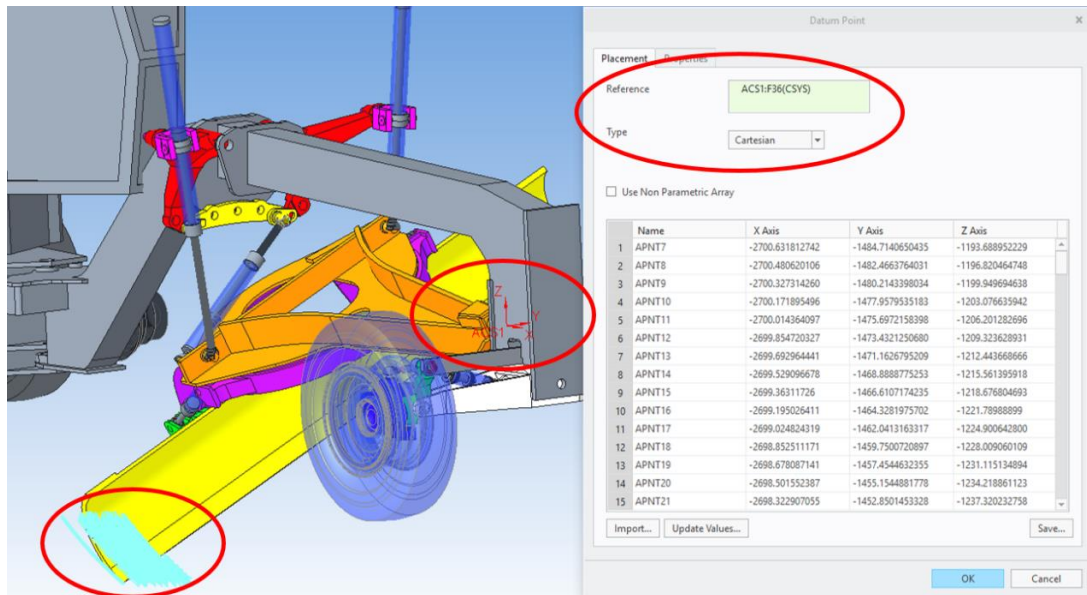


**Figure 2.13: Analysis, Step 5**

The steps mentioned above are continued until the maximum stroke value is reached. If the maximum stroke is called as  $n$ ,  $(n + 1) \times (n + 1)$  matrix is obtained for B1 and B4 points as a result of the analysis.

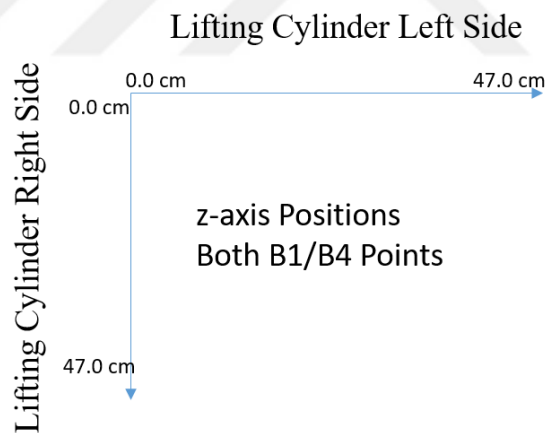


**Figure 2.14: Data Set Representation**

Evaluation of the XYZ axis values obtained as result of the analysis according to the reference point provides convenience in terms of the analysis. However, the location of the reference point may change due to factors such as the terrain's shape, the machine's position, tire diameter and tire pressure. So, it would be more appropriate to choose the neutral position as the starting position and accept the value of the B1 and B4 points in the z-axis as 0 mm for this analysis to always work correctly.

The B1 and B4 points in the X, Y and Z axes are shown in Figures 2.15 – 2.20 with respect to right and left lifting cylinder stroke values. For both points, the graphs shows the points' behavior almost linear. In the analysis, the maximum stroke value was taken as 47 cm for both sides.

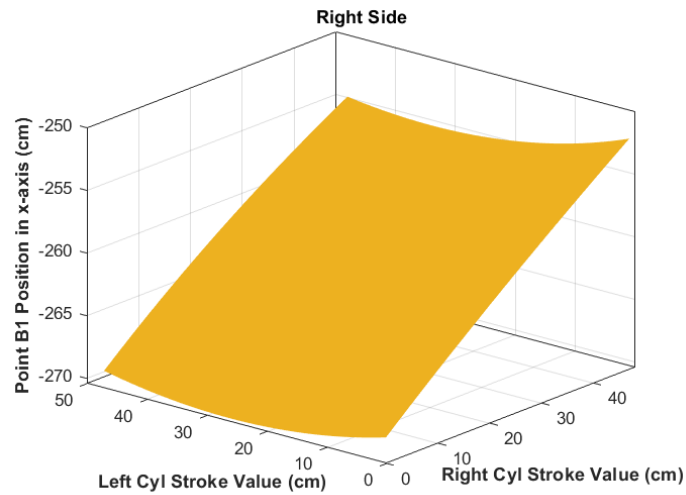


**Figure 2.15:** Data Set Graph for B1 Point in x-axis

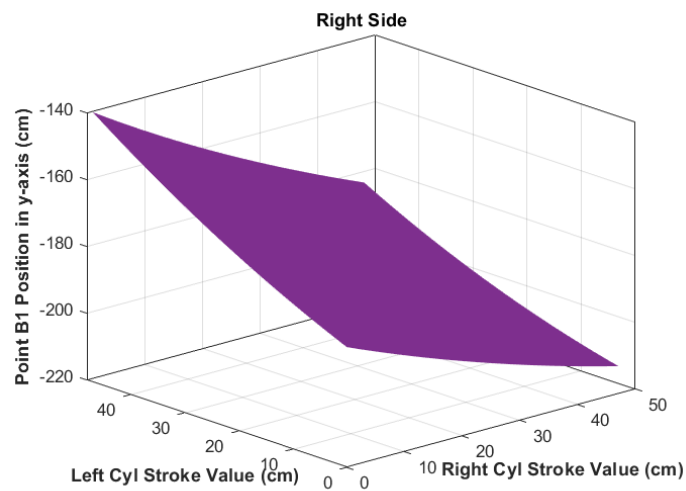


**Figure 2.16:** Data Set Graph for B1 Point in the y-axis

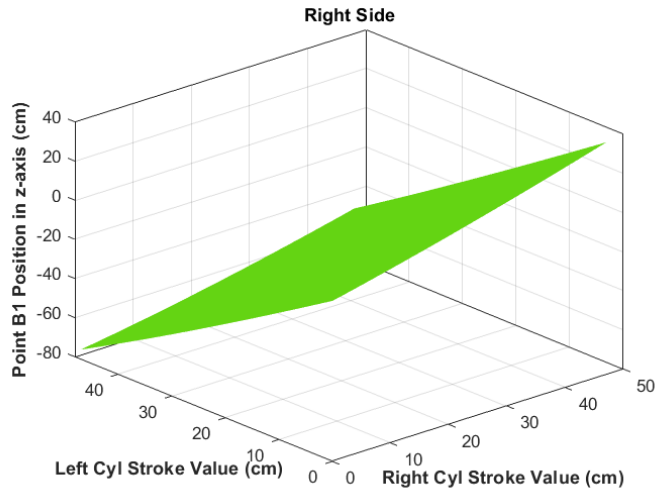


**Figure 2.17:** Data Set Graph for B1 Point in the z-axis

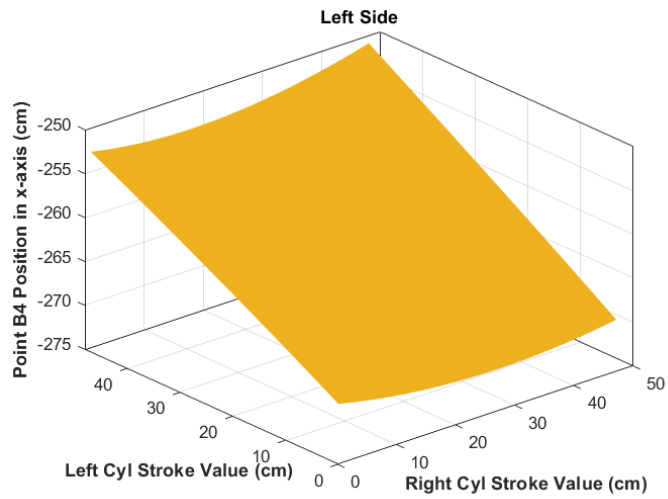


**Figure 2.18:** Data Set Graph for B1 Point in x-axis

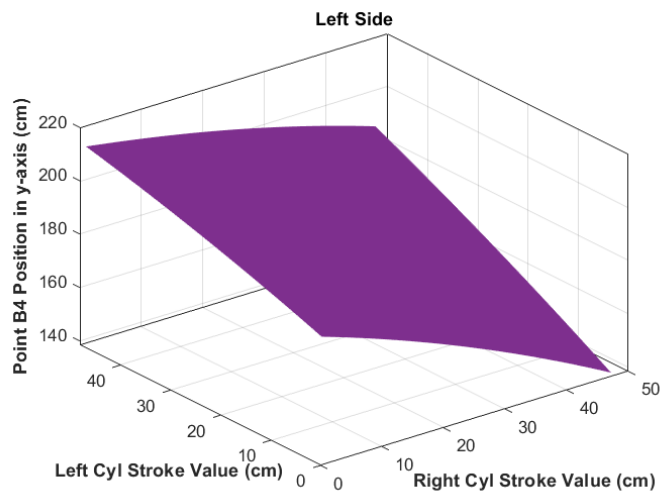


**Figure 2.19:** Data Set Graph for B1 Point in y-axis

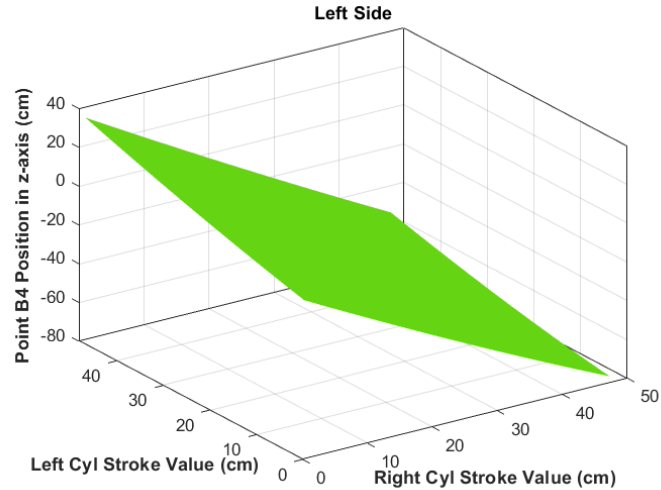


**Figure 2.20:** Data Set Graph for B1 Point in z-axis

As a result of this analysis, the positions of the cutting edges of the blade can be known for certain stroke values. The position of the stroke-blade edge can be matched using positions obtained with a resolution of 10 mms in the range of 0-470 mms. However, for unknown stroke values, the positions should be known.

The position of the edge of the blade in all three axes depends on two variables. There are also certain constraints factors such as the constant distance between B1 and B4 points, the closed loop parallel mechanism, etc. The function outputs obtained with the existing data should be obtained optimally, closest to the real values. Therefore, the problem can be formulated as an optimization problem.

## 2.1. PROBLEM DESCRIPTION AND SOLUTION

The problem at hand has been described as an optimization problem. It is solved using Quasi-Newton Approximation. In this problem, the functions obtained for B1 and B4 points should be minimized, because the error between the real data and the function outputs should be as minimal as possible.

A bivariate quadratic curve equation was used to define the graphs obtained above depending on two variables.

$$f(rs, ls) = x(1) * (rs)^2 + x(2) * (ls)^2 + x(3) * (rs) + x(4) * (ls) + x(5) * (rs * ls) + x(6) \quad (2.1)$$

In the defined equation, at least one of the equations  $x_1$ ,  $x_2$ ,  $x_3$ ,  $x_4$ ,  $x_5$  and  $x_6$  should not be zero.  $r_s$  and  $l_s$  are function variables. For this equation,  $r_s$  denotes the stroke of the right lifting cylinder, and  $l_s$  is the stroke of the left lifting cylinder.

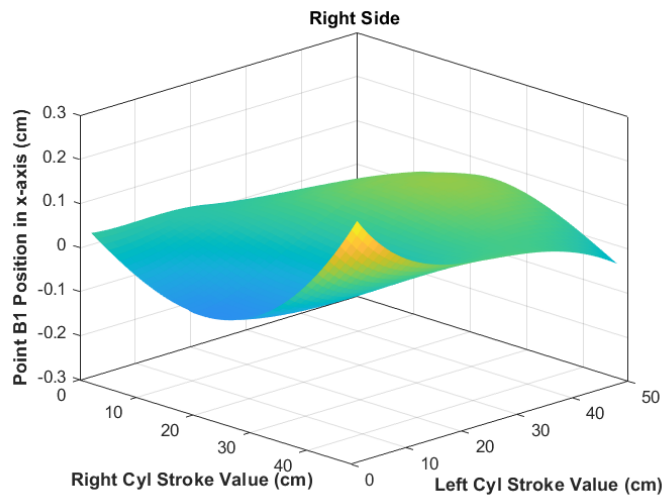
The equation coefficients calculated by the Broyden-Fletcher-Goldfarb-Shanno (BFGS) method are given in Table 2.1.

The Matlab Optimization Toolbox 'fmincon' function was used to obtain the equations.

**Table 2.1:** Coefficients for all Axes Equations

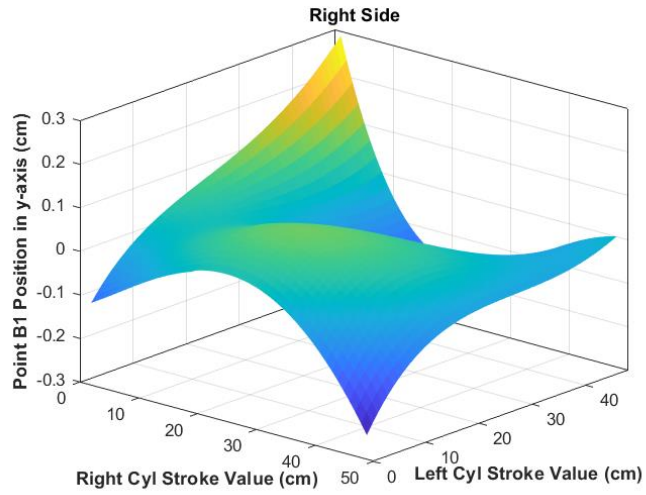
	x(1)	x(2)	x(3)	x(4)	x(5)	x(6)
B1 <sub>x</sub>	0.0028	-0.0011	-0.1404	0.3939	-8.8174e-04	-268.6465
B1 <sub>y</sub>	0.0054	0.0036	0.6905	-0.7575	-0.0069	-184.901
B1 <sub>z</sub>	0.0019	0.0027	-1.7416	0.6594	-0.0040	0.0301
B4 <sub>x</sub>	-5.7715e-04	0.0031	0.3580	-0.1666	0.0013	-268.5751
B4 <sub>y</sub>	-0.0028	-0.0049	0.7010	-0.7578	0.0095	185.109
B4 <sub>z</sub>	0.0028	0.0022	0.6124	-1.7855	-0.0044	-0.0068

Figure 2.21 to Figure 2.23 shows the error graphs for B1 point (right side) between the real data set and the optimization function result. Figure 2.24 to Figure 2.26 shows the same graphs for the B4 point (left side).



**Figure 2.21:** Optimization Result Error Graph for B1 Point in x-axis

Looking at the error graph for the x-axis of the B1 point, one of the function outputs obtained as a result of the optimization, it is seen that the sensitivity is around 0.1 cm. the functions obtained for the x-axis of point B1 can be used in automatic function control. See Figure 2.21.



**Figure 2.22:** Optimization Result Error Graph for B1 Point in y-axis

The error graphs obtained for values on the y and z axes of the B1 point also show sensitivity at the level on 0.1 cm. Likewise, these functions can also be used. See Figure 2.22 and Figure 2.23.

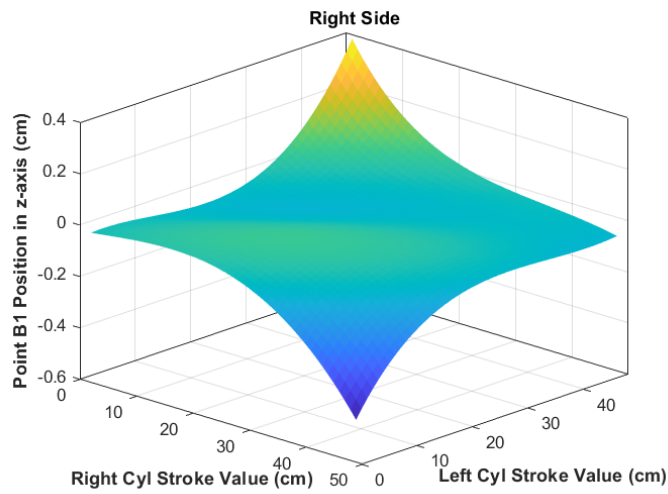


**Figure 2.23:** Optimization Result Error Graph for B1 Point in the z-axis.

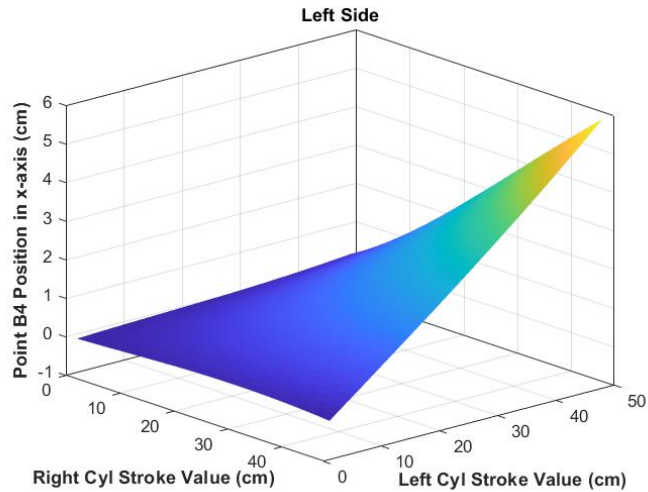


**Figure 2.24:** Optimization Result Error Graph for B4 Point in the x-axis.

When the error graphs obtained for the B4 point are examined, the sensitivity for the x-axis increases to 1cm while the y-axis reaches 10 cm. In this case, very precise functions could not be obtained. The x and y axis equations for point B4 are unsuitable. However, the sensitivity for the z-axis is still in the order of 0.1 cm. while the equations in three axes can be used for the B1 point, only the function obtained from the z-axis is suitable for the B4 point.

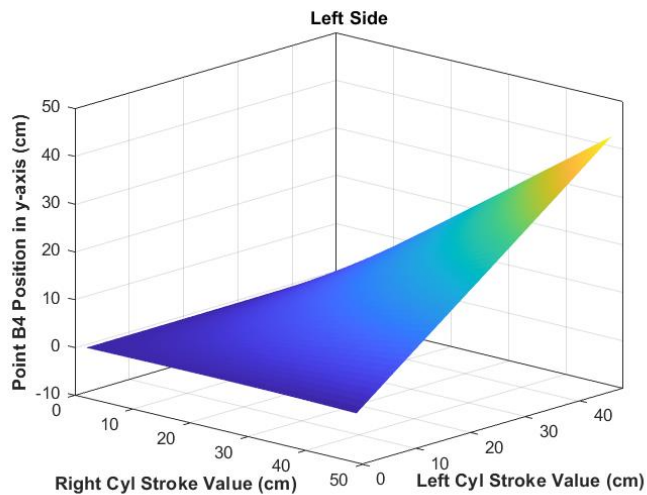


**Figure 2.25:** Optimization Result Error Graph for B4 Point in y-axis

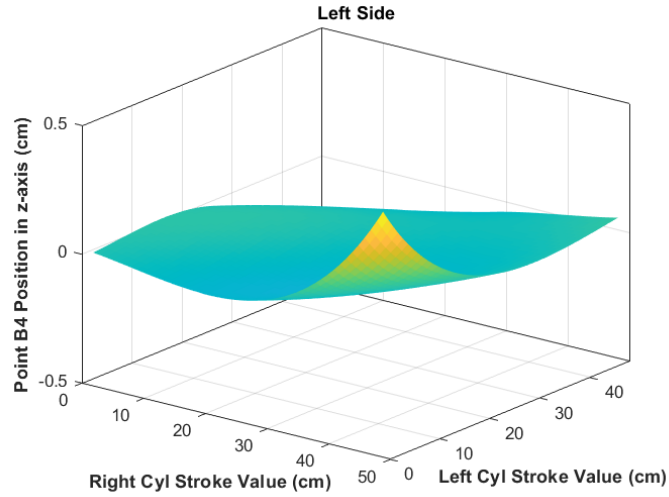


**Figure 2.26:** Optimization Result Error Graph for B4 Point in the z-axis

## 2.2.POLYNOMIAL SURFACE FITTING

As another method, polynomial surface fitting can be used. In this method, a polynomial surface formed by the data sets is tried to be expressed with the most appropriate degree of functions. Using eqn. 2.2 expansion, a function of any degree can be obtained.

$$f(s, t) = \sum_{m=0}^r \sum_{k=0}^m p_{mk} s^m t^k \quad (2.2)$$

Where,  $f: D \subset \mathbb{R}^2 \rightarrow \mathbb{R}$ ,  $r + m \leq \text{Polynomial Degree}$ ,  $s$ ,  $t$  and  $p$  represents inputs, and polynomial coefficient, respectively.

The degree of a polynomial is very important to finding the optimum polynomial coefficients.

The polynomial coefficients are calculated using the Least square adjustment method. When the function calculated in the above equation is expressed as  $f$  and the data set matrix as  $f^*$ , the general linear equation representation is as follows,

$$f * p = f^* \quad (2.3)$$

The QR decomposition method can divide the function matrix  $f$  into  $Q$  orthogonal and  $R$  upper triangular matrix.



$$f = Q * R \quad (2.4)$$

Using the Gram-Schmidt method, f columns are converted to orthonormal sets.

$$Q * R * p = f^* \quad (2.5)$$

$$Q' * Q * R * p = Q' * f^* \quad (2.6)$$

$$R * p = Q' * f^* \quad (2.7)$$

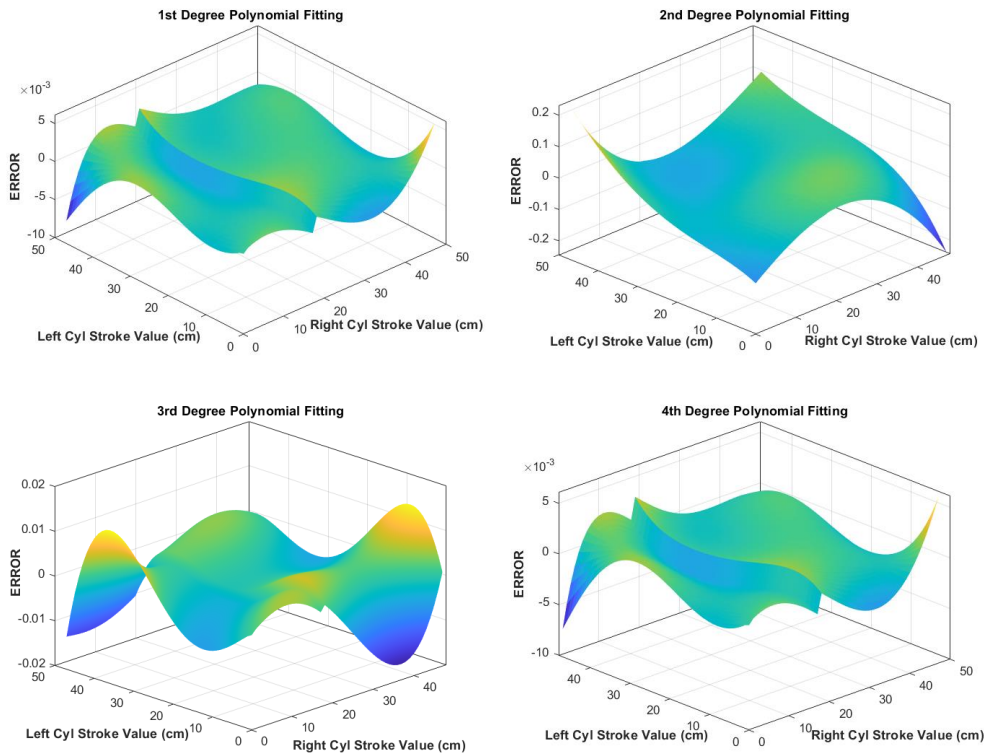
$$p = R \setminus Q' * f^* \quad (2.8)$$

The error between the function output and the data set can give information about the coefficients' accuracy.

$$error = \min \|f_{(r_s, l_s)} - f^*_{(r_s, l_s)}\| \quad (2.9)$$

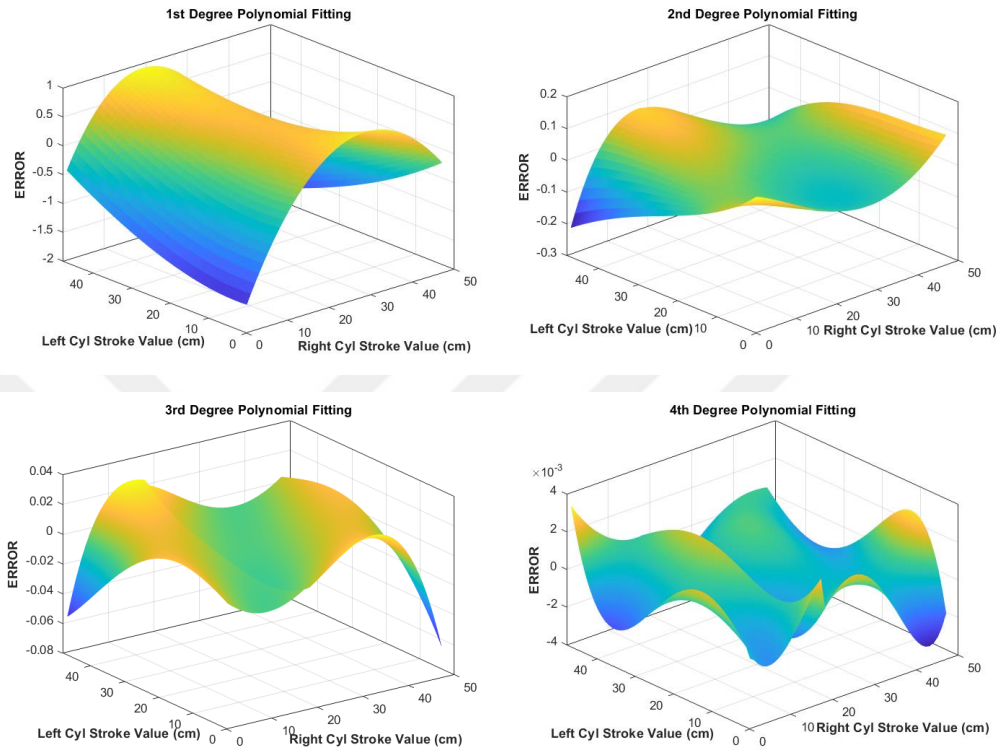
$$f(r_s, l_s) = p_{00} + p_{10} * r_s + p_{01} * l_s + p_{20} * r_s^2 + p_{11} * r_s * l_s + p_{02} * l_s^2 + p_{30} * r_s^3 + p_{21} * r_s^2 * l_s \dots \dots \quad (2.10)$$

For this reason, polynomial fitting processes from the 1st to the 4th degree were applied for the equation whose explanation was given above, and error graphs were obtained.



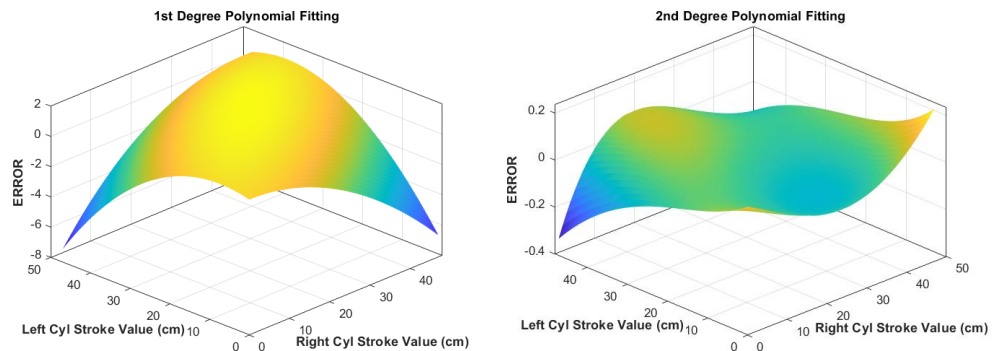
**Figure 2.27:** Error Graphs for Polynomial Fitting in x-axis data for B1 Point, RH

Figure 2.27 shows the polynomial surface fitting error graphs made for the x-axis values of the B1 point. The first and last graphs showed very similar results, but considering the other axis values, the coefficients were preferred over the 4<sup>th</sup>-degree polynomial fitting coefficients.



**Figure 2.28:** Error Graphs for Polynomial Fitting in x-axis data for B4 Point, LH

For the x-axis values on the left side, the 4<sup>th</sup> degree gave the lowest error. Compared to the B1 point, the 1<sup>st</sup>-degree error value was higher but still at acceptable levels. Polynomial coefficients were accepted according to the 4<sup>th</sup>-degree polynomial fitting results.



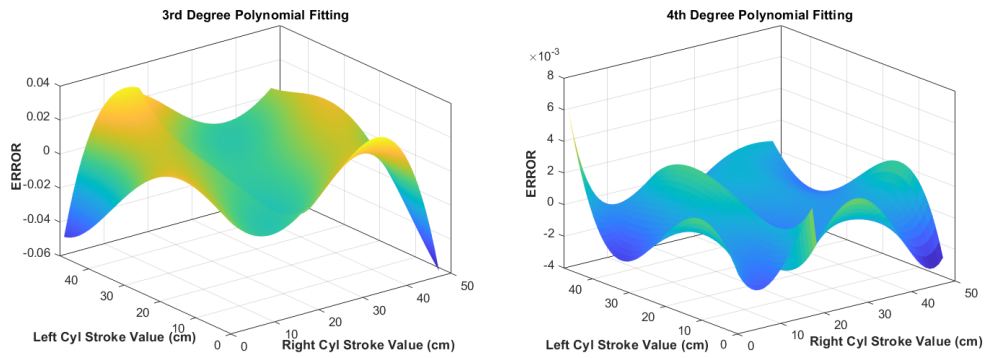


**Figure 2.29:** Error Graphs for Polynomial Fitting in y-axis data for B1 Point, RH

The fitting process shows the values of the B1 and B4 points on the y axis; the 4<sup>th</sup>-degree fitting gives the best result. Therefore, the coefficients are preferred according to this process.

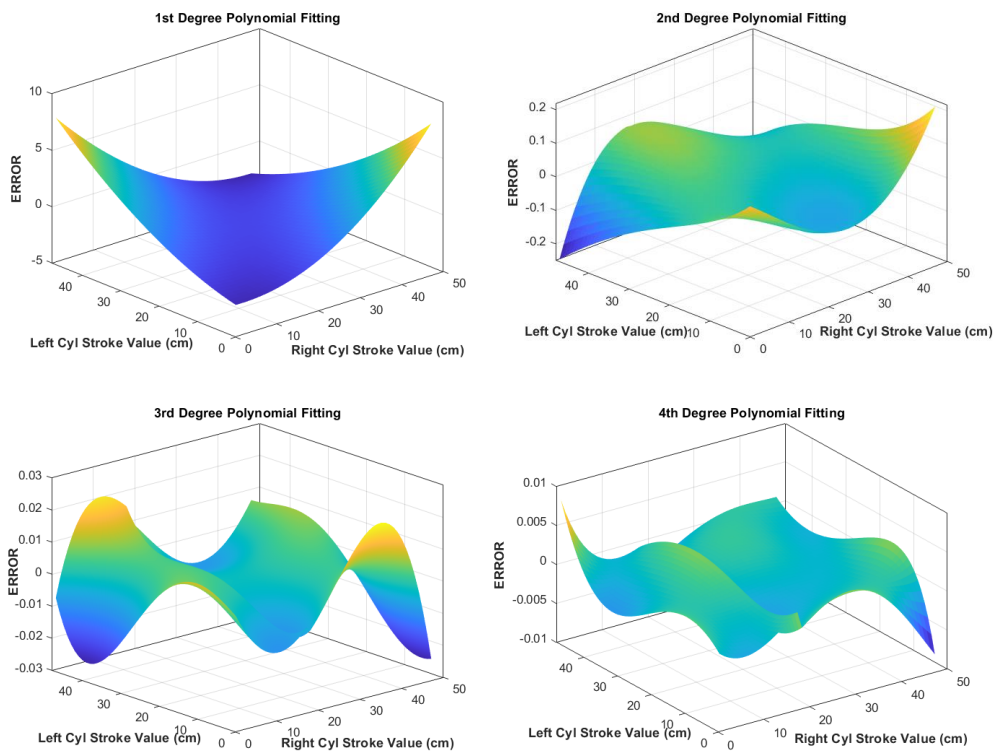


**Figure 2.30:** Error Graphs for Polynomial Fitting in y axis data for B4 Point, LH

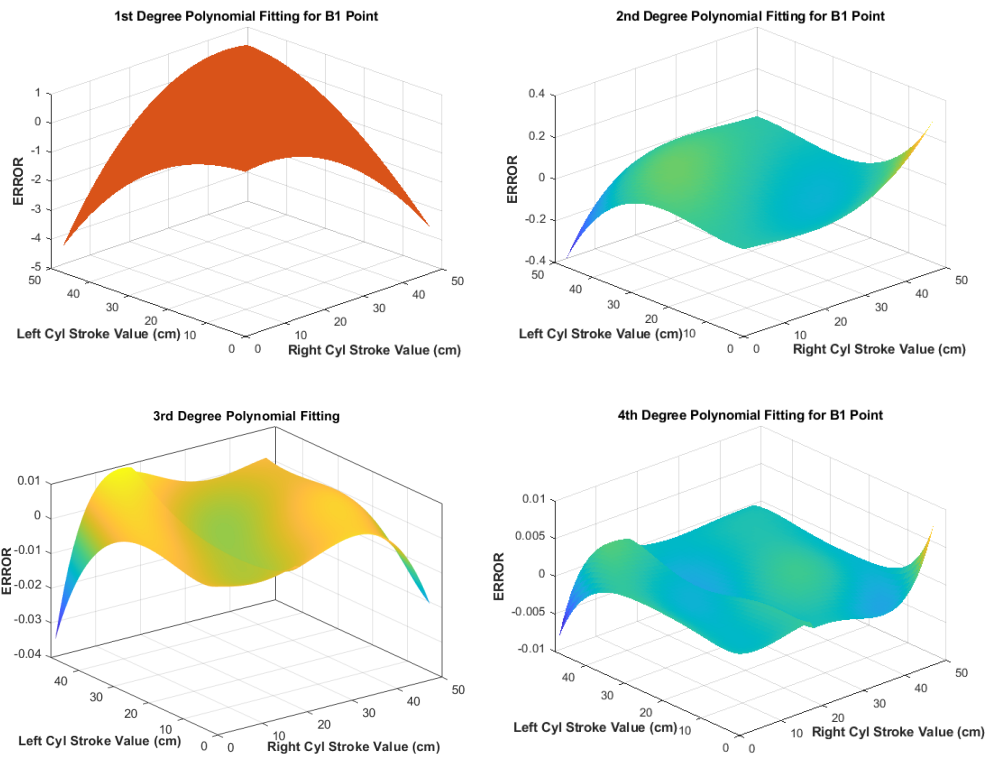


**Figure 2.31:** Error Graphs for Polynomial Fitting in z-axis data for B1 Point, RH

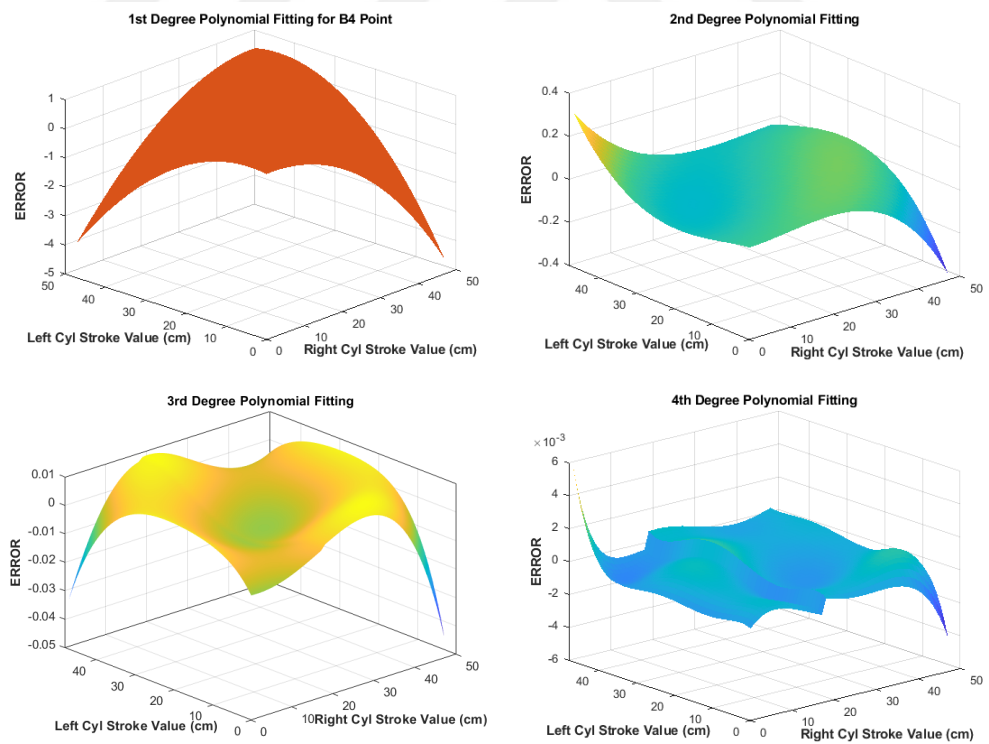


**Figure 2.32:** Error Graphs for Polynomial Fitting in z-axis data for B4 Point, LH

Similar results were obtained for the z axis values as well. The function coefficients for B1 and B4 points are selected according to the 4th-degree polynomial fitting. The coefficients can be seen in Table 2.2.

**Table 2.2.** Polynomial Coefficients.

	x-axis data		y-axis data		z-axis data	
	B1	B4	B1	B4	B1	B4
p00	-268.6129	-268.6134	-185.0204	185.0196	4.09e-04	-0.0026
p10	-0.14267	0.36613	0.7085	0.7085	-1.7400	0.6140
p01	0.38502	-0.1615	-0.7499	-0.7499	0.6600	-1.7900
p20	0.00307	-8.4386	0.0047	-0.0031	0.0015	0.0029
p11	-4.2360e-04	5.1801e-04	-0.0077	0.0087	-0.0039	-0.0043
p02	-0.00105	0.0034	0.0039	-0.0047	0.0028	0.0021
p30	-1.09955e-05	6.4533e-06	1.3328e-05	9.9631e-06	1.23e-05	-1.0826e-05
p21	1.25251e-05	-5.023e-06	-1.3334e-05	-8.2562e-06	-1.71e-05	1.3603e-05
p12	-2.12052e-05	2.49963e-05	3.2537e-05	2.9459e-05	1.70e-05	-1.5087e-05
p03	7.06766e-06	-1.4166e-05	-1.5992e-05	-1.3807e-05	-9.78e-06	8.7925e-06
p40	7.61488e-08	-2.5305e-08	-6.5255e-08	-6.2981e-08	-9.88e-09	5.5665e-08
p31	-9.3167e-08	1.0743e-09	2.9519e-08	8.4625e-08	-3.39e-08	-4.7121e-08
p22	2.1516e-09	1.8002e-07	1.7352e-07	3.0067e-08	7.61e-08	1.4619e-07
p13	6.5710e-08	-2.741e-07	-2.8845e-07	-1.7944e-07	-9.18e-08	-9.6225e-08
p04	-3.874e-08	1.0655e-07	1.2054e-07	8.1139e-08	5.51e-08	9.7931e-09

## CHAPTER III

### HYDRAULIC SYSTEM AND SYSTEM IDENTIFICATION

Automatic levelling control model can be separated as hydraulic model and mechanism. Chapter II mentions the studies carried out for the mechanism analysis. The machine has a hydraulic system consisting of a hydraulic motor, hydraulic valve, and hydraulic cylinders, and the system is controlled with electro-hydraulically. Figure 3.1 shows the hydraulic system schematics.

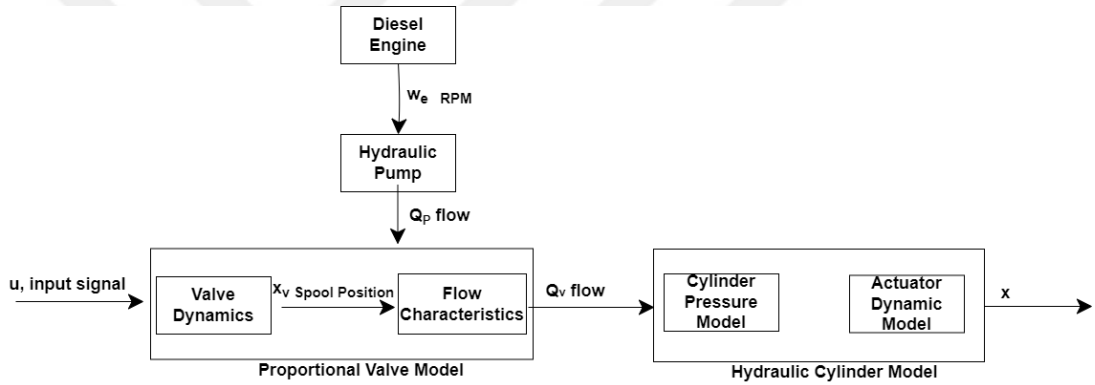


**Figure 3.1:** Schematic of Electro-Hydraulic System

The hydraulic pump is directly connected to the diesel engine. The flow is generated by hydraulic pump using rotation rate of diesel engine. Then, the flow is transferred to the hydraulic system. The flow amount is proportional to the engine's angular velocity and displacement of the pump. General flow equation is in Equation 3.1.

$$Q = \frac{V * n * \eta_{vol}}{1000} \left[ \frac{l}{min} \right] \quad (3.1)$$

Where, Q is volume flow (l/min), V is nominal volume (cm<sup>3</sup>), n is drive speed of the pump (min<sup>-1</sup>) and  $\eta_{vol}$  is the volumetric efficiency.

The hydraulic valve is energized with an analog signal (voltage, current etc.), and the valve spool is activated. The flow is generated by the hydraulic pump. Then, it is transferred to the continuation of the hydraulic system according to the internal structure of the valve. The hydraulic valve can be open or closed centered and the flow paths can be four or more. The amount of flow, and the flow direction is related to the valve characteristics.

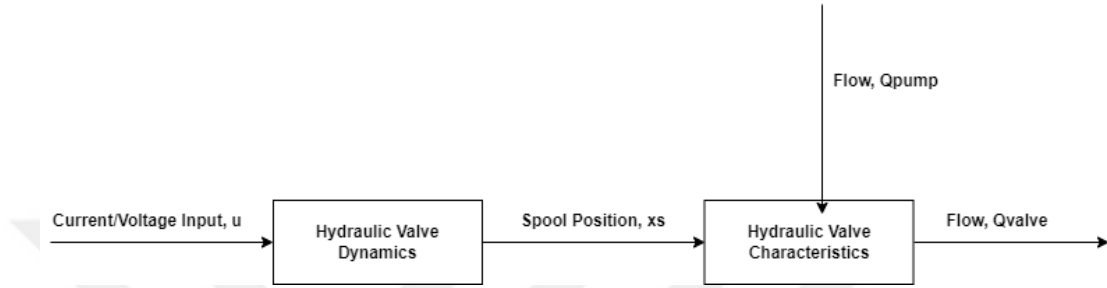


**Figure 3.2:** Representation of Valve Model

$$Q = C_d w x_s \sqrt{\frac{2}{\rho} \Delta p} \quad (3.2)$$

Where,  $C_d$  is discharge coefficient,  $w$  is peripheral width of the orifice,  $x_s$  is the spool position,  $\Delta p$  is pressure difference between input and output of the orifice and  $\rho$  is the hydraulic fluid density.

The extraction and retraction of the hydraulic cylinder occur with the pressure created by the hydraulic fluid filling its chambers. The flow equations can be written as in Equations 3.3 and 3.4.

$$Q_1 = A_1 * \dot{x}_{stroke} + \frac{V_1}{\beta} * \frac{dp_1}{dt} \quad (3.3)$$

$$Q_2 = A_2 * \dot{x}_{stroke} - \frac{V_2}{\beta} * \frac{dp_2}{dt} \quad (3.4)$$

Where,  $Q_1$  is the pump flow,  $Q_2$  is the return flow,  $V_1$  is the volume of the side 1 of the cylinder and  $V_2$  is the side 2 volume.  $A_1$ , and  $A_2$  area of the side 1 and side 2, respectively.  $\dot{x}_{stroke}$  is the cylinder velocity.  $\beta$ , is the bulk modulus of the hydraulic fluid and  $p_1$  and  $p_2$  are the chamber pressures.

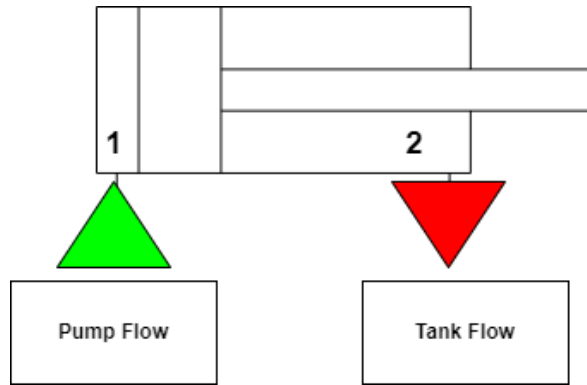


**Figure 3.3:** Representation of Hydraulic Cylinder

Orifice equations, cylinder volume, pressure equations, and hydraulic pump flow equations can be written to express the system dynamically. However, obtaining these equations can be challenging when there are many unknowns, such as the diameter and length of the valve spool, hydraulic pump displacements, leakages, etc. [4]. The hydraulic pump can produce enough flow to fulfill the machine's functions. The electrohydraulic valve block also provides the flow produced by the pump to the hydraulic group. PWM energizes electrohydraulic valve. As a result, depending on the extraction and retraction of the cylinder, the valve spool moves in the +/- direction and the flow passes.

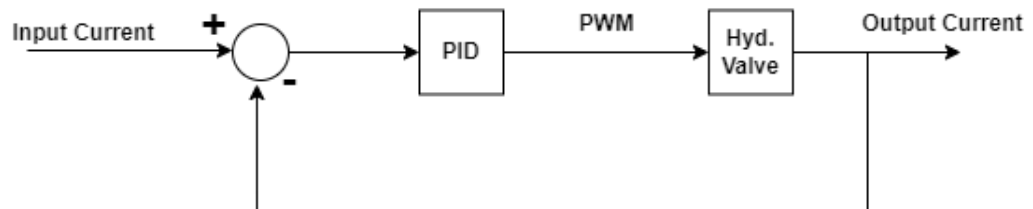


**Figure 3.4:** Electro-Hydraulic Valve Working Principle

In the existing system, an analog signal is generated with the movement of the joystick on the X/Y axis. The generated signal is proportional to the axis position. The joystick value is 0 in the neutral state. It takes values from 0-100 in the positive or negative direction on the axes. This range can be expressed in % (this value will be referred to as Joystick Value - JV). The joystick value corresponds to a current value according to the valve characteristics. The generated current is converted to PWM with the PID controller and the electro-hydraulic valve spool is activated. The larger the current, the larger the PWM and the spool more open. This means that the flow



generated by the pump fills the cylinders more quickly. That is, the cylinder movements accelerate. Figure 3.4 shows the working principle of the system.

A test setup can be prepared to find the cylinder motion characteristic. Draw-wire encoders are mounted on the real mechanism. These sensors are used to measure the cylinder stroke. 'Desired Stroke Value' is given to the system as an input, and the stroke value read from the sensor becomes the 'Actual Stroke Value' as an output.

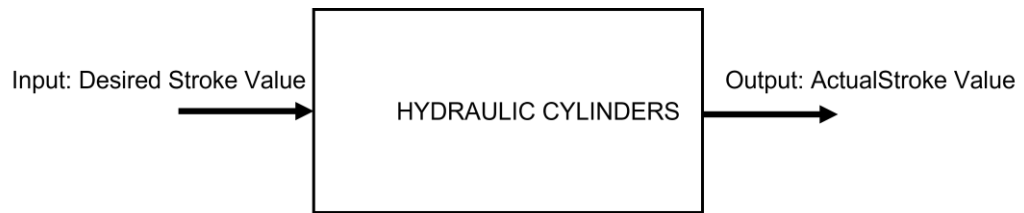


**Figure 3.5:** Test Setup

In the notation given in Figure 3.5 the 'Desired Stroke Value' and the 'Actual Stroke Value' read from the draw wire encoders are constantly compared. PWM continues to be produced until the two values are equal. The propositions are as follows.

Desired Stroke Value-Actual Stroke Value>0, Up Direction

Desired Stroke Value-Actual Stroke Value<0, Down Direction

Desired Stroke Value-Actual Stroke Value=0, No Movement



**Figure 3.6:** Siko Draw-Wire Encoder

Draw-wire encoders consist of the wire and encoder mechanism. The wire is attached to the piston when the cylinder is fully closed. Then, when the cylinder starts to open, each turn of the wire mechanism represents a length value. Draw-wire encoders can be easily mounted without drilling the cylinder piston, so they are very

easy to use. The sensors must withstand high pressure and temperature because they work in hydraulic oil. The illustration of the draw-wire sensor mounted in a hydraulic cylinder can be seen in Figure 3.7.



**Figure 3.7:** Draw-Wire Encoder Representation Mounted in Cylinder

In this thesis, the Siko Draw-Wire Encoder SGH25 [20] was mounted on the right and left lift cylinders. The measuring range of the encoder is 0 to 2500 mm. It has pressure resistance up to 450 bar. The sensor has 4-20 mA analog/current output. It has a 12-bit resolution.



**Figure 3.8:** Sensor Mounted on Cylinder

Using the input/output relationship of various experiments to be performed on the real mechanism (See Figure 3.5), the system's transfer function can be obtained using system identification techniques.

System identification is the mathematical expression of a dynamic system using the input/output relationship. System identification consists of 3 steps.

- ✓ Input/output measurements of the dynamic system (time or frequency domain)
- ✓ Choosing the appropriate structural model
- ✓ Obtaining appropriate coefficients for the structural model using input/output data [28].

A series of tests were performed on the machine for input/output measurements. Desired Stroke Value was entered into the system as input  $u(t)$  and output values defined as Actual Stroke  $y(t)$  were recorded with measurements from the encoders. During the test, three different joystick values were recorded. These values represent slow, medium and fast states. The machine runs in Parking Mode and at 800 RPM engine speed during recordings. Measurements were recorded at 100 ms (10 Hz) intervals. Records were taken separately for the right and left lifting cylinders.

$$u(t) = [u(Ts), u(2Ts), \dots, u(NTs)] \quad (3.5)$$

$$y(t) = [y(Ts), y(2Ts), \dots, y(NTs)] \quad (3.6)$$

$$Ts = 0.1 \text{ sec} \quad (3.7)$$

Structural models for the estimation can be transfer functions, state space equations, and pole-zero gain models. In this study, the estimation model was chosen as the transfer function.

$$G(s) = \frac{y(s)}{u(s)} \quad (3.8)$$

Then, transfer functions are obtained by using the interior point method. Matlab System Identification Toolbox was used for to obtain the function coefficients. When the measurement graphics were examined, it was seen that there was a delay between the input/output.

### 3.1. Slow (20% Joystick Value)

First, up and down movement records were taken for the 20% joystick value.

### 3.1.1. Down Direction

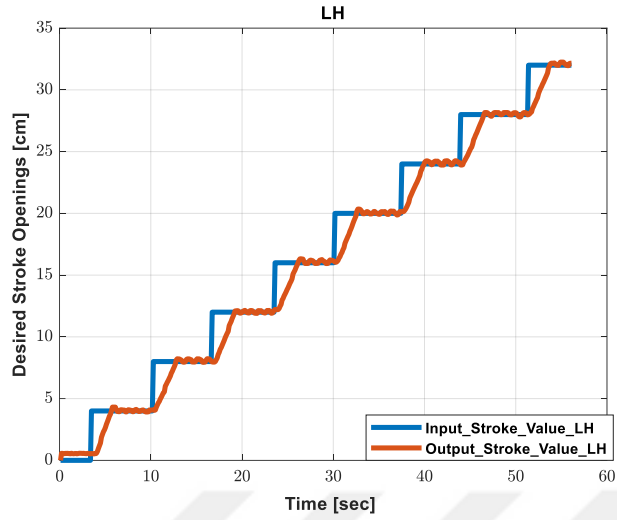


**Figure 3.9:** Down Direction for Left Lifting Cylinder, Joystick Value 20 %

$$TFLH = e^{-0.214s} \frac{0.1453s + 1.5471}{s^2 + 1.7544s + 1.5467} \quad (3.9)$$

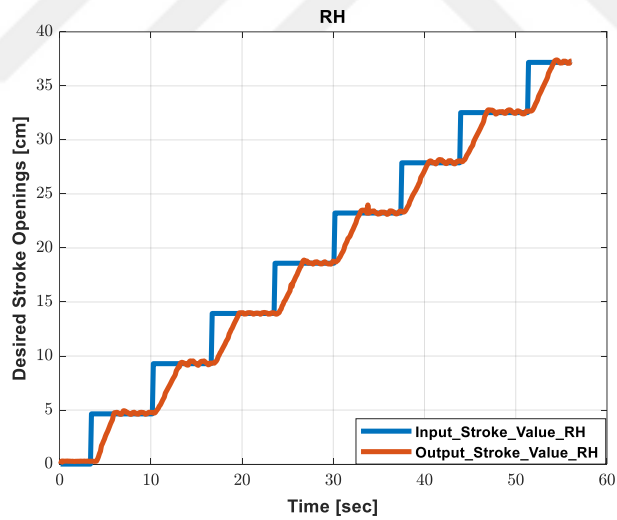


**Figure 3.10:** Down Direction for Right Lifting Cylinder, Joystick Value 20 %

$$TFRH = e^{-0.428s} \frac{0.3036s + 1.2182}{s^2 + 1.6008s + 1.2182} \quad (3.10)$$

### 3.1.2. Upper Direction

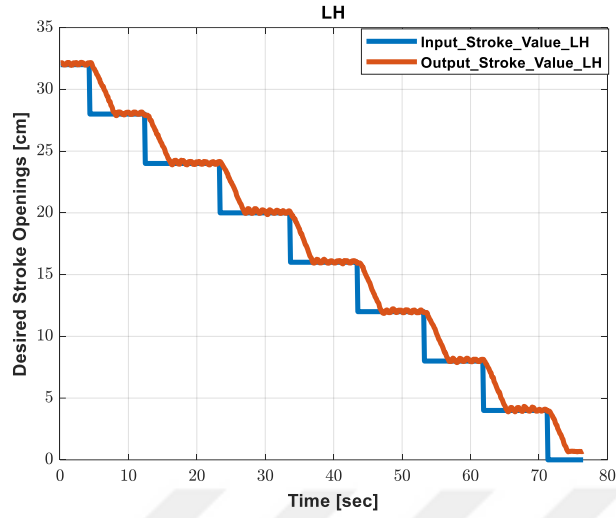


**Figure 3.11:** Up Direction for Left Lifting Cylinder, Joystick Value 20 %

$$TFLH = e^{-0.226s} \frac{0.5920s + 0.0582}{s^2 + 0.6698s + 0.0571} \quad (3.11)$$

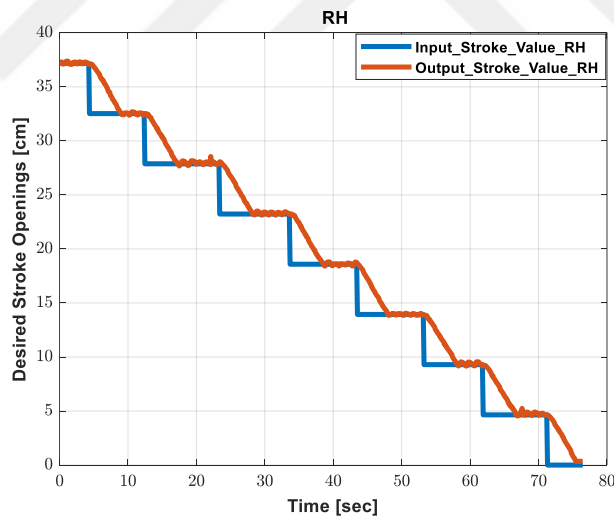


**Figure 3.12:** Up Direction for Right Lifting Cylinder, Joystick Value 20 %

$$TFRH = e^{-0.339s} \frac{0.3301s^2 - 0.4684s + 0.8756}{s^2 + 1.9911s + 0.8749} \quad (3.12)$$

### 3.2. Intermediate (50% Joystick Value)

Secondly, records were taken for 50% joystick value.

### 3.2.1. Down Direction

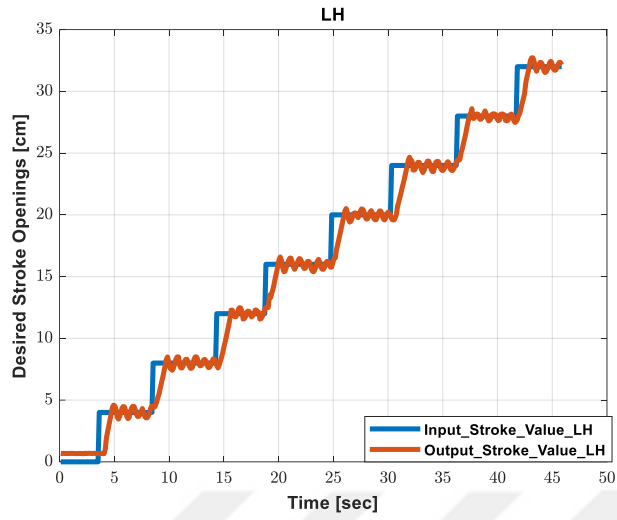


**Figure 3.13:** Down Direction for Left Lifting Cylinder, Joystick Value 50 %

$$TFLH = e^{-0.448s} \frac{2.9405s + 0.0081}{s^2 + 3.0894s + 2.6888e - 07} \quad (3.13)$$

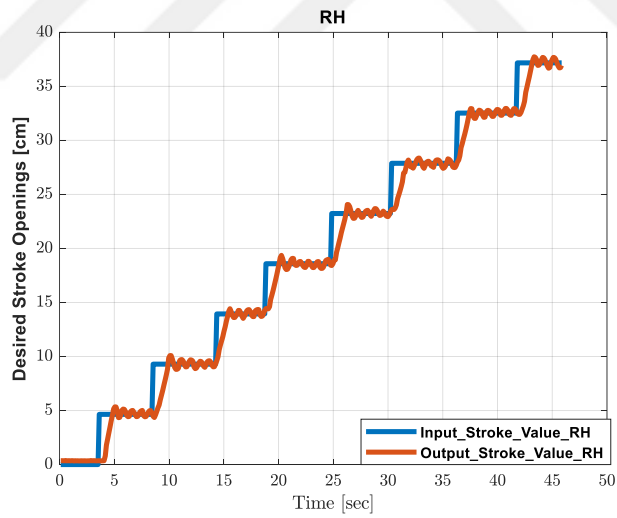


**Figure 3.14:** Down Direction for Right Lifting Cylinder, Joystick Value 50 %

$$TFRH = e^{-0.224s} \frac{0.4206s + 6.7877}{s^2 + 3.7987s + 6.7865} \quad (3.14)$$

### 3.2.2. Upper Direction

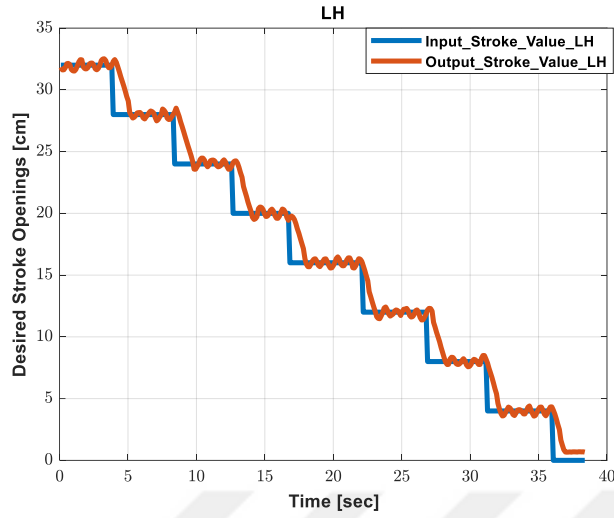


**Figure 3.15:** Up Direction for Left Lifting Cylinder, Joystick Value 50 %

$$TFLH = e^{-0.107s} \frac{0.5847s^2 + 6.2425s + 3.4954}{s^3 + 4.3231s^2 + 7.1579s + 3.4927} \quad (3.15)$$

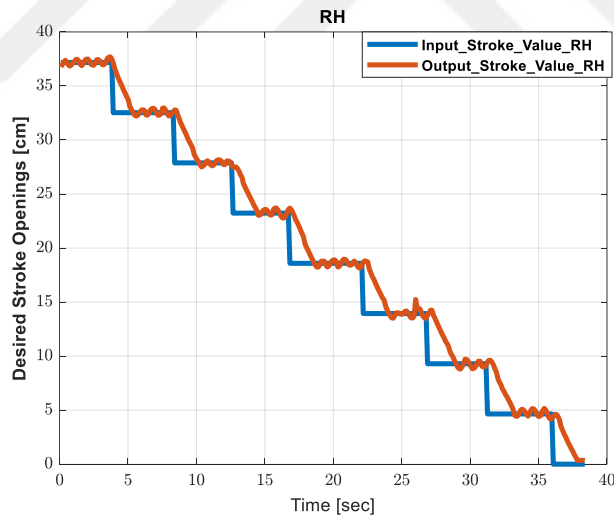


**Figure 3.16:** Up Direction for Right Lifting Cylinder, Joystick Value 50 %

$$TFRH = e^{-0.107s} \frac{3.7556s^2 + 8.1285s + 0.9952}{s^3 + 6.4634s^2 + 9.5547s + 1.0245} \quad (3.16)$$

### 3.3. Fast (80 % Joystick Value)

Finally, 80 % joystick values were recorded.

### 3.3.1. Down Direction

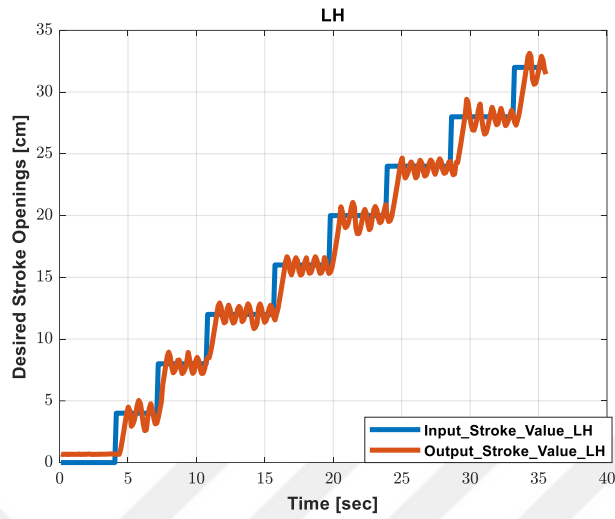


**Figure 3.17:** Down Direction for Left Lifting Cylinder, Joystick Value 80 %

$$TFLH = e^{-0.33s} \frac{3.3075s + 30.4757}{s^2 + 8.1376s + 30.7286} \quad (3.17)$$

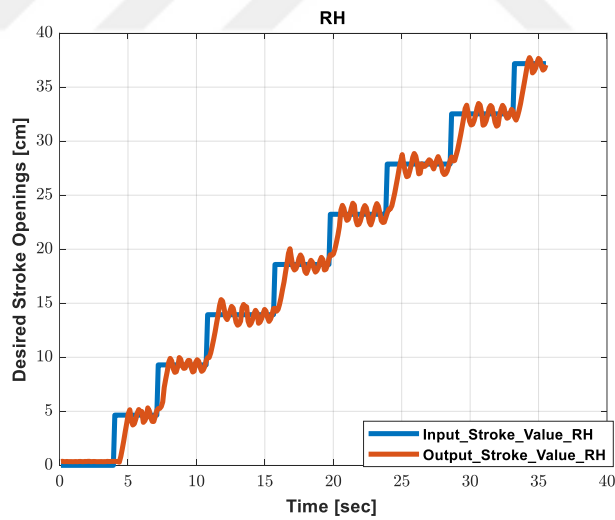


**Figure 3.18:** Down Direction for Right Lifting Cylinder, Joystick Value 80 %

$$TFRH = e^{-0.22s} \frac{2.8559s + 0.5924}{s^2 + 2.9175s + 0.6003} \quad (3.18)$$



### 3.3.2. Upper Direction

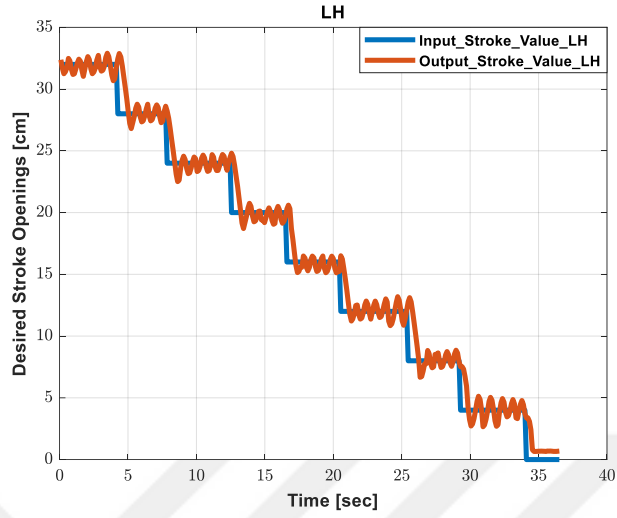


**Figure 3.19:** Up Direction for Left Lifting Cylinder, Joystick Value 80 %

$$TFLH = e^{-0.109s} \frac{3.2118s^2 + 30.5728s + 4.8761}{s^3 + 21.0958s^2 + 31.3992s + 4.9164} \quad (3.19)$$

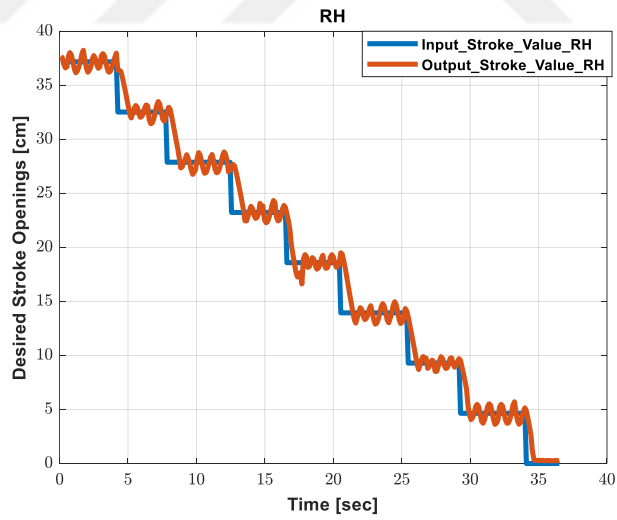


**Figure 3.20:** Up Direction for Right Lifting Cylinder, Joystick Value 80 %

$$TFRH = e^{-0.218s} \frac{0.4865s^2 + 4.0128s + 0.6463}{s^2 + 4.0948s + 0.6424} \quad (3.20)$$

While the highest joystick value is 100 %, the records were taken at 80 % because of the sudden vibrations that occur in the machine due to the retraction and

extraction of hydraulic cylinder that occur while trying to equalize the input/output values, as mentioned in the propositions. These vibrations shake the machine very much and endanger safe operation during the test.

It has been observed that there is a delay between input/output in the transfer functions obtained from Figure 3.9 to 3.20. Delay may occur due to electronic or hydraulic reasons. PWM/Current records taken during the tests can be examined to understand whether electronic reasons cause the delay or not. Because in reality, as mentioned in Figure 3.4, the joystick value corresponds to a current, and the current is converted to PWM value with PID controller. For this reason, Joystick value, PWM and, Current graphs were drawn in Figures 3.21 to 3.26 and compared.

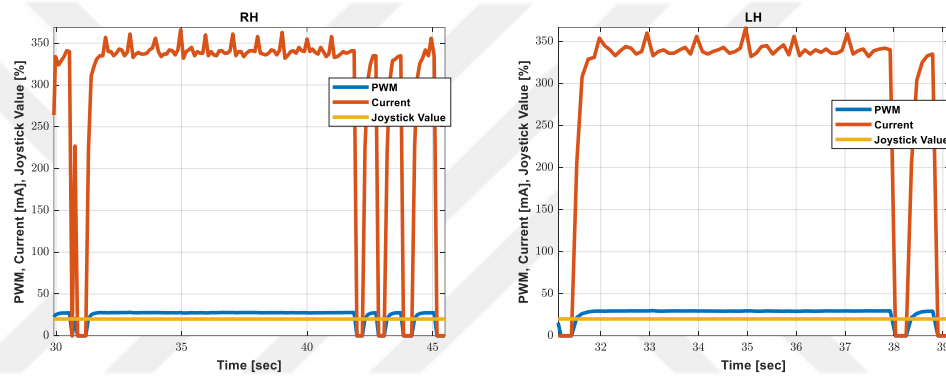


**Figure 3.21:** Up Direction, 20% Joystick Value/PWM/Current Start Time Comparison RH and LH

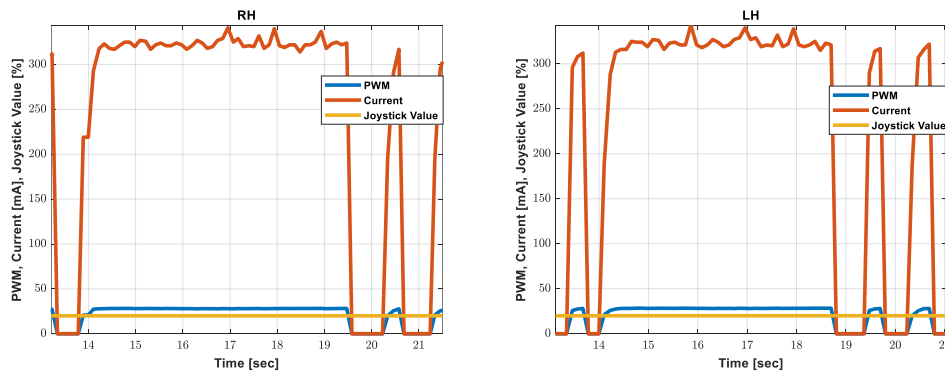


**Figure 3.22:** Down Direction, 20% Joystick Value/PWM/Current Start Time Comparison RH and LH

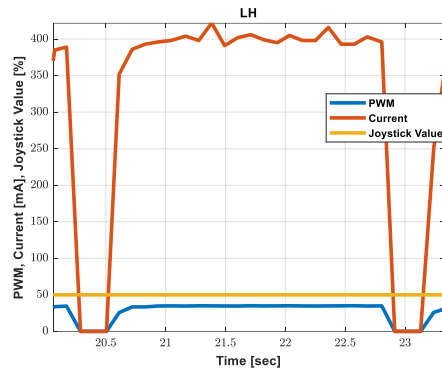
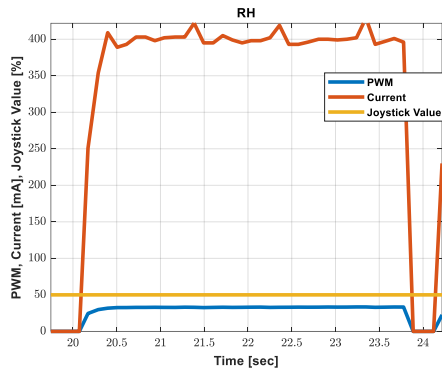


**Figure 3.23:** Up Direction, 50% Joystick Value/PWM/Current Start Time Comparison RH and LH

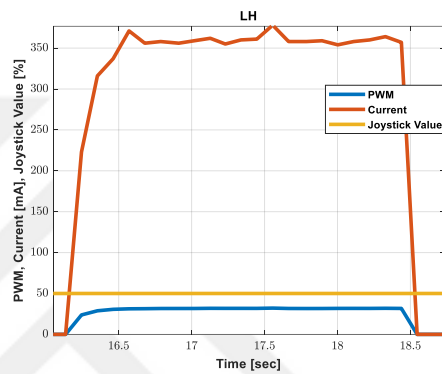
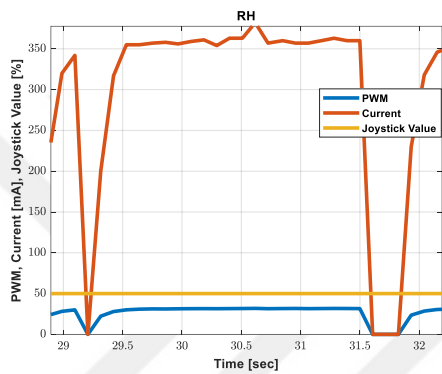


**Figure 3.24:** Down Direction, 50% Joystick Value/PWM/Current Start Time Comparison RH and LH

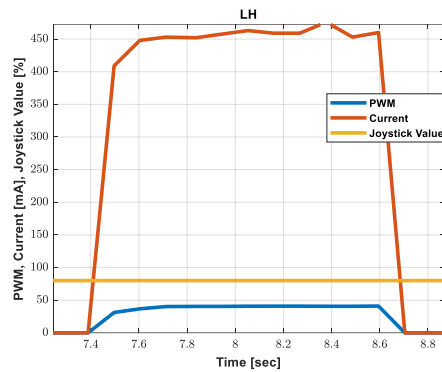
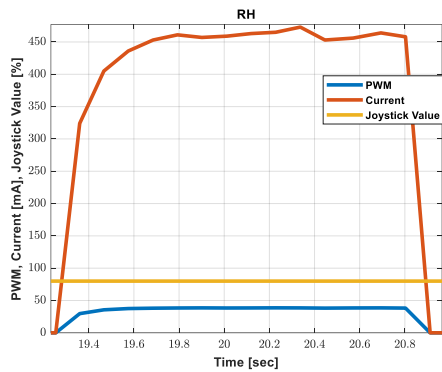


**Figure 3.25:** Up Direction, 80% Joystick Value/PWM/Current Start Time Comparison RH and LH

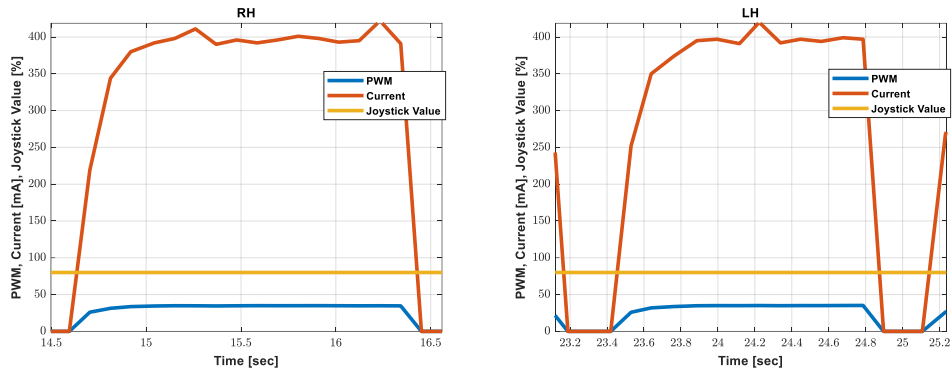


**Figure 3.26:** Down Direction, 80% Joystick Value/PWM/Current Start Time Comparison RH and LH

Figures 3.27 to 3.32 can be examined to understand whether the delay is due to hydraulic reasons. In graphs, a stroke value is given to the system then the new stroke value is given, enabling the cylinder to move in the opposite direction during its movement.

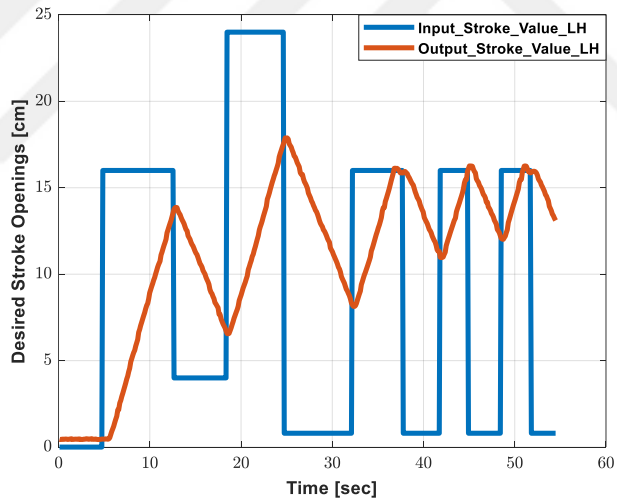


**Figure 3.27:** Up and Down Directions, 20% Joystick Value, LH

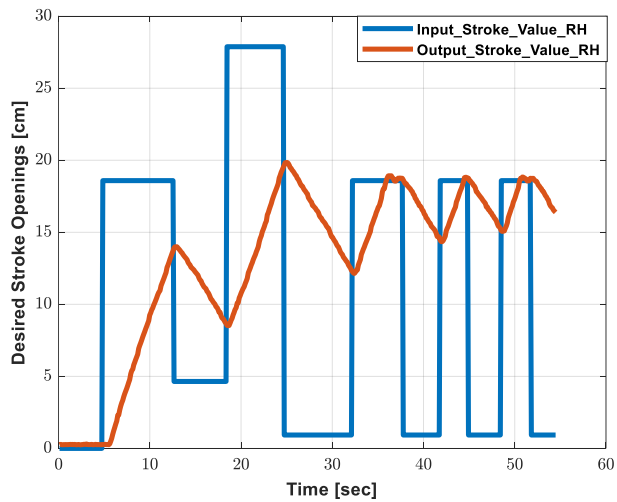


**Figure 3.28:** Up and Down Directions, 20% Joystick Value, RH

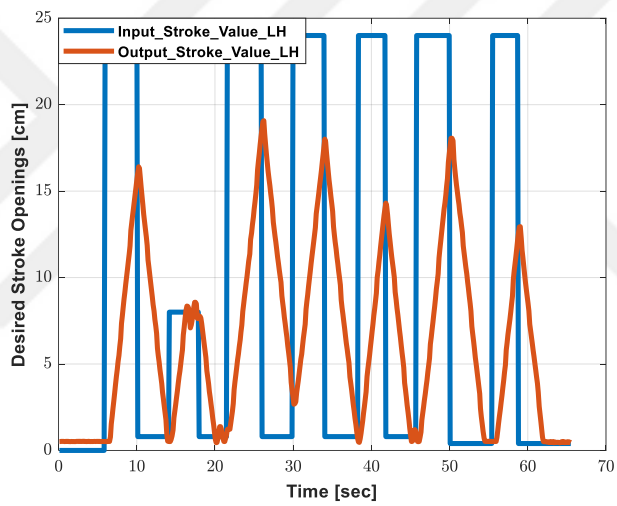


**Figure 3.29:** Up and Down Directions, 50% Joystick Value, LH

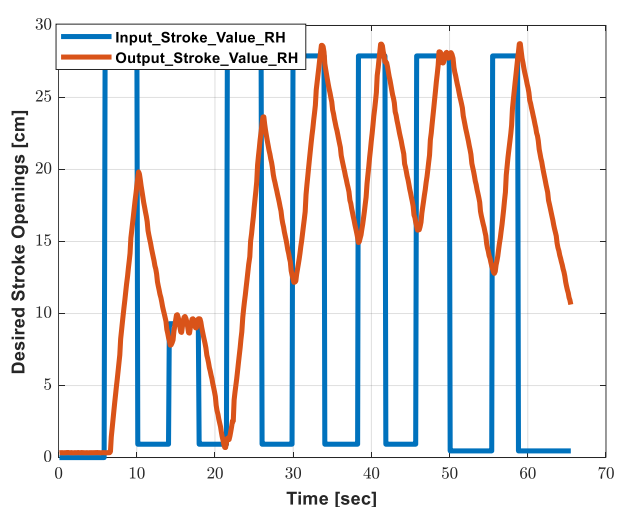


**Figure 3.30:** Up and Down Directions, 50% Joystick Value, RH

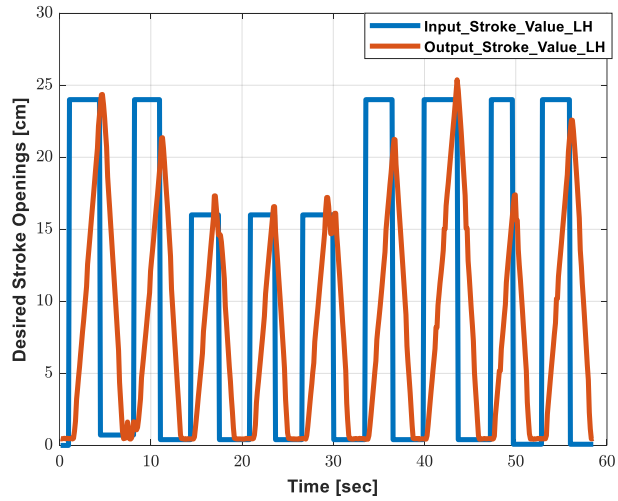


**Figure 3.31:** Up and Down Directions, 80% Joystick Value, LH

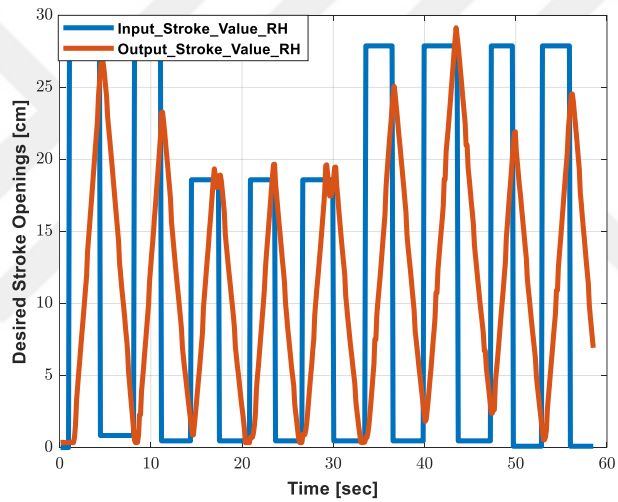


**Figure 3.32:** Up and Down Directions, 80% Joystick Value, RH

The graphs from Figure 3.27 to 3.29 show that the reason for the delay is hydraulically. In cases where the cylinder movement direction changes, it takes time for the current to increase for that direction. Therefore, the valve spool opens slowly and takes time for the hydraulic oil to fill or drain from the cylinders.

Since the behaviors are similar for each joystick value, Figures 3.33 and 3.35 are plotted for 50% Joystick Value. Figures 3.34 and 3.36 are zoomed-in versions of Figures 3.33 and 3.35 to observe the behavior.

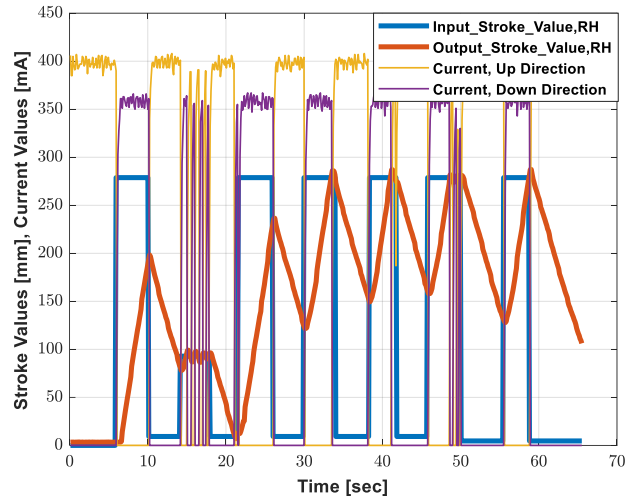


**Figure 3.33:** Up and Down Direction vs Current Graph, 50% Joystick Value, RH

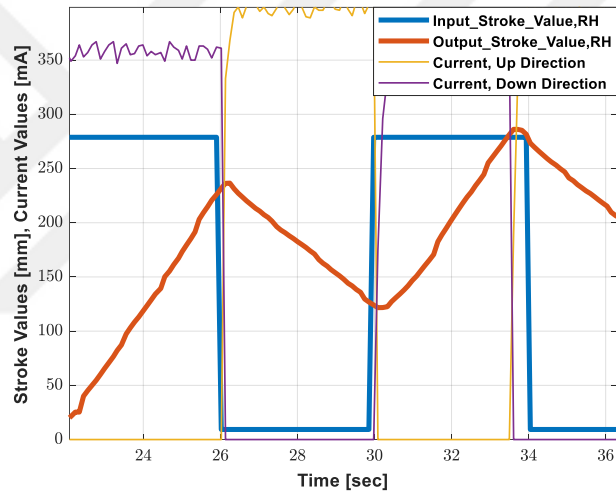


**Figure 3.34:** Closer look to Figure 3.32

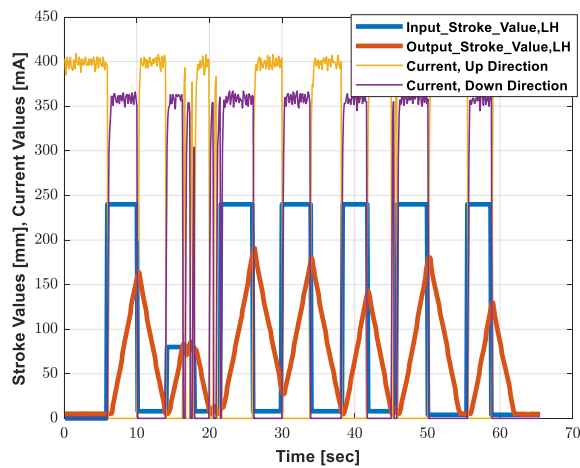


**Figure 3.35:** Up and Down Direction vs Current Graph, 50% Joystick Value, LH

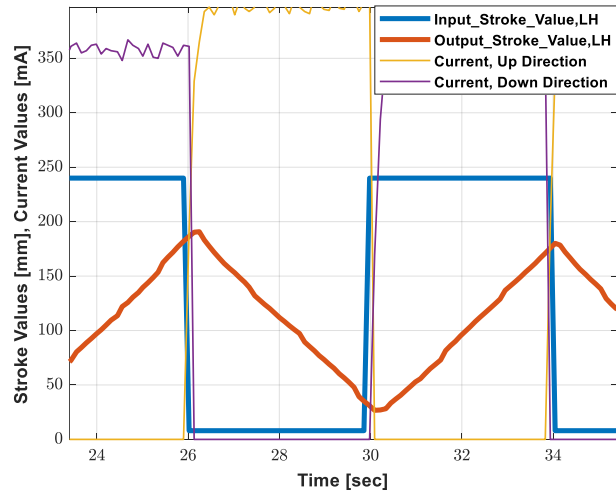


**Figure 3.36:** Close look to Figure 3.34



## CHAPTER IV

### CONTROLLER DESIGN

In Chapter III, it has been observed that the system behaviors are quite similar for three different Joystick Values. The pole-zero graphs can be used to compare the transfer functions so the mentioned similarities can become more pronounced. The poles of the transfer functions are obtained for the downward and upward movements in Figures 4.1 and 4.2, respectively.

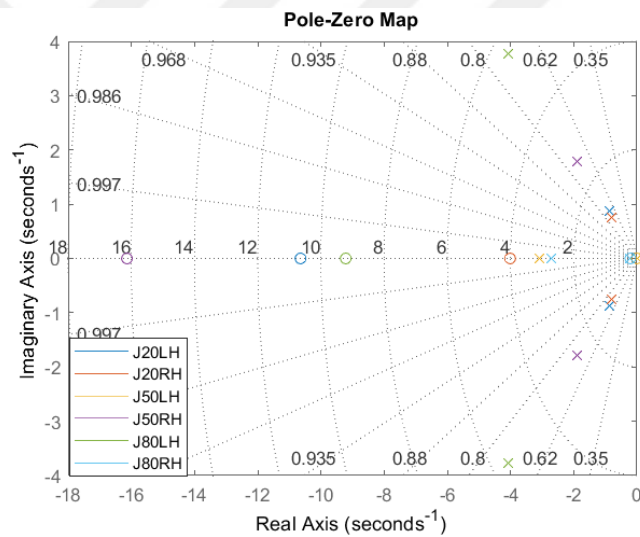


**Figure 4.1:** Pole-Zero Map for Down Direction

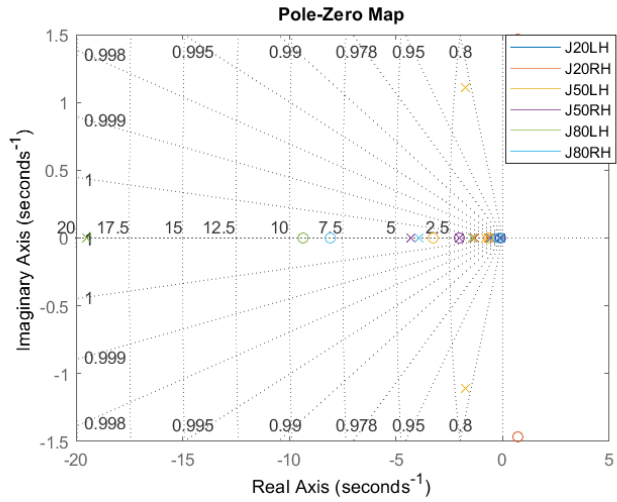


**Figure 4.2:** Pole-Zero Map for Up Direction

Then, 50 % Joystick Value was chosen to create a Matlab Simulink model. The controller to be designed will then be tested in other transfer functions, and the system behaviors will be examined. Even with a single joystick value, four different transfer functions have been obtained.

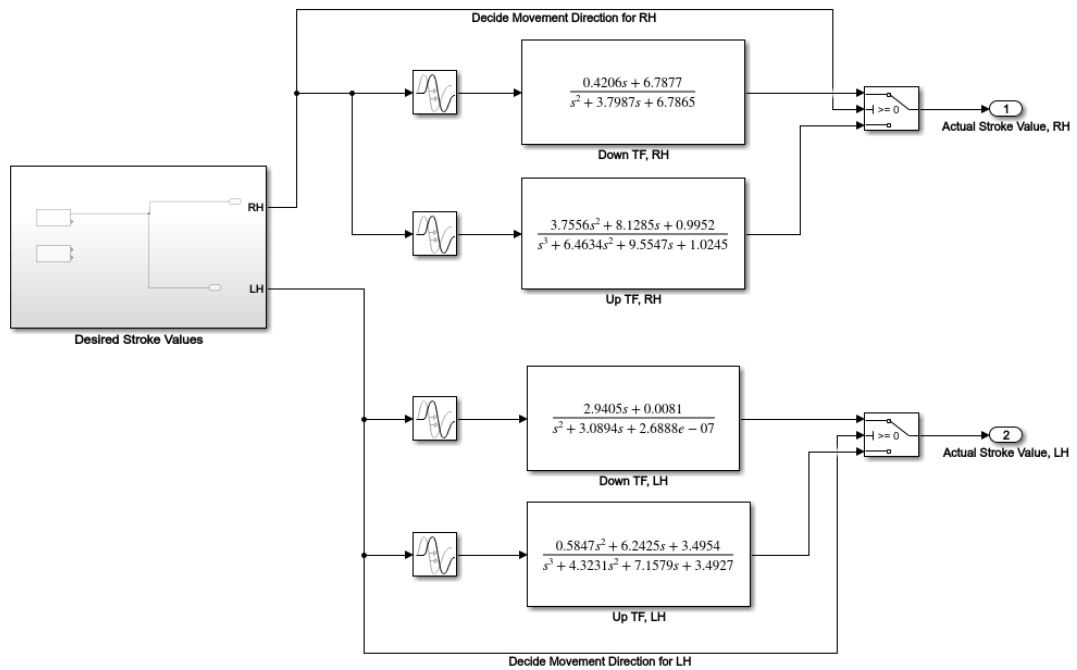


**Figure 4.3:** Matlab Simulink Model for 50 % Joystick Value's Transfer Functions

Matlab Simulink model represents that if the Desired Stroke Value is greater than zero, the movement is in the down direction; if it is smaller than zero, the

movement is in the upward direction. The down direction represents the extraction, and the latter refers to the retraction of the cylinder.

Figures 4.4 and 4.5 show the behavior of the right and left liftings, respectively. The given step input is 30 centimeters in the down direction for both cylinders, and the simulation sample time is taken as fixed-step 1e-2.

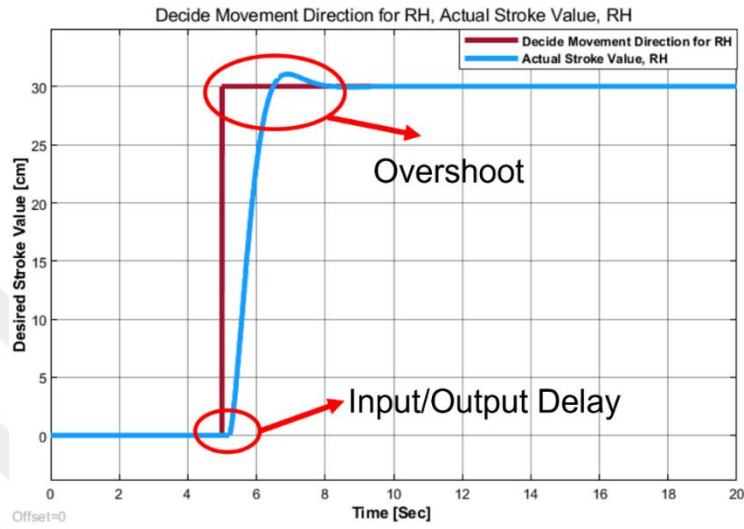


**Figure 4.4:** Matlab Simulink Model for 50 % Joystick Value's Transfer Functions

$$TFRH = e^{-0.224s} \frac{0.4206s + 6.7877}{s^2 + 3.7987s + 6.7865} \quad (4.1)$$

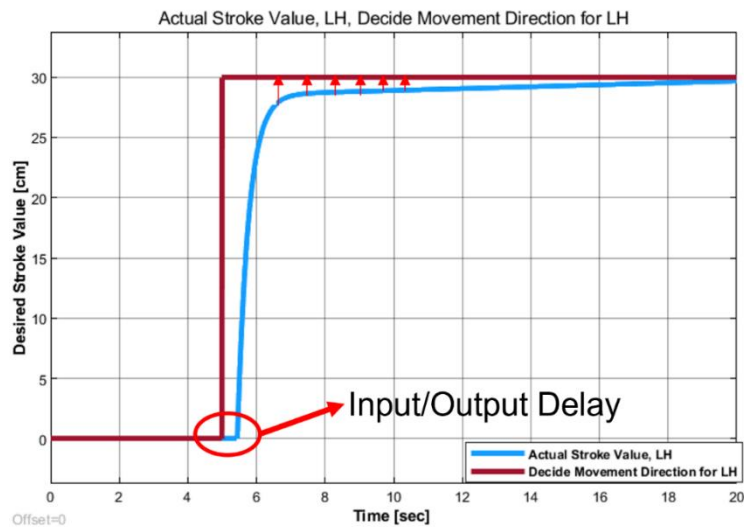


**Figure 4.5:** Matlab Simulink Model for 50 % Joystick Value's Transfer Functions

$$TFLH = e^{-0.448s} \frac{2.9405s + 0.0081}{s^2 + 3.0894s + 2.6888e - 07} \quad (4.2)$$

In Figure 4.4, the stroke value reaches the Desired Stroke Value in 8 seconds, but initially, it overshoots. Figure 4.5 takes more than 20 seconds for the stroke value to reach the Desired Value.

In time-delayed systems, the exponential transfer function can be expressed rationally by using the pade approximation. In order to express the above-mentioned time-delayed transfer functions without time-delay, the ‘pade’ command can be used in Matlab. For example, eqn. 4.1 can be expressed as eqn. 4.3 and eqn 4.2 can be expressed as eqn. 4.4 using 1st order pade approximation.

$$TFLH_{pade} = \frac{-0.4206s^2 - 3.032s + 60.6}{s^3 + 12.73s^2 + 40.7s + 60.59} \quad (4.3)$$

$$TFLH_{pade} = \frac{-2.941s^2 + 13.12s + 0.03616}{s^3 + 7.554s^2 + 13.79s + 1.2e - 06} \quad (4.4)$$

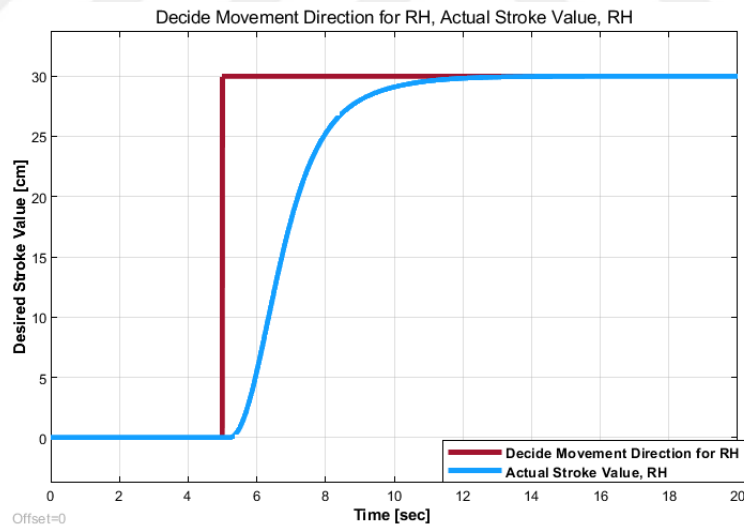


**Figure 4.6:** Down Direction, 50 % Joystick Value RH with PI Controller

$$P_{RH}=0.05 \quad (4.3)$$

$$P_{LH}=0.001 \quad (4.4)$$

$$I = \frac{0.05}{s} \quad (4.5)$$

Then, the applied PI controller was tested with the same joystick value at the -30 cm desired stroke input, and Figures 4.7 and 4.8 were obtained.

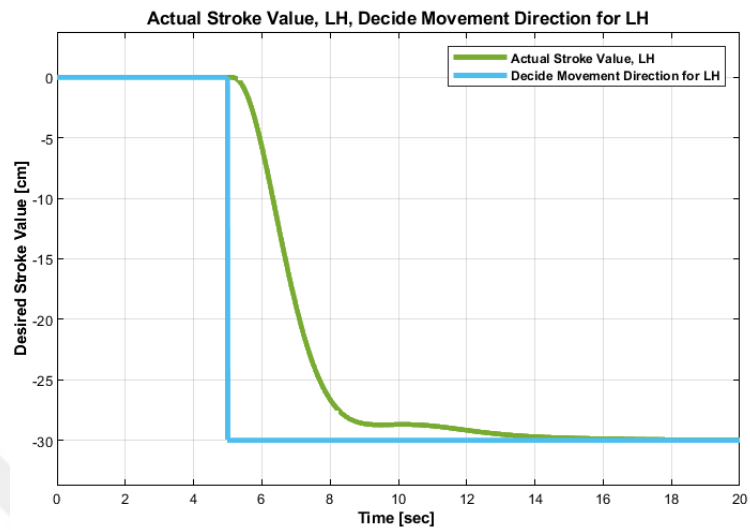


**Figure 4.7:** Up Direction, 50 % Joystick Value LH with PI Controller

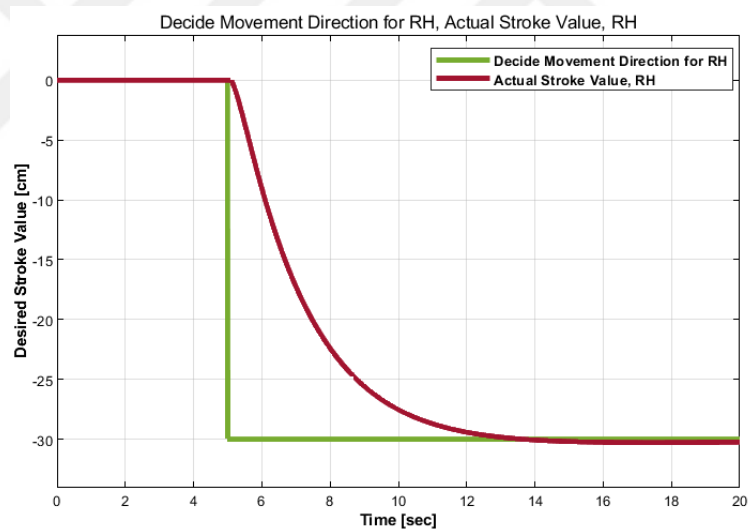


**Figure 4.8:** Up Direction, 50 % Joystick Value RH with PI Controller

The PI controller designed for the model created in Figure 4.3 gives suitable outputs for the 50 % joystick value both in the up and down movement. However, it is necessary to see the reaction of these PI coefficients for other transfer functions.

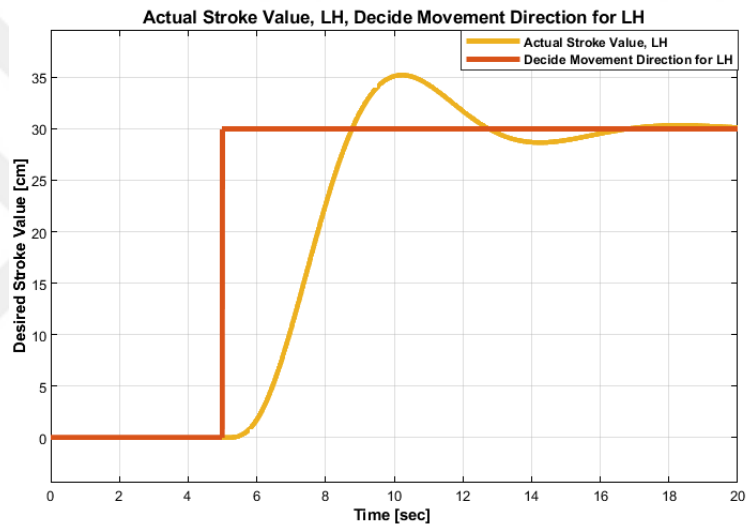
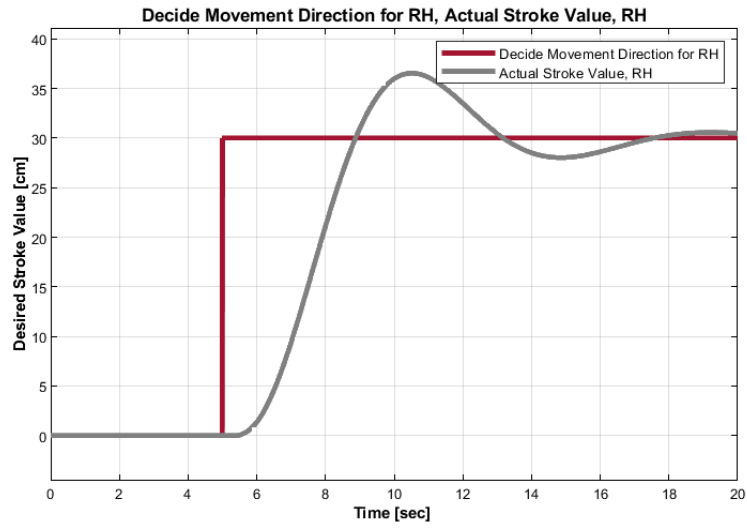


**Figure 4.9:** Down Direction, 20 % Joystick Value with PI Controller RH and LH

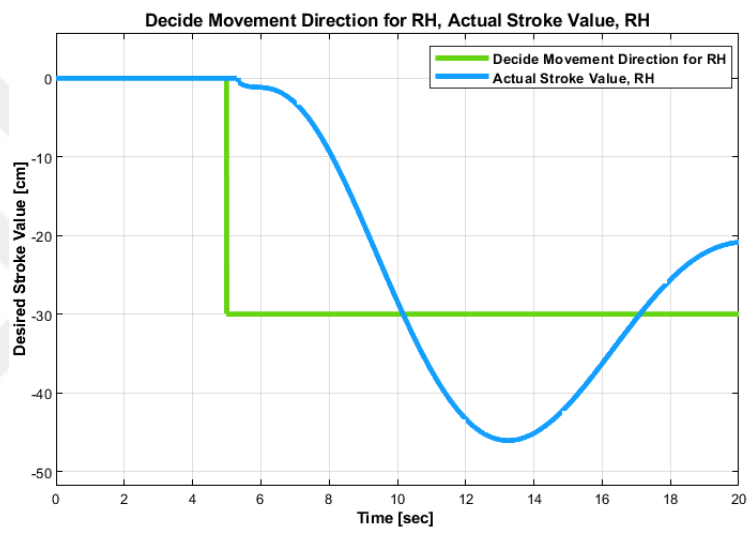
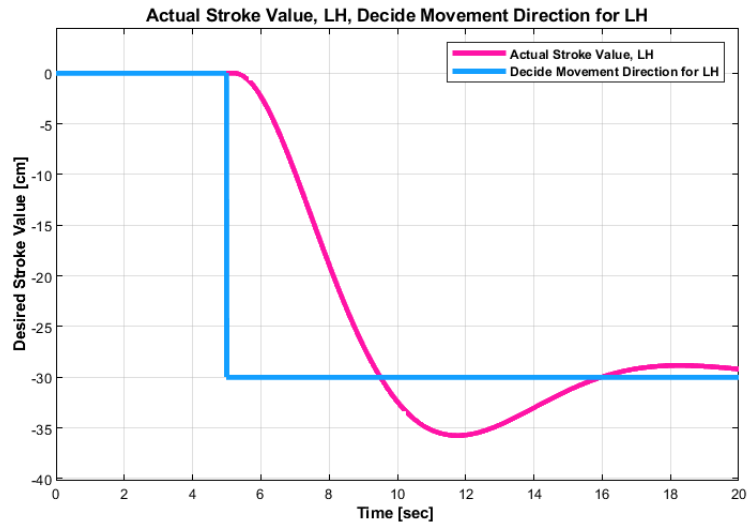


**Figure 4.10:** Up Direction, 20 % Joystick Value with PI Controller RH and LH

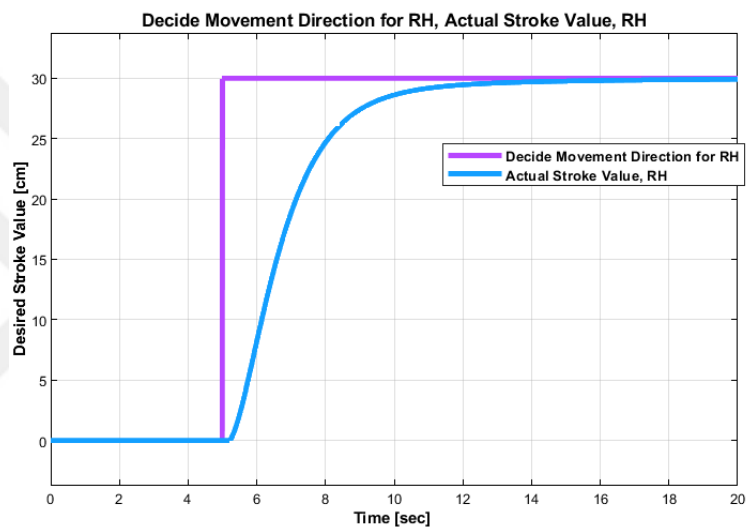
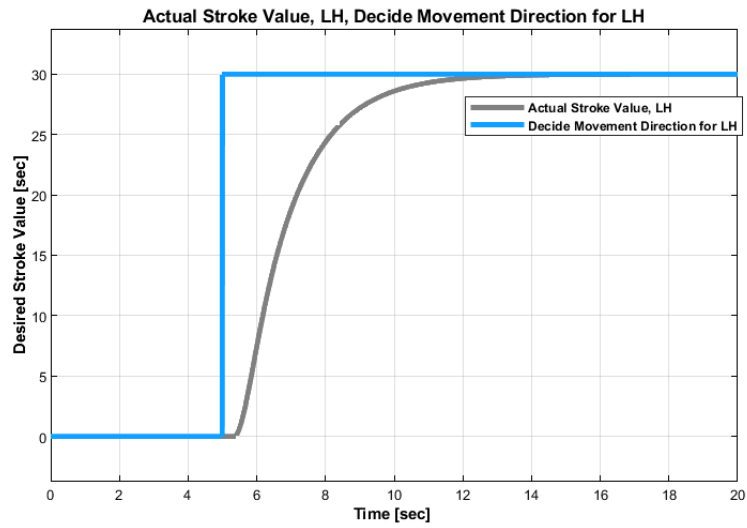


**Figure 4.11: Down Direction, 80 % Joystick Value with PI Controller RH and LH**



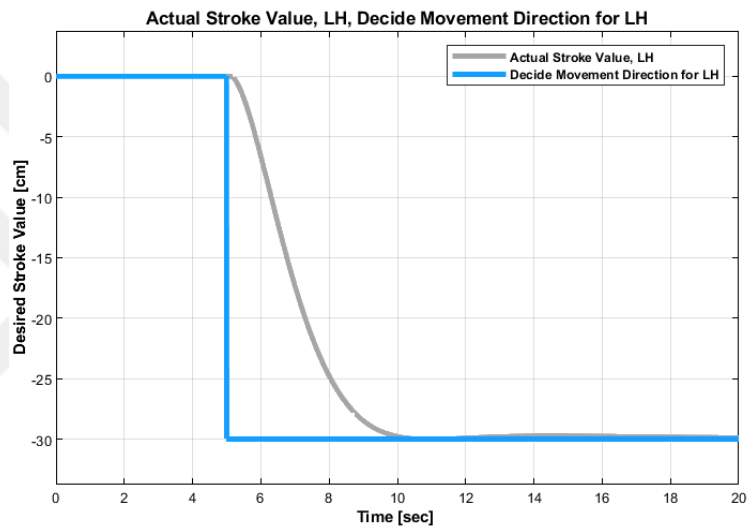
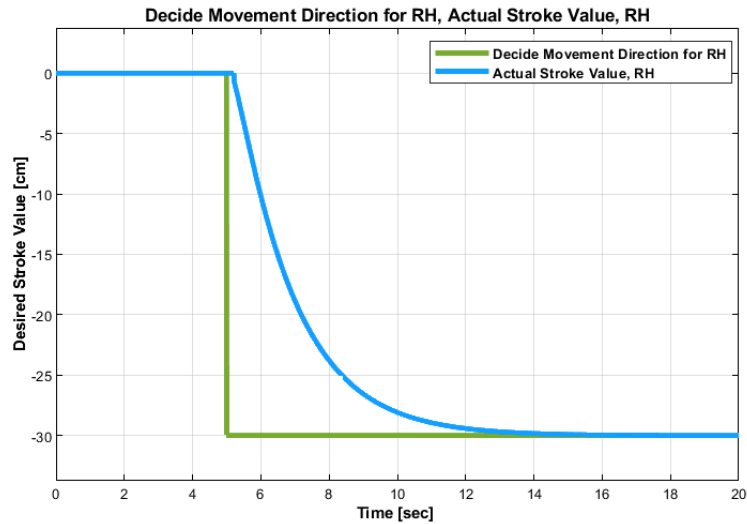


**Figure 4.12:** Up Direction, 80 % Joystick Value with PI Controller RH and LH

The controller designed for 50 % JV is also used for 20% and 80%. While the controller's behavior did not give proper results for 20 % JV (See Figures 4.9 and 4.10), it was suitable for 80 % JV (See Figures 4.11 and 4.12). However, it should be noted that at least four different transfer functions are obtained only for 800 RPM pump speed. The hydraulic pump speed varies between 800 RPM to 2200 RPM. For this reason, paying attention to other joystick percents and RPM values when designing the controller is necessary. This means that different transfer functions require different controllers.

When the graphs from Figures 3.9 to 3.20 are re-examined, the output of the given step input is always in the form of ramp output. This means that the hydraulic system always reacts as an integrator. Only the cylinder velocities are different. The fact that the system behavior is similar, only the cylinder speeds are different, raises

the possibility of designing a common controller. Graphs of three different joystick values can be used to see the relationship of the cylinder velocities with JVs. The slope of the graphs will give the cylinder velocity in cm/sec.

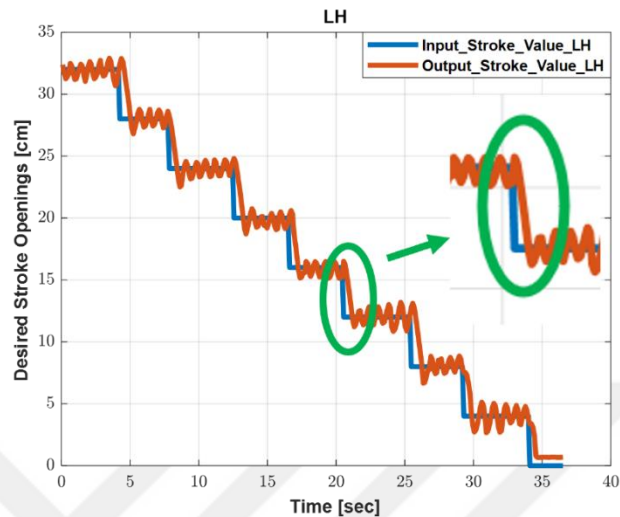


**Figure 4.13:** Cylinder Speed Calculation using Test Data

Table 4.1 shows the calculated speeds for all test results.

**Table 4.1** Calculated Cylinder Speeds

cm/sec	J20_Down	J20_Up	J50_Down	J50_Up	J80_Down	J80_Up
RH	1.075	1.680	2.900	4.800	6.480	5.880
LH	1.075	1.725	3.500	3.950	6.980	6.170

In Table 4.1, it is seen that the downward movement is faster than the upward movement. The most important reason for this is gravity's effect on the blade's downward movement.

Then, the cylinder speeds specified in Table 4.1 were also calculated for other JVs. As a result, Table 4.2 was obtained.

**Table 4.2** Calculated Cylinder Speeds for other JVs

cm/sec	JV=10	JV=20	JV=30	JV=40	JV=50	JV=60	JV=70	JV=80
Left_Up	1.170	1.725	2.200	2.950	3.950	4.500	5.850	6.170
Left_Down	0.370	1.075	1.670	2.550	3.500	4.950	6.000	6.980
Right_Up	1.170	1.680	2.350	3.650	4.800	5.070	6.800	5.880
Right_Down	0.500	1.075	1.550	1.900	2.900	4.250	5.800	6.480

Joystick Value vs. Cylinder Speed graphs were drawn using Matlab Basic Fitting with the values in Table 4.2, and the fitting equations were obtained. When Figure 4.14 is examined, a very close to linear behavior is seen. In particular, the same velocity can be taken for right and left cylinders up to 30 % JV.

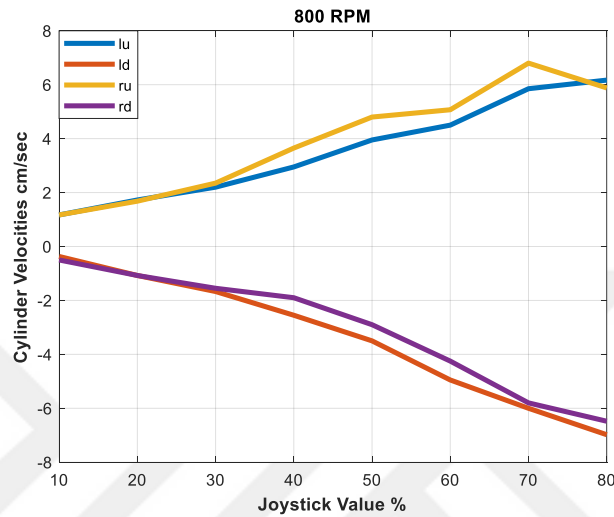


**Figure 4.14:** Cylinder Speed Calculation using Test Data

$$lu = 0.076x + 0.16 \quad (4.6)$$

$$ld = -0.097x + 0.99 \quad (4.7)$$

$$ru = 0.081x + 0.29 \quad (4.8)$$

$$rd = -0.089x + 0.94 \quad (4.9)$$

Where  $lu$  is up, and  $ld$  is down direction cylinder velocities for left lifting cylinder,  $ru$  is up, and  $rd$  is down direction cylinder velocities for right cylinder in cm/sec.  $x$  is joystick value in %.

The model can use a feedforward controller until the cylinder reaches the desired stroke value. During the movement, a fixed joystick value is given to the system. As seen in Figure 4.14, it is appropriate for this value to be 30 % JV.

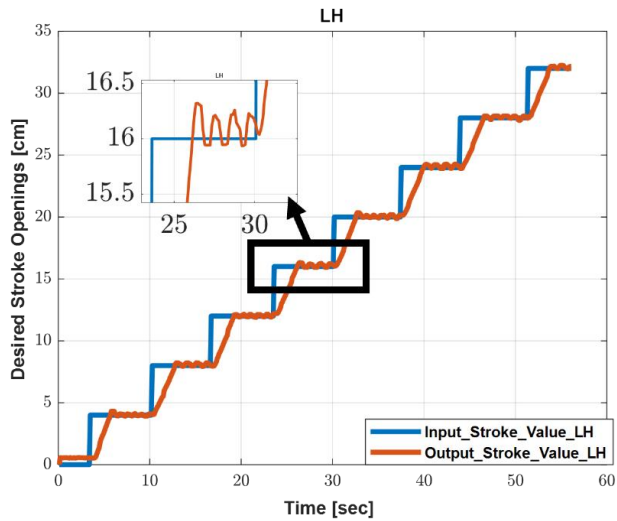


**Figure 4.15:** 20 % JV Graphic to Show JV Effects to Equalize the Desired and Actual Stroke Openings

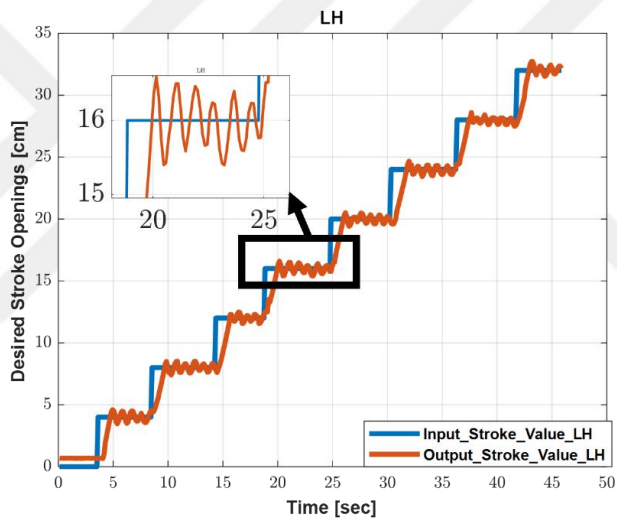


**Figure 4.16:** 50 % JV Graphic to Show JV Effects to Equalize the Desired and Actual Stroke Openings

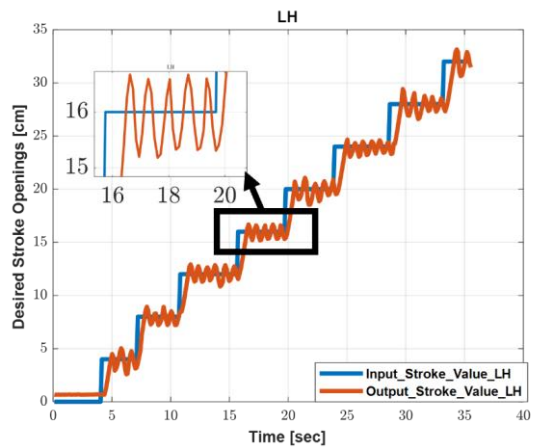


**Figure 4.17:** 80 % JV Graphic to Show JV Effects to Equalize the Desired and Actual Stroke Openings

When Figures 4.15, 4.16 and 4.17 are examined, it is seen that it is more difficult to equate the desired stroke value with the actual stroke value at high JV values. This is due to the valve characteristics. Feedback controllers can be used for sensitive control. In other words, after the cylinders extract to a certain length with feedforward, the feedback controller is activated to provide precise control. During the feedback controller, the cylinder velocities were calculated from equations 4.6 to 4.9. The switch shown in Figure 4.18 provides the transition between the controllers by referring to the determined minimum stroke openings.

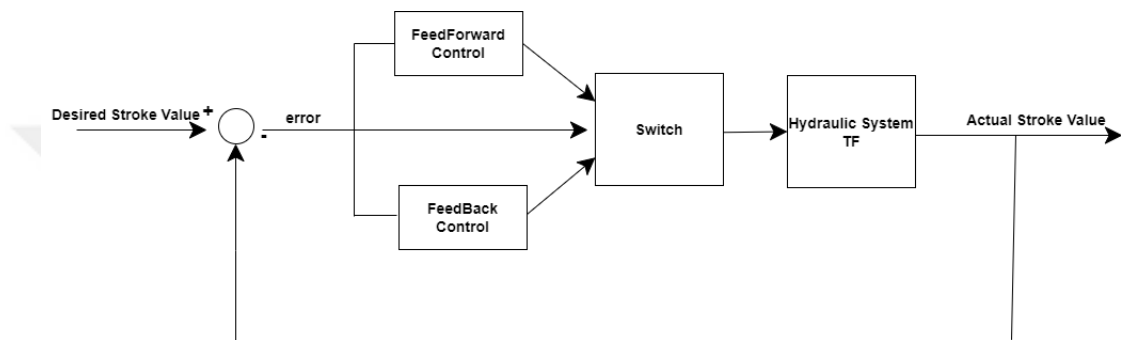


**Figure 4.18:** Overall Control Concept for Hydraulic System

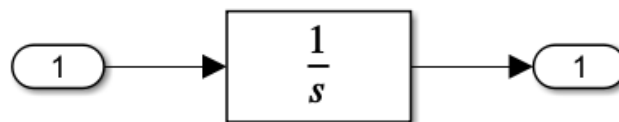


**Figure 4.19:** Valve Characteristics as an Integrator (Hydraulic System TF)

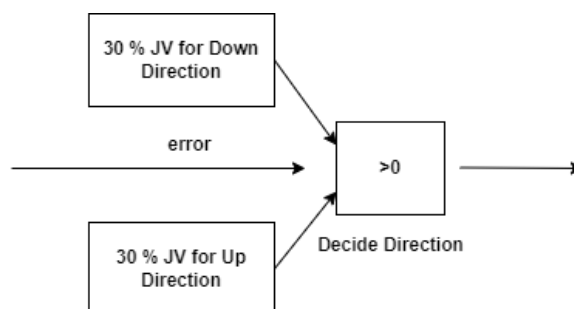


**Figure 4.20:** Feedforward Control

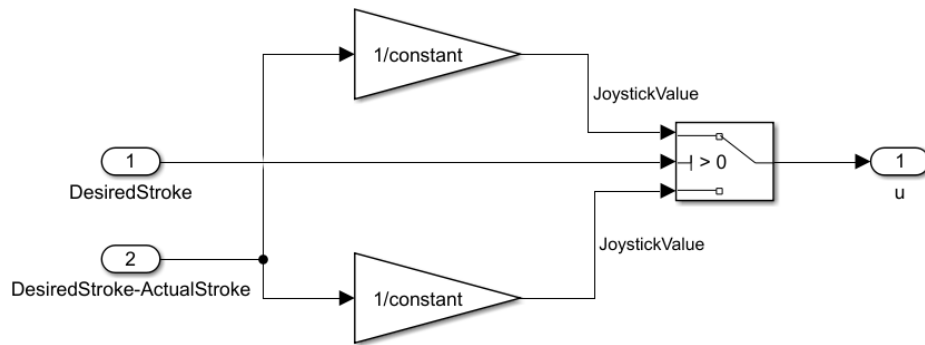


**Figure 4.21:** Feedback Control

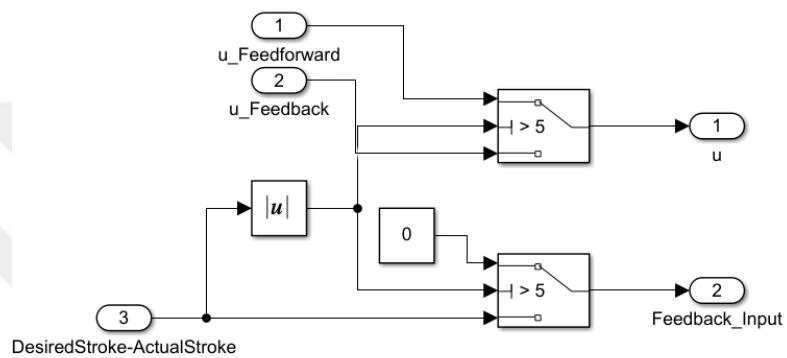


**Figure 4.22:** Switch

Figure 4.23 shows the Simulink model created for the hydraulic system control. The behavior of the model against the Desired Stroke values given as input is seen in Figures 4.24 and 4.25. In Chapter V, the test results obtained on the real machine will be compared with Simulink model outputs.

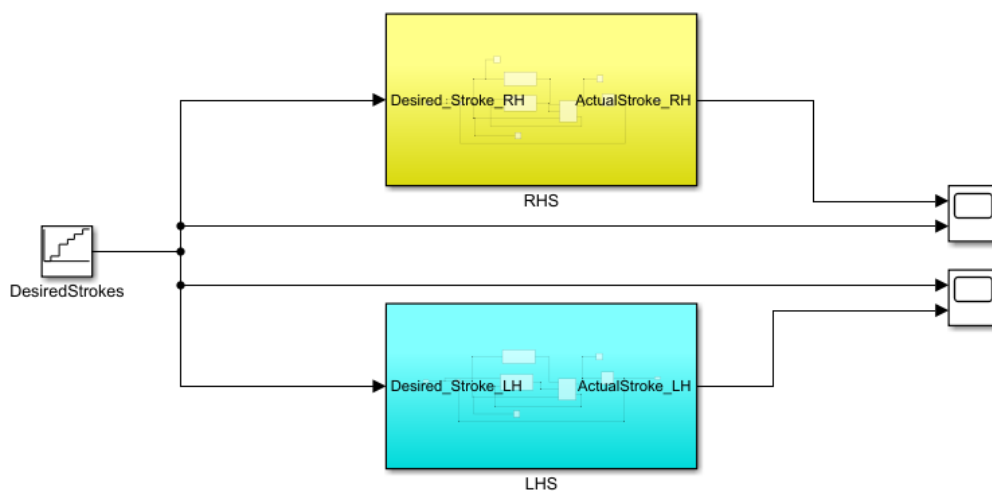


**Figure 4.23:** Simulink model of Hydraulic System Control

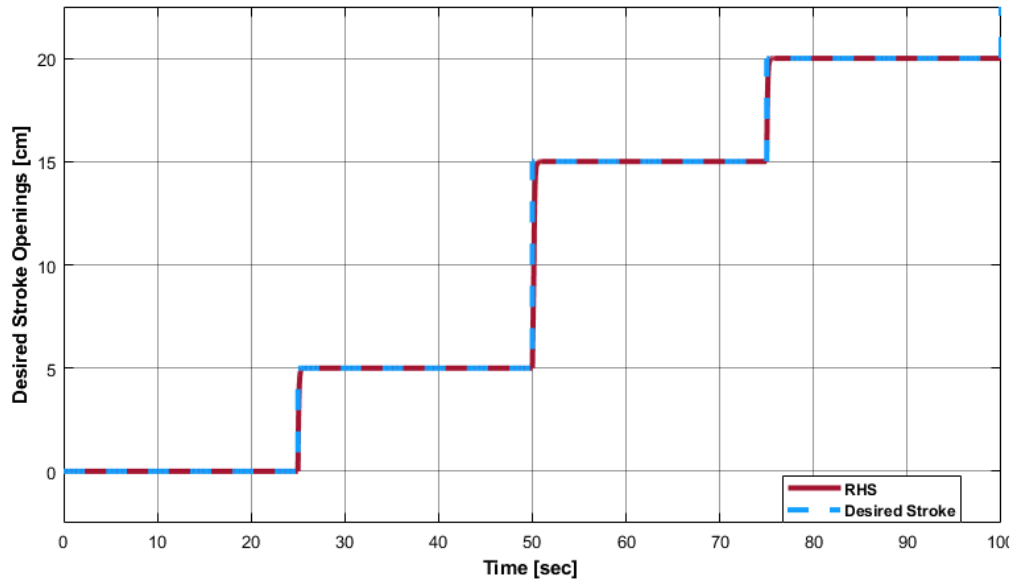


**Figure 4.24:** Simulink output for Right Lifting Cylinder

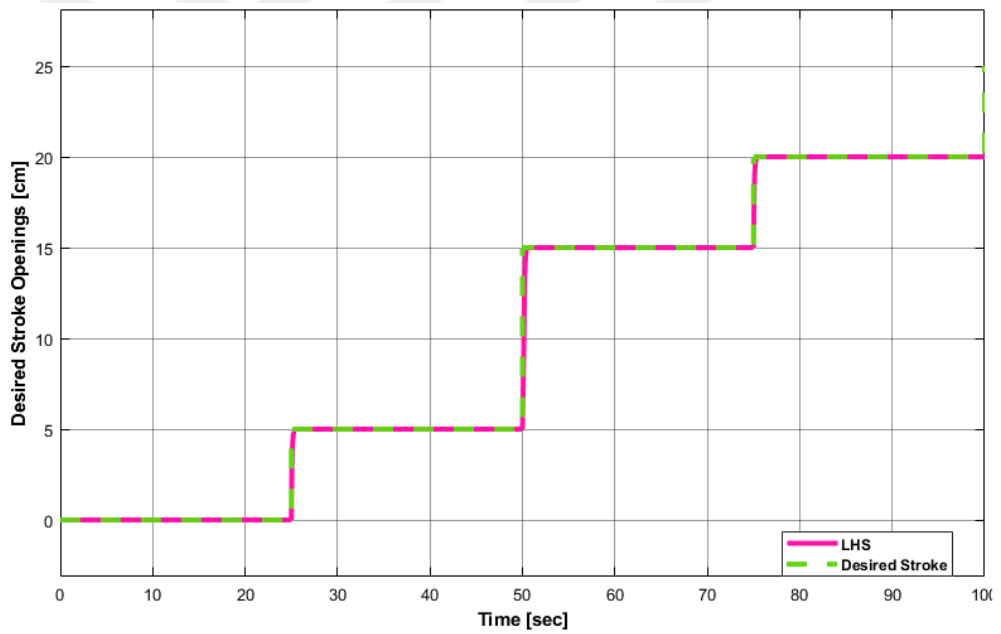


**Figure 4.25:** Simulink output for Left Lifting Cylinder

**CHAPTER V**  
**TEST RESULTS, SIMULATIONS AND MATHEMATICAL MODEL FOR**  
**FUTURE WORKS**

**5.1. TEST RESULTS FOR HYDRAULIC SYSTEM AND HEIGHT**  
**SIMULATIONS**

The model created in Chapter IV has been tested on a real machine. In Figure 4.23 and 4.24, it has been observed that the model works sensitively and accurately. However, when the test records taken on the real machine were examined, it was seen that there were differences between the input/output. In Figure 5.1, there are approximately 0,5 cm difference between input/output.

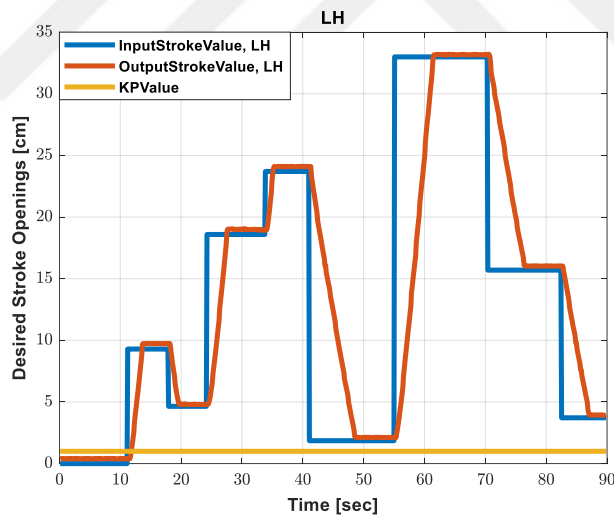


**Figure 5.1:** KP Value 1, Test Result for Left Lifting Cylinder up/down directions

Then, it is desired to observe the system behavior for the input values in different ranges. For this, records were taken at different KP values and the best results were obtained when KP value was 2,5. This value is the same for both the right and left liftings. Test results recorded at 100 ms intervals.



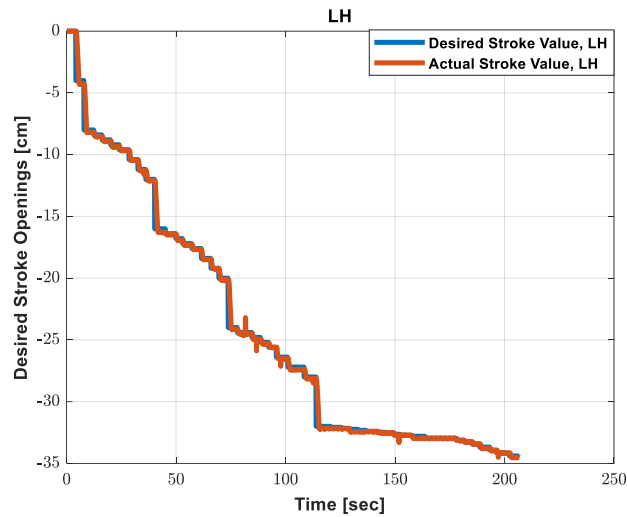


**Figure 5.2:** KP Value 2,5, Test Result for Left Lifting Cylinder down direction

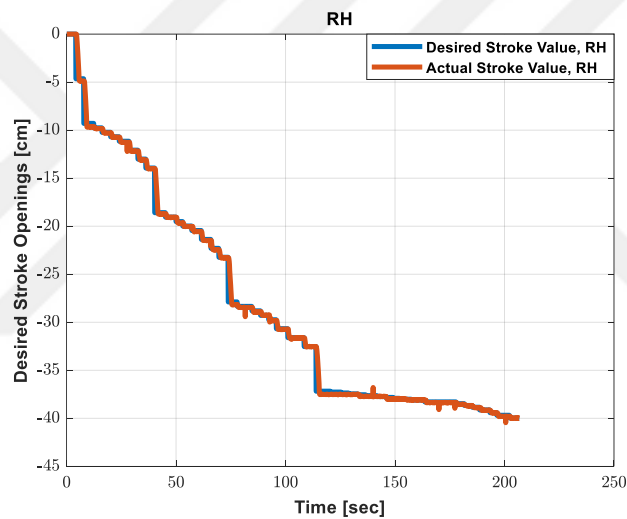


**Figure 5.3:** KP Value 2.5, Test Result for Right Lifting Cylinder down direction

After creating the appropriate model for the hydraulic system and obtaining the appropriate sensitivities, the Simulink model was developed to observe the Desired Height/Actual Height relationship. Accordingly, the position of both edges of the blade in 3-axes is obtained in return for the Desired Height given as input. Using the model in Figure 4.22, the values of the right and left liftings are obtained. Then, using the functions obtained in Chapter II, the positions of the right and left edges on the axes can be determined.

The Height/Stroke relationship was provided by the data matrices obtained in Chapter II. In the new model, a stroke value should be calculated for a height value entered and the control model created for the hydraulic system should work. For this, the data matrices obtained in Chapter II can be used. Data matrices contain values

recorded with a resolution of 1 cm in the range of 0-48 cm. In order to increase the sensitivity, the range was doubled and a 95x95 matrix was obtained. Matlab interp3 command was used for this calculation.

$$B1Z = \begin{bmatrix} \dots & \dots & \dots \\ \vdots & \ddots & \vdots \\ \dots & \dots & \dots \end{bmatrix}_{95 \times 95} \quad (5.1)$$

$$B4Z = \begin{bmatrix} \dots & \dots & \dots \\ \vdots & \ddots & \vdots \\ \dots & \dots & \dots \end{bmatrix}_{95 \times 95} \quad (5.2)$$

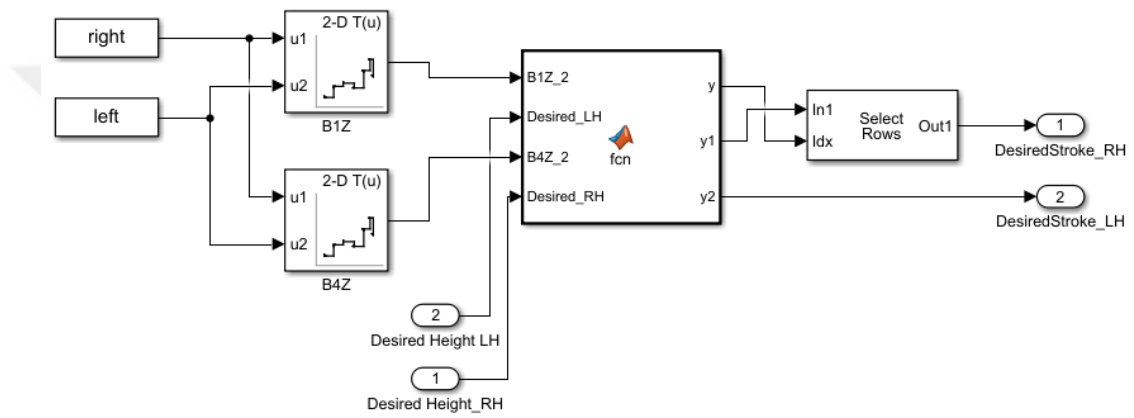


**Figure 5.4:** Calculation model for Desired Stroke when input is Desired Height

$$Z = \text{abs}(B1Z + \text{DesiredHeight}_{rh}) + \text{abs}(B4Z + \text{DesiredHeight}_{lf}) \quad (5.3)$$

$$[aa \ bb] = \min(\min(Z)) \quad (5.4)$$

$$[row, col] = \text{find}(Z == aa) \quad (5.5)$$

$$\text{DesiredStroke}_{B1Z} = row \quad (5.6)$$

$$\text{DesiredStroke}_{B4Z} = col \quad (5.7)$$

A new matrix is obtained by using equation 5.3 with a Desired Height value entered in Figure 5.4. then, the minimum value of the matrix was calculated as in equation 5.4. Then, row and column values have this minimum value were obtained. The row represents the desired stroke for the right lifting cylinder and the column represents the desired stroke for the left lifting cylinder. the green box in Figure 5.5 represents the above operations.

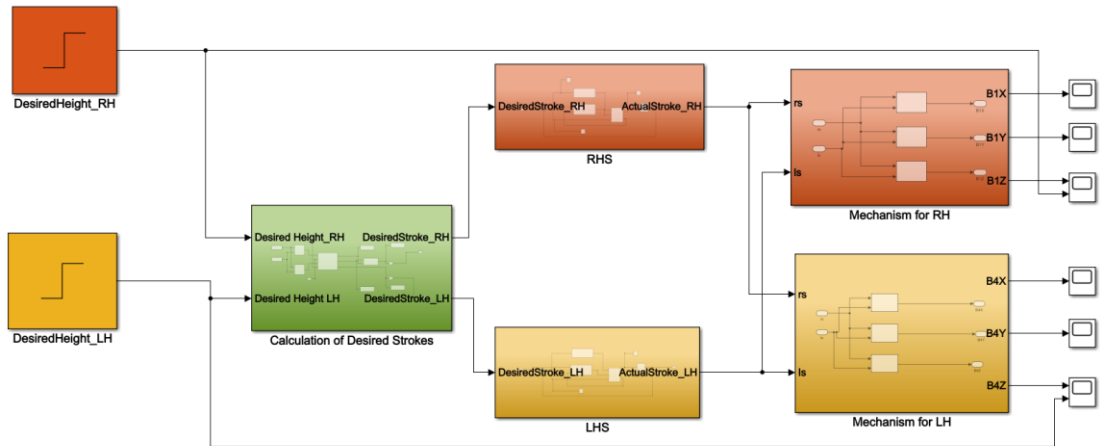


**Figure 5.5: Overall Height Model**

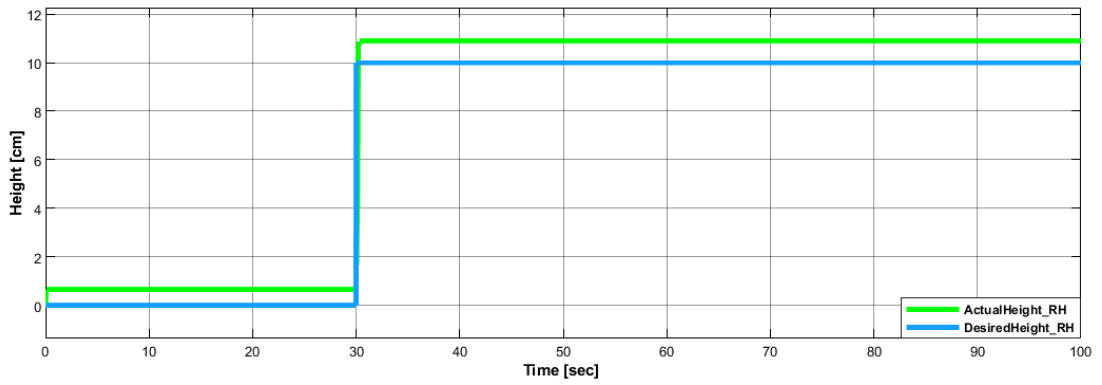


**Figure 5.6: Blade right edge desired and actual output with approximately 0,5 cm difference**

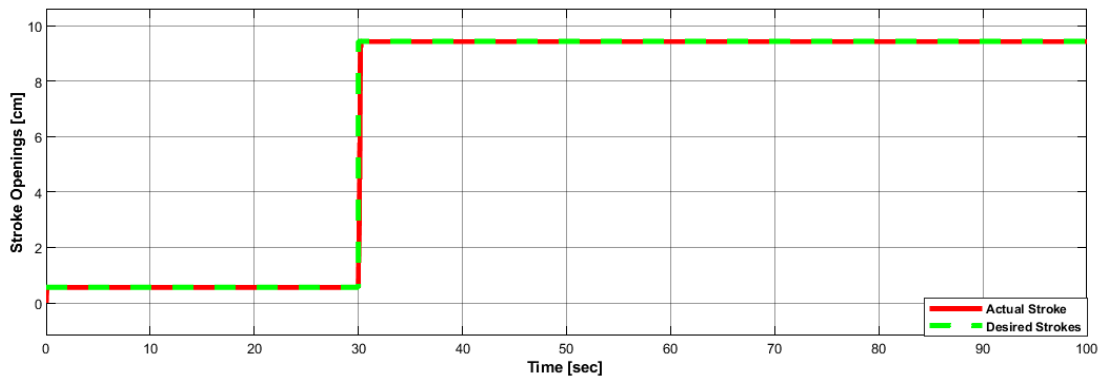


**Figure 5.7: Right lifting cylinder desired and actual stroke openings**

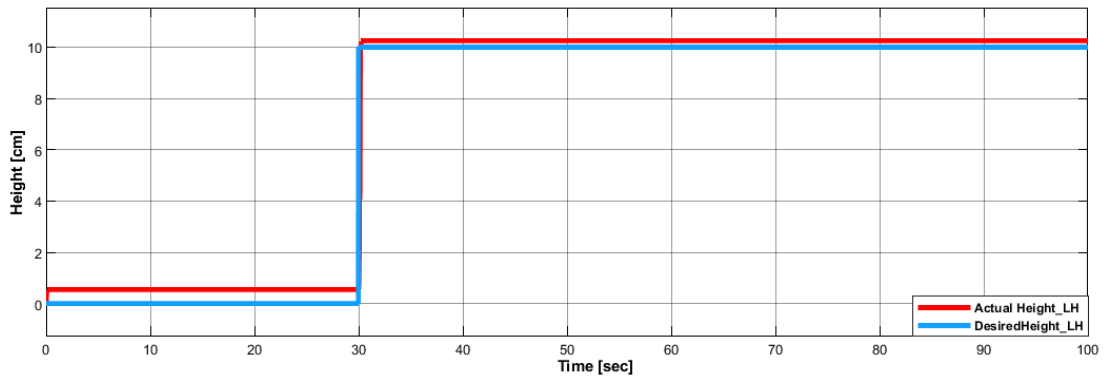


**Figure 5.8:** Blade left edge desired and actual output with approximately 0,3 cm difference

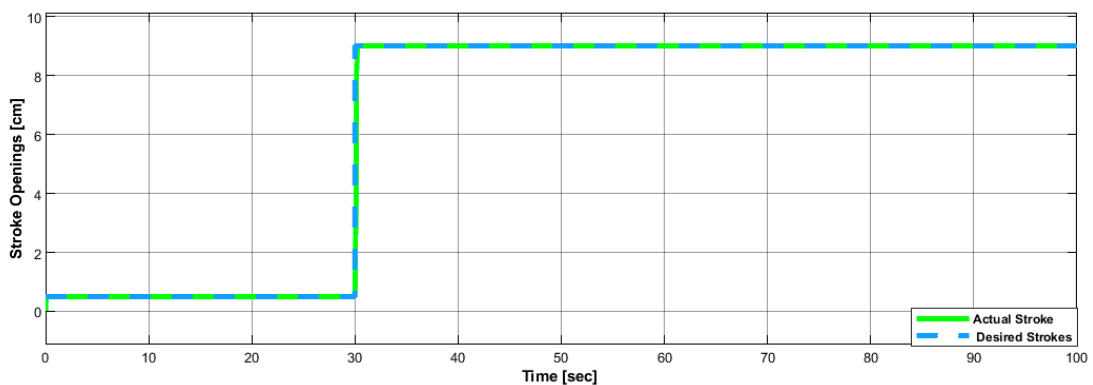


**Figure 5.9:** Left lifting cylinder desired and actual stroke openings

## 5.2. TERRAIN DESIGN

The Hydraulic system can be easily tested in a real machine environment. Draw wire encoders on the machine can also provide information about the desired-actual stroke values. However, since the aim is height control, a test environment should also be created for the desired-actual height. Topics such as the height of the soil, how high the blade runs during operation, etc. are too complex to compare with actual test results. For this reason, a simulation was created in the Matlab environment. During the simulation, the blade will level a pile of soil that is randomly laid in front of the vehicle and has a certain average height. The simulation environment is also illustrated in Figures 5.10 and 5.11.

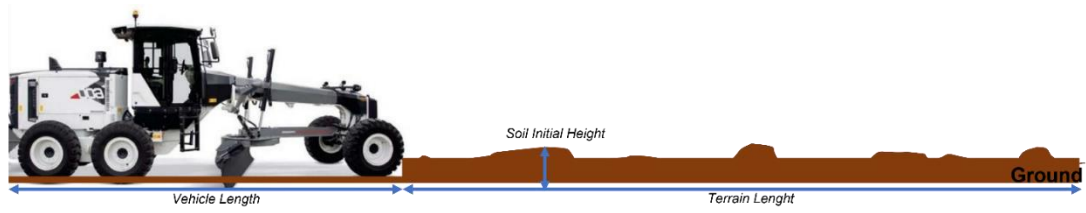


**Figure 5.10:** Side view from y-axis

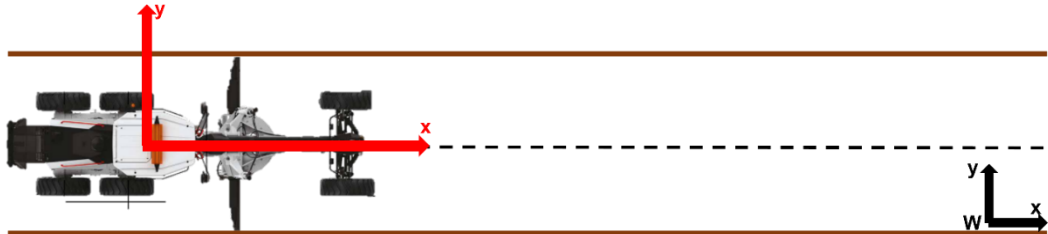


**Figure 5.11:** Top view from z-axis

The desired height on the road increases and decreases continuously in order to observe the sensitivity of the controller. The values taken by both the right and left edges of the blade are plotted according to the desired input height value.

### 5.3. MATHEMATICAL MODEL FOR FUTURE WORKS

#### 5.3.1. Different RPM-JV Relationship

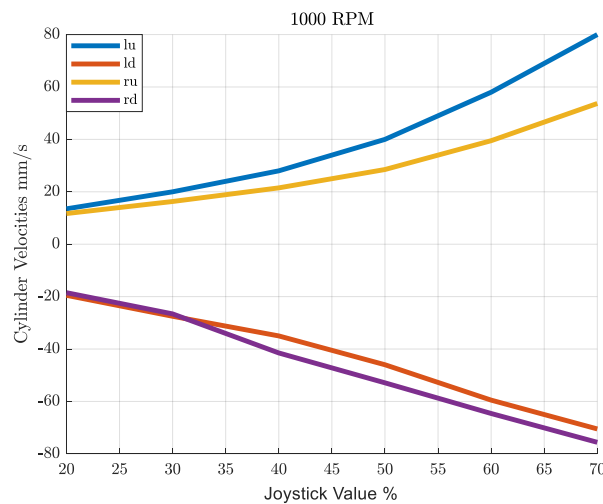


**Figure 5.12:** Cylinder Speed Calculation using Test Data for 1000 RPM

$$Lu = 0.131x - 1.903 \quad (5.1)$$

$$Ld = -0.1034x + 0.3543 \quad (5.2)$$

$$ru = 0.08189x - 0.8315 \quad (5.3)$$

$$rd = -0.1174x + 0.6213 \quad (5.4)$$

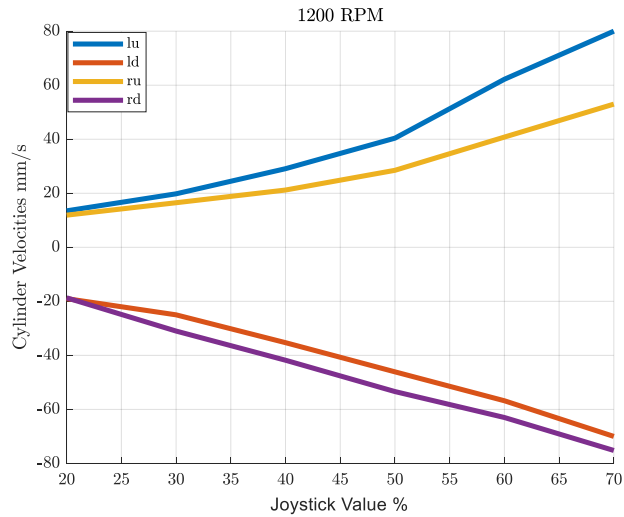


**Figure 5.13:** Cylinder Speed Calculation using Test Data for 1200 RPM

$$Lu = 0.1346x - 1.972 \tag{5.5}$$

$$Ld = -0.1032x + 0.4407 \tag{5.6}$$

$$ru = 0.08163x - 0.8083 \tag{5.7}$$

$$rd = -0.1115x + 0.2972 \tag{5.8}$$

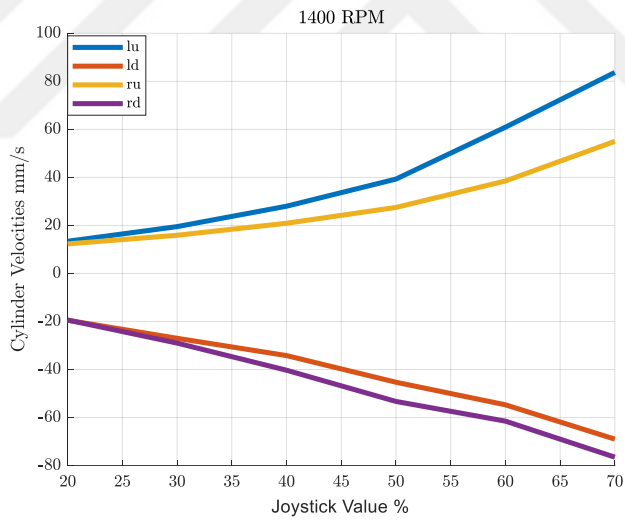


**Figure 5.14:** Cylinder Speed Calculation using Test Data for 1400 RPM

$$Lu = 0.1391x - 2.181 \tag{5.9}$$

$$Ld = -0.0976x + 0.2316 \tag{5.10}$$

$$ru = 0.08226x - 0.8666 \tag{5.11}$$

$$rd = -0.1131x + 0.4248 \tag{5.12}$$

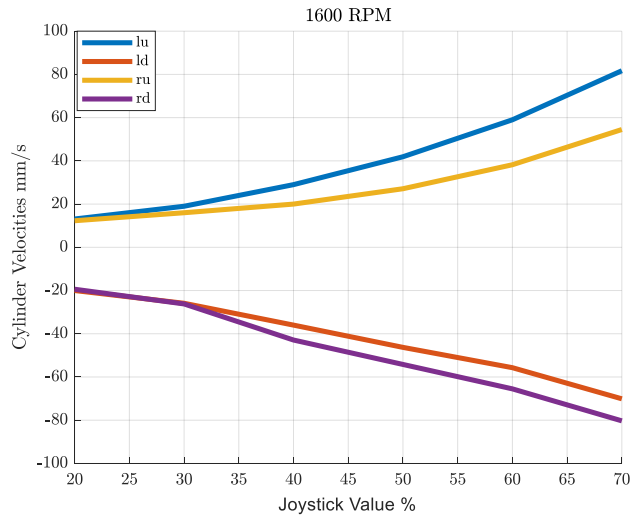


**Figure 5.15:** Cylinder Speed Calculation using Test Data for 1600 RPM

$$Lu = 0.136x - 2.057 \tag{5.13}$$

$$Ld = -0.1001x + 0.2692 \tag{5.14}$$

$$ru = 0.08134x - 0.8588 \tag{5.15}$$

$$rd = -0.1239x + 0.7678 \tag{5.16}$$

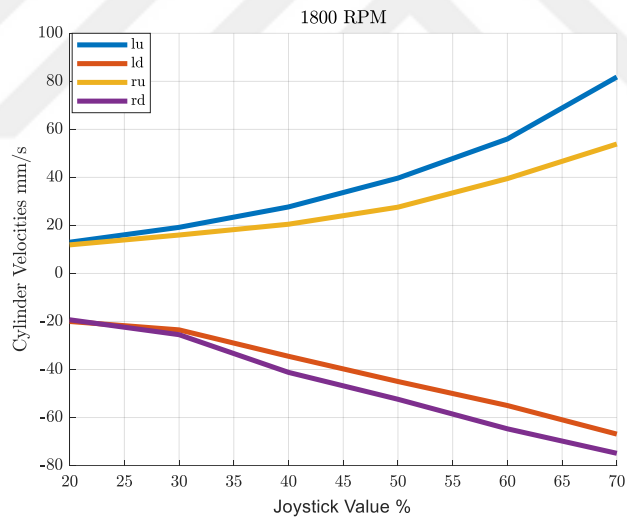


**Figure 5.16:** Cylinder Speed Calculation using Test Data for 1800 RPM

$$Lu = 0.1333x - 2.04 \tag{5.17}$$

$$Ld = -0.097x + 0.2833 \tag{5.18}$$

$$ru = 0.08217x - 0.8744 \tag{5.19}$$

$$rd = -0.1162x + 0.597 \tag{5.20}$$

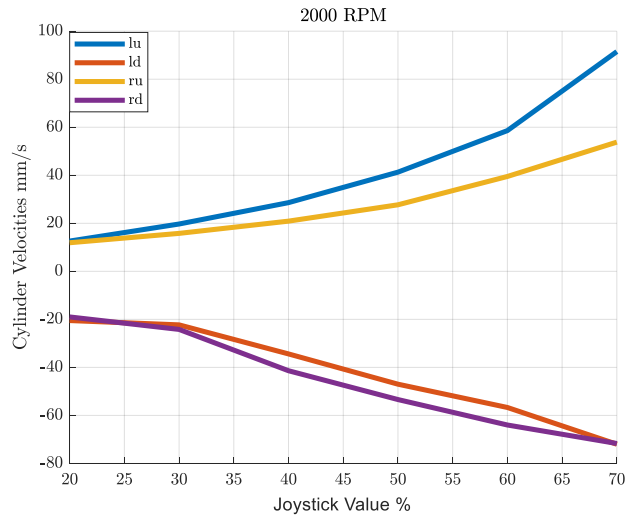


**Figure 5.17:** Cylinder Speed Calculation using Test Data for 2000 RPM

$$Lu = 0.1497x - 2.531 \tag{5.21}$$

$$Ld = -0.1067x + 0.5846 \tag{5.22}$$

$$ru = 0.08211x - 0.8685 \tag{5.23}$$

$$rd = -0.1128x + 0.5156 \tag{5.24}$$

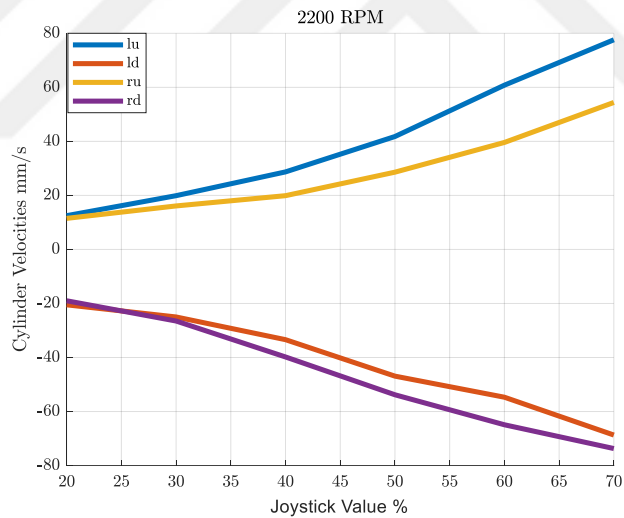


**Figure 5.18:** Cylinder Speed Calculation using Test Data for 2200 RPM

$$Lu = 0.1318x - 1.909 \tag{5.25}$$

$$Ld = -0.0981x + 0.2644 \tag{5.26}$$

$$ru = 0.0839x - 0.9411 \tag{5.27}$$

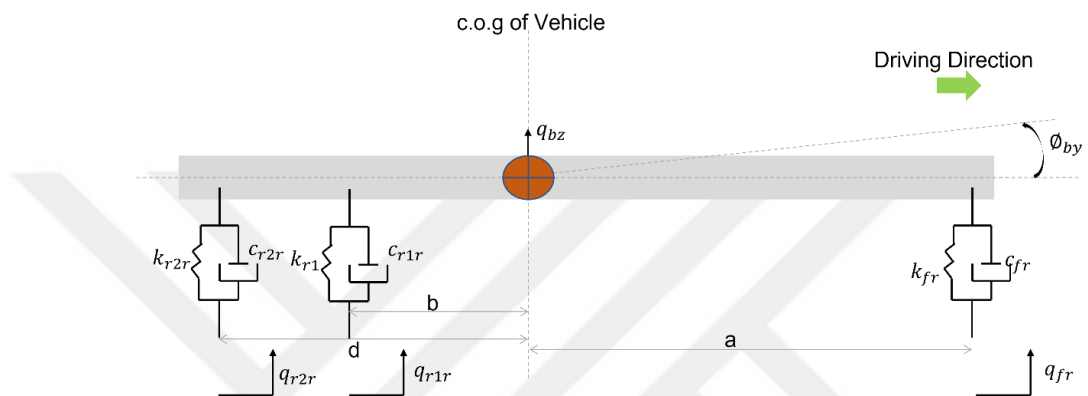
$$rd = -0.1151x + 0.5492 \tag{5.28}$$

### 5.3.2. Disturbances

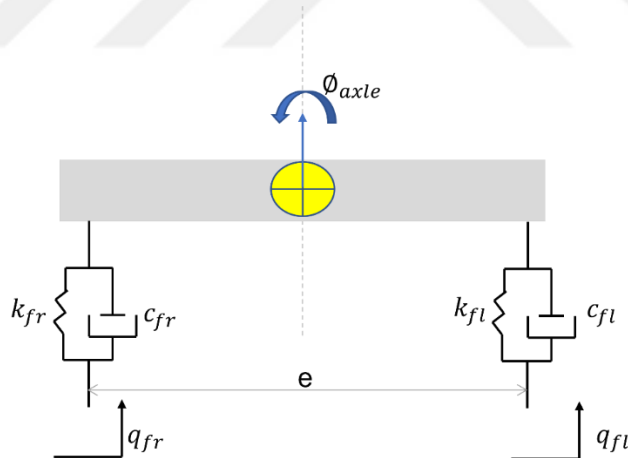
The vehicle has three dynamic movements, pitch, roll and jump. These movements occur as a result of the vehicle wheels passing over a bump. The below



figure shows the half vehicle model of motor grader. The pitching and jumping movements of the vehicle body against a bump are shown in figure. Motor grader wheels do not have a suspension system compared to the other vehicles. For this reason, the wheels are only expressed with the spring damper relationship. In this thesis, parts such as cabin and seat are not included in the half-car model, since it is desired to examine the effects on the position of the blade only when the wheels pass over a bump.



**Figure 5.19:** Side view from y-axis



**Figure 5.20:** Front view from x-axis

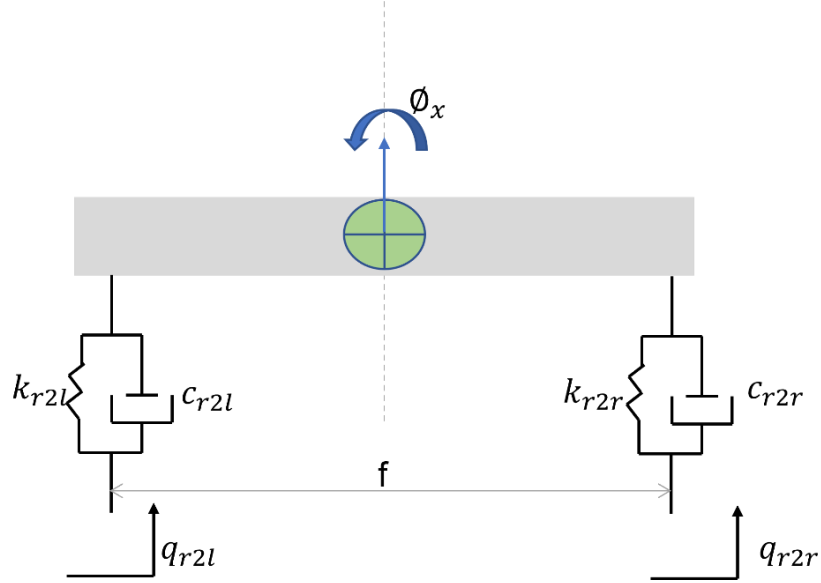


**Figure 5.21:** Back view from x-axis

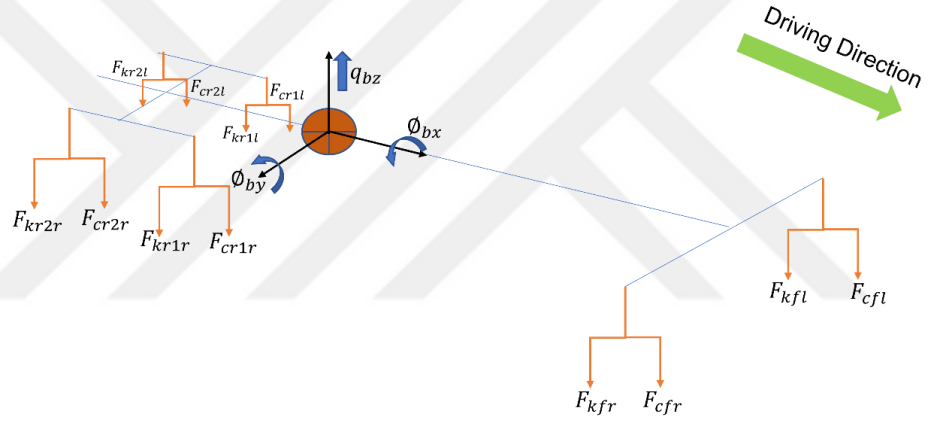


**Figure 5.22:** Spring-Damper Forces on Machine Schematics

CCW and up directions are selected as positive. Then,

$$F_{kfr} = k_{fr}(q_{fr} + \Phi_{axle} \frac{e}{2} + \Phi_{bx} \frac{e}{2} - q_{bz} - a\Phi_{by}) \quad (5.29)$$

$$F_{cfr} = c_{fr}(\dot{q}_{fr} + \dot{\Phi}_{axle} \frac{e}{2} + \dot{\Phi}_{bx} \frac{e}{2} - \dot{q}_{bz} - a\dot{\Phi}_{by}) \quad (5.30)$$

$$F_{kfl} = k_{fl}(q_{fl} - \Phi_{axle} \frac{e}{2} - \Phi_{bx} \frac{e}{2} - q_{bz} - a\Phi_{by}) \quad (5.31)$$

$$F_{cfl} = c_{fl}(\dot{q}_{fl} - \dot{\Phi}_{axle} \frac{e}{2} - \dot{\Phi}_{bx} \frac{e}{2} - \dot{q}_{bz} - a\dot{\Phi}_{by}) \quad (5.32)$$

$$F_{kr1r} = k_{r1r}(q_{r1r} + \Phi_{bx} \frac{f}{2} - \Phi_{tr} \frac{d-b}{2} - q_{bz} + \Phi_{by} \frac{d+b}{2}) \quad (5.33)$$

$$F_{cr1r} = c_{r1r}(\dot{q}_{r1r} + \dot{\Phi}_{bx} \frac{f}{2} - \dot{\Phi}_{tr} \frac{d-b}{2} - \dot{q}_{bz} + \dot{\Phi}_{by} \frac{d+b}{2}) \quad (5.34)$$

$$F_{kr1l} = k_{r1r}(q_{r1r} - \Phi_{bx} \frac{f}{2} - \Phi_{tl} \frac{d-b}{2} - q_{bz} + \Phi_{by} \frac{d+b}{2}) \quad (5.35)$$

$$F_{cr1_l} = c_{r1_l}(\dot{q}_{r1_l} - \dot{\phi}_{bx} \frac{f}{2} - \dot{\phi}_{tl} \frac{d-b}{2} - \dot{q}_{bz} + \dot{\phi}_{by} \frac{d+b}{2}) \quad (5.36)$$

$$F_{kr2_r} = k_{r2_r}(q_{r2_r} + \phi_{bx} \frac{f}{2} + \phi_{tr} \frac{d-b}{2} - q_{bz} + \phi_{by} \frac{d+b}{2}) \quad (5.37)$$

$$F_{cr2_r} = c_{r2_r}(\dot{q}_{r2_r} + \dot{\phi}_{bx} \frac{f}{2} + \dot{\phi}_{tr} \frac{d-b}{2} - \dot{q}_{bz} + \dot{\phi}_{by} \frac{d+b}{2}) \quad (5.38)$$

$$F_{kr2_l} = k_{r2_r}(q_{r2_r} - \phi_{bx} \frac{f}{2} + \phi_{tl} \frac{d-b}{2} - q_{bz} + \phi_{by} \frac{d+b}{2}) \quad (5.39)$$

$$F_{cr2_l} = c_{r2_l}(\dot{q}_{r2_l} - \dot{\phi}_{bx} \frac{f}{2} + \dot{\phi}_{tl} \frac{d-b}{2} - \dot{q}_{bz} + \dot{\phi}_{by} \frac{d+b}{2}) \quad (5.40)$$

- Rear Axle Pitch Motion

$$I_{t_r} \ddot{\phi}_{t_r} + \frac{d-b}{2} (-F_{kr1_r} - F_{cr1_r} + F_{kr2_r} + F_{cr2_r}) = 0 \quad (5.41)$$

$$I_{t_l} \ddot{\phi}_{t_l} + \frac{d-b}{2} (-F_{kr1_l} - F_{cr1_l} + F_{kr2_l} + F_{cr2_l}) = 0 \quad (5.42)$$

- Front Axle Roll Motion

$$I_{axle} \ddot{\phi}_{axle} + \frac{e}{2} (-F_{kf_l} - F_{cf_l} + F_{kf_r} + F_{cf_r}) = 0 \quad (5.43)$$

- Body Jump Motion

$$m_{bz} \ddot{q}_{bz} - F_{kf_r} - F_{cf_r} - F_{kf_l} - F_{cf_l} - F_{kr1_r} - F_{cr1_r} - F_{kr2_r} - F_{cr2_r} - F_{kr1_l} - F_{cr1_l} - F_{kr2_l} - F_{cr2_l} = 0 \quad (5.44)$$

- Body Pitch Motion

$$I_{by} \ddot{\phi}_{by} - aF_{kf_r} - aF_{cf_r} - aF_{kf_l} - aF_{cf_l} + \frac{d+b}{2} [F_{kr1_r} + F_{cr1_r} + F_{kr2_r} + F_{cr2_r} + F_{kr1_l} + F_{cr1_l} + F_{kr2_l} + F_{cr2_l}] = 0 \quad (5.45)$$

- Body Roll Motion

$$I_{bx} \ddot{\phi}_{bx} + \frac{e}{2} F_{kf_r} + \frac{e}{2} F_{cf_r} - \frac{e}{2} F_{kf_l} - \frac{e}{2} F_{cf_l} + \frac{f}{2} (F_{kr1_r} + F_{cr1_r} + F_{kr2_r} + F_{cr2_r}) - \frac{f}{2} (F_{kr1_l} + F_{cr1_l} + F_{kr2_l} + F_{cr2_l}) = 0 \quad (5.46)$$

Force-moment balance equations can be written in matrix form as follows,

$$\begin{aligned}
[M]_{6 \times 6} \begin{bmatrix} \ddot{\phi}_{tr} \\ \ddot{\phi}_{tl} \\ \ddot{\phi}_{axle} \\ \ddot{q}_{bz} \\ \ddot{\phi}_{by} \\ \ddot{\phi}_{bx} \end{bmatrix}_{6 \times 1} + [C]_{6 \times 6} \begin{bmatrix} \dot{\phi}_{tr} \\ \dot{\phi}_{tl} \\ \dot{\phi}_{axle} \\ \dot{q}_{bz} \\ \dot{\phi}_{by} \\ \dot{\phi}_{bx} \end{bmatrix}_{6 \times 1} + [K]_{6 \times 6} \begin{bmatrix} \phi_{tr} \\ \phi_{tl} \\ \phi_{axle} \\ q_{bz} \\ \phi_{by} \\ \phi_{bx} \end{bmatrix}_{6 \times 1} & \quad (5.47) \\
= [F]_{6 \times 12} \begin{bmatrix} q_{fr} \\ q_{fl} \\ q_{r1r} \\ q_{r1l} \\ q_{r2r} \\ q_{r2l} \\ \dot{q}_{fr} \\ \dot{q}_{fl} \\ \dot{q}_{r1r} \\ \dot{q}_{r1l} \\ \dot{q}_{r2r} \\ \dot{q}_{r2l} \end{bmatrix}_{12 \times 1} &
\end{aligned}$$

General state space representation is as follows,

$$\{\dot{x}\} = [A]\{x\} + [B]\{u\} \quad (5.48)$$

$$\{y\} = [C]\{x\} + [D]\{u\} \quad (5.49)$$

Where,  $\{x\}$  is state vector,  $\{u\}$  is input vector and  $\{y\}$  is the output vector.

$$\{u\} = \begin{bmatrix} q_{fr} \\ q_{fl} \\ q_{r1r} \\ q_{r1l} \\ q_{r2r} \\ q_{r2l} \\ \dot{q}_{fr} \\ \dot{q}_{fl} \\ \dot{q}_{r1r} \\ \dot{q}_{r1l} \\ \dot{q}_{r2r} \\ \dot{q}_{r2l} \end{bmatrix} \quad (5.50)$$

$$\{x\} = \begin{bmatrix} \phi_{tr} \\ \phi_{tl} \\ \phi_{axle} \\ q_{bz} \\ \phi_{by} \\ \phi_{bx} \\ \dot{\phi}_{tr} \\ \dot{\phi}_{tl} \\ \dot{\phi}_{axle} \\ \dot{q}_{bz} \\ \dot{\phi}_{by} \\ \dot{\phi}_{bx} \end{bmatrix} \quad (5.51)$$

$$\{\dot{x}\}_{12 \times 1} = [A]_{12 \times 12} \cdot \{x\}_{12 \times 1} + [B]_{12 \times 12} \cdot \{u\}_{12 \times 1} \quad (5.52)$$

$$\{\dot{x}\} = \begin{bmatrix} [0] & [I] \\ -[M]^{-1}[K] & -[M]^{-1}[C] \end{bmatrix} \{x\} + \begin{bmatrix} [0] \\ -[M]^{-1}[F] \end{bmatrix} \{u\} \quad (5.53)$$

Dynamic movements occurring in the center of gravity of the machine are expressed by the 4th, 5th, and 6th equations. These movements are called jumping, pitching and Rolling, respectively. Jump occurs along the z-axis, pitch along the y-axis and roll along the x-axis. Rotation and translation matrices can be used to Express the effect of these movements occurring in the center of gravity of the machine on the two cutting edges of the blade. Then,

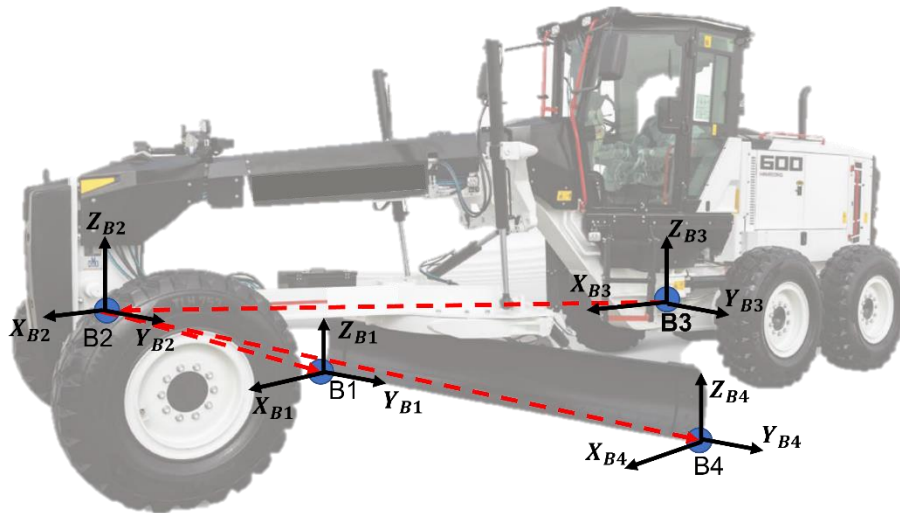


**Figure 5.23:** Configuration of the coordinate frames

Point B3 shown in Figure 5.23 represents the center of gravity of the machine, points B1 and B2 represent the right and left cutting edges of the blade, and point B2

represents the connection point between the drawbar and front frame. To find the effect of the movement at the B3 point of the B1 and B2 points, the B3 point is moved to the B2 point and the B2 point to the B1 and B4 points with using rotation and translation matrices. So,

Rotation in x axis,

$$Rotation(x, \phi_x) = \begin{bmatrix} 1 & 0 & 0 & 0 \\ 0 & \cos\phi_x & -\sin\phi_x & 0 \\ 0 & \sin\phi_x & \cos\phi_x & 0 \\ 0 & 0 & 0 & 1 \end{bmatrix} \quad (5.54)$$

Rotation in y axis,

$$Rotation(y, \phi_y) = \begin{bmatrix} \cos\phi_y & 0 & \sin\phi_y & 0 \\ 0 & 1 & 0 & 0 \\ -\sin\phi_y & 0 & \cos\phi_y & 0 \\ 0 & 0 & 0 & 1 \end{bmatrix} \quad (5.55)$$

Translation in z axis,

$$Translation(z, q_z) = \begin{bmatrix} 1 & 0 & 0 & 0 \\ 0 & 1 & 0 & 0 \\ 0 & 0 & 1 & q_z \\ 0 & 0 & 0 & 1 \end{bmatrix} \quad (5.56)$$

Roll-Pitch-Yaw Convention for B3 point (cog of machine),

$$T_{B3} = Rot(x, \phi_x) * Rot(y, \phi_y) * Trans(z, q_z) \quad (5.57)$$

$$T_{B3} = \begin{bmatrix} 1 & 0 & 0 & 0 \\ 0 & \cos\phi_x & -\sin\phi_x & 0 \\ 0 & \sin\phi_x & \cos\phi_x & 0 \\ 0 & 0 & 0 & 1 \end{bmatrix} * \begin{bmatrix} \cos\phi_y & 0 & \sin\phi_y & 0 \\ 0 & 1 & 0 & 0 \\ -\sin\phi_y & 0 & \cos\phi_y & 0 \\ 0 & 0 & 0 & 1 \end{bmatrix} * \begin{bmatrix} 1 & 0 & 0 & 0 \\ 0 & 1 & 0 & 0 \\ 0 & 0 & 1 & q_z \\ 0 & 0 & 0 & 1 \end{bmatrix} \quad (5.58)$$

$$T_{B3} = \begin{bmatrix} 1 & 0 & 0 & 0 \\ 0 & \cos\phi_x & -\sin\phi_x & 0 \\ 0 & \sin\phi_x & \cos\phi_x & 0 \\ 0 & 0 & 0 & 1 \end{bmatrix} * \begin{bmatrix} \cos\phi_y & 0 & \sin\phi_y & \sin\phi_y * q_z \\ 0 & 1 & 0 & 0 \\ -\sin\phi_y & 0 & \cos\phi_y & \cos\phi_y * q_z \\ 0 & 0 & 0 & 1 \end{bmatrix} \quad (5.59)$$

$$T_{B3} = \begin{bmatrix} \cos\phi_y & 0 & \sin\phi_y & \sin\phi_y * q_z \\ -\sin\phi_x * \sin\phi_y & \cos\phi_x & -\sin\phi_x * \cos\phi_y & -\sin\phi_x * \cos\phi_y * q_z \\ -\sin\phi_y * \cos\phi_x & \sin\phi_x & \cos\phi_x * \cos\phi_y & \cos\phi_y * \cos\phi_x * q_z \\ 0 & 0 & 0 & 1 \end{bmatrix} \quad (5.60)$$

Then, B2 point can be found using B3 point convention,

$$P_{B2} = T_{B3} * \begin{matrix} B2 \\ B3 \end{matrix} P = T_{B3} * \begin{bmatrix} l_{xb3b2} \\ l_{yb3b2} \\ l_{zb3b2} \\ 1 \end{bmatrix} \quad (5.61)$$

Then, B1 and B4 positions can be found using B2 coordinates,

$$P_{B1} = \begin{matrix} B1 \\ B2 \end{matrix} P * P_{B2} \quad (5.62)$$

$$P_{B4} = \begin{matrix} B4 \\ B2 \end{matrix} P * P_{B2} \quad (5.63)$$

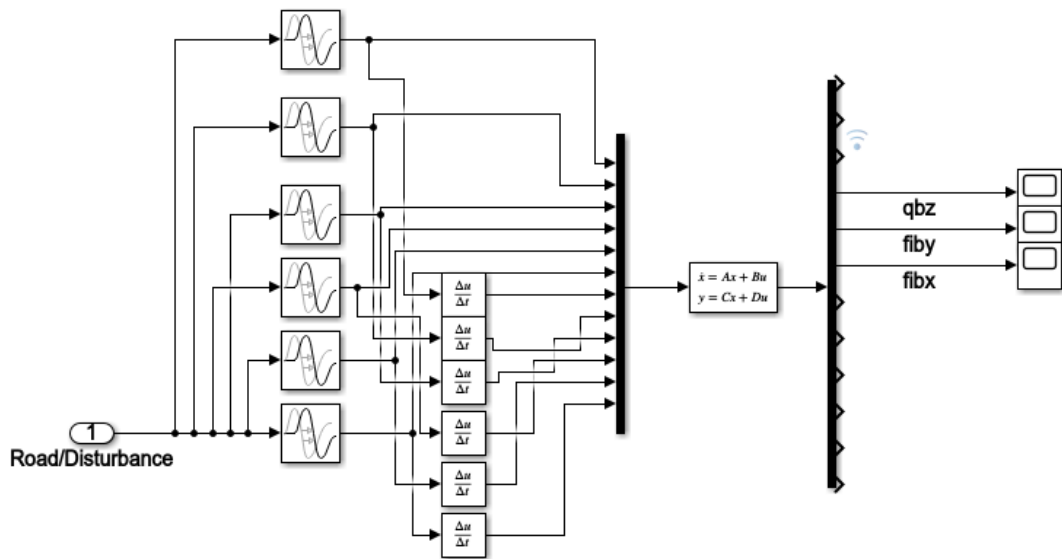


**Figure 5.24:** Simulink Model for Pitch, Roll and Jump Motion of Machine COG

## CHAPTER VI

### CONCLUSION

In this thesis, it is aimed to automatically control the height of the motor grader blade. First of all, the blade mechanism was analyzed. The mechanism has various degree of freedoms. Therefore, it is quite difficult to obtain its analysis with kinematic equations. By using the 3D CAD model of the mechanism, the position changes of the edges of the blade were obtained as a result of the movements of the cylinders. Blade edge and cylinder stroke value equations were obtained with optimization methods. Then, the hydraulic system was examined and its equations were obtained. However, it is very difficult to obtain these equations as some properties are not clear between the components. For this reason, the transfer functions of the hydraulic system were obtained with the tests on the real vehicle by using System Identification. The transfer function is different for each speed of the cylinder, but it also gives similar results. For this reason, one of the transfer functions whose pole-zero graphs were examined was selected and a suitable controller was designed. Then, this controller was tested in other transfer functions and their behavior was observed.

The repeated test results on the real system were examined and it was observed that the behavior of the system is ramp output versus step input. This shows that the system acts as an integrator against a given step input. Accordingly, the transfer function of the system was taken as the integrator and a new model was obtained with the equations formed from the cylinder speeds. Then, the hydraulic system outputs were placed in the mechanism equations calculated at the beginning and the tip positions of the blade were obtained in all three axes.

A terrain created in the Matlab/Simulink environment, the responses of the hydraulic system to various height inputs were observed. Then, using the equations obtained with the principle of the vehicle dynamics, the changes in the center of gravity of the vehicle in all three axes were found. These changes give the positions of the vehicle in three axes in the face of a disturbance from the road. Then, these changes in



the center of gravity were transferred to the blade by using rotation matrices and the system behavior was observed.

Various sensors can be added to the system to measure the blade-ground distance in the continuation of the study. The reaction of the blade can be examined by using the model created for different orientations of the blade. Improvements can be made if necessary.



## REFERENCES

- [1] Iowa Transportation Center University Extension (1991), *Motor Grader Operator Maintenance of Granular Surfaced Roads. Tips from Iowa Operators*, Iowa State University of Science and Technology.
- [2] SOBCZYK Andrzej, TORA Grzegorz (1998), "Grader blade stabilization system", *Automation in Construction* 7, pp. 385-389.
- [3] SAKAI Yukihiisa (2002), Development of Combined Automatic Blade Control for Snow-Removing Grader, *Komatsu Technical Report*, Vol. 48 No.150.
- [4] FALES Roger C., KELKAR Atul G., SPENCER Erik, CHIPPERFIELD Kurt, WAGNER Francis (2003), "Modelling and Control of a Construction Machine with a Human-In-The-Loop Assessment in Virtual Reality", *International Mechanical Engineering Congress IMECE*, November 15-21.
- [5] JALON Javier Garcia, CALLEJO Alfonso (2011), "A straight methodology to include multibody dynamics in graduate and undergraduate subjects", *Mechanism and Machine Theory*.
- [6] HYASHI Kazuhiko, SHIMADA Kenjiro, ISHIBASHI Eiji, OKAMOTO Kenji, YONEZAWA Yasuhito (2013), "Development of D61EXi/PXi-23 Bulldozer with automatic control system of work equipment", *Komatsu Technical Report*, Vol.59 No. 166.
- [7] PAN Yongjun, CALLEJO Alfonso (2016), "Identification, design and kinematic analysis of an earthmoving mechanism", *Journal of Terramechanics* 66, pp. 27-39.
- [8] PAN Yongjun, HOU Liang (2017), "Lifting and parallel lifting optimization by using sensitivity and fuzzy set for an earthmoving mechanism", *Journal of Automobile Engineering*, Vol. 231(2), pp. 192-203.
- [9] SUN D.I., KIM S.H., LEE Y.S., LEE S.K., HAN C.S. (2017), "Pose and Position Estimation of Dozer Blade in 3-dimensional by Integration of IMU with Two RTK GPSs", *34th International Symposium on Automation and Robotics in Construction (ISARC 2017)*.

- [10] KIM Sang-Ho, LEE Yong-Seok, SUN Dong-Ik, LEE Sang-Keun, YU Bo-Hyun, JANG Sung-Hoon, KIM Wansoo, HAN Chang-Soo (2019), "Development of bulldozer sensor system for estimating the position of blade cutting edge", *Automation in Construction* 106, 102890.
- [11] KORYTOV M.S., SHCHERBAKOV V.S., TITENKO V.V. (2019), "Effects of the angles of the earth-moving machine moldboard on the cross slope of the graded surface", *IOP Conf. Series: Journal of Physics: Conf. Series* 1210 (2019)012070.
- [12] Michigan's Local Technical Assistance Program (1997), *Motor Grader Operator's Training Manual*.
- [13] TOPCON Positioning System (2007), *Motorgrader System Five Operator's Manual For the 9164 Control Box*. Part Number 7010-0344. Re. E.
- [14] OZKAN Ekin Cansu, ERGEZER Halit (2022), "Kinematic Analysis and Position Control of Motor Grader Blade Mechanism for Automatic Levelling", *8th International Conference on Control, Decision and Information Technologies (CoDIT)*.
- [15] <https://www.caterpillar.com/en/news/caterpillarNews/h/the-origin-of-motor-graders-produced-by-caterpillar-began-110-years-ago.html> (Access Date: 13.7.2022).
- [16] <https://www.hidromek.com.tr/30/detail/hmk-600-mg> (Access Date: 13.7.2022).
- [17] <https://www.deere.com/en/campaigns/smartgrade-motor-graders/> (Access Date: 13.7.2022)
- [18] [https://www.cat.com/en\\_US/products/new/technology/grade.html](https://www.cat.com/en_US/products/new/technology/grade.html) (Access Date: 13.7.2022)
- [19] <https://leica-geosystems.com/products/machine-control-systems/grader> (Access Date: 13.7.2022)
- [20] <https://www.siko-global.com/en-de/products/linearline-draw-wire-encoders/position-sensors-for-hydraulic-cylinders> (Access Date: 16.7.2022)
- [21] <https://www.mathworks.com/products/matlab.html> (Access Date: 16.7.2022)
- [22] <https://www.ptc.com/en/products/creo> (Access Date: 16.7.2022)
- [23] STAICU Stefan (2009), "Dynamics of the spherical 3-UPS/S parallel mechanism with prismatic actuators", *Multibody Syst Dyn*, Vol. 22, pp. 115-132.

- [24] RETSCHER Günther (1998), "Evaluation concepts for application of multi-sensor systems", *XXI International Congress FIG '98*, pp.104-117, Brighton, UK.
- [25] RETSCHER Günther (2002), "Multi-Sensor Systems for Machine Guidance and Control", *TS6.7 Engineering Surveys for Transportation and Utility Lines FIG XXII International Congress*", USA.
- [26] SHEVCHENKO V., BEZTSENNAYA Zh. (2015), "A Method to Estimate Loading of a Motor-Grader Blade Control Hydraulic Cylinders", *International Scientific Journal "Machines. Technologies. Materials."* Vol. 12, pp. 75-77.
- [27] FALES Roger, KELKAR Atul (2009), "Robust control design for a Wheel loader using Hco and feedback linearization based methods", *ISA Transactions*, Vol.48, pp.312-320.
- [28] LJUNG Lennart (1999), *System Identification Theory for the User Second Edition*, Printice Hall PTR, pp. 6-14.
- [29] EROL Bihter (2011), "An automated height transformation using precise geoid models", *Scientific Research and Essays*, Vol. 6(6), pp. 1351-1363.
- [30] CATERPILLAR Inc. (2011), *Cat Motor Grader Application Guide*, AEGQ0947.
- [31] UNLUSOY Y. Samim (2017), *Industrial Fluid Power Lecture Notes*, Mechanical Engineering Department, Middle East Technical University, Ankara.
- [32] ÇİFTÇİ Murat (2009), *Basit Ağır Araç Modelleri (Yüksek Lisans Tezi)*, İstanbul Teknik Üniversitesi Fen Bilimleri Enstitüsü, İstanbul.
- [33] GÖZTAŞ Durmuş Ali (2010), *Ride Model and Simulation of a Backhoe-Loader (Yüksek Lisans Tezi)*, Middle East Technical University The Graduate School of Natural and Applied Sciences, Ankara.
- [34] AKOVA Hayrettin Ulaş (2014), *Design, Construction and Control of an Electro-Hydraulic Load Simulator for Testing Hydraulic Drives (Yüksek Lisans Tezi)*, Middle East Technical University The Graduate School of Natural and Applied Sciences, Ankara